UNIVERSITEIT VAN PRETORIA
UNIVERSITY OF PRETORIA
YUNIBESITHI YA PRETORIA

Electrical characterisation of Schottky barrier diodes fabricated on GaAs by electron beam metallisation

by

Enoch Mpho Sithole

Submitted in partial fulfillment of the
requirements for the degree

MSc (Physics)

in the

Faculty of Natural and Agricultural Sciences.

University of Pretoria
Pretoria

October 2001

Supervisor: Prof F. D. Auret
Co-supervisor: Prof G. Myburg

© University of Pretoria

UNIVERSITEIT VAN PRETORIA
UNIVERSITY OF PRETORIA
YUNIBESITHI YA PRETORIA

Acknowledgements

I would like to thank the following persons for their contribution towards the completion of this study:

My supervisor, Prof F. D. Auret for his guidance, support, and encouragement.

My co-supervisor, Prof G. Myburg, for encouragement and helpful suggestions during the experimental part of this study.

The National Research Foundation (NRF) of South Africa for their financial support throughout my studies.

My wife, Mmapula for her support and encouragement during this study.

My parents for providing me with the opportunity to further my education.

Objectives

Metallisation of semiconductors is a critical processing step during device fabrication. Electron beam (EB) evaporation is very popular for the deposition of metals on semiconductors, especially due to its ability to evaporate high melting point metals under high vacuum conditions. It has also been found that EB deposition enhances the adhesion of the deposited layer onto the substrate. However, apart from the advantages, EB evaporation also has some disadvantages. It has been found that when the electrons strike the molten metal x-rays of varies energies are produced. Particles backscattered from the molten target as well as particles originating at the region of the filament reach the substrate. A metal shield has been used to prevent some of these particles from reaching the substrate but it could not prevent all particles from reaching the substrate.

The aim of this study was to apply more physics to eliminate the effect of the particles on the substrate. Positive and negative voltages were applied respectively to the substrate to prevent particles from reaching the substrate. The effect of biasing the sample during Schottky contact fabrication by EB deposition on GaAs will be investigated. The quality of the electrical characteristics of Schottky contacts will be evaluated by current-voltage (I-V) and capacitance-voltage (C-V) measurements as a function of applied voltage. Deep level transient spectroscopy (DLTS) will be used to identify and characterize the induced defects in the material and comparing their electrical properties with those previously detected from GaAs.

UNIVERSITEIT VAN PRETORIA
UNIVERSITY OF PRETORIA
YUNIBESITHI YA PRETORIA

Summary

Electrical characterisation of Schottky barrier diodes fabricated on GaAs by electron beam metallisation

by

Enoch Mpho Sithole

Supervisor: Prof F. D. Auret
Co-supervisor: Prof G. Myburg

The electrically active defects introduced in GaAs by electron beam deposition (EB) of Ta were characterised. The effect of electron beam deposition on the electrical properties of GaAs was evaluated by current-voltage (I-V), capacitance-voltage (C-V) and deep level transient spectroscopy (DLTS). However, when electronic devices are formed by EB, defects may be introduced into the semiconductor material, depending on the properties of the metal being deposited. Depending on the application, these defects may have either advantages or detrimental effects on the performance of such a device.

I-V measurements indicated that the EB induced damage results in an increase in ideality factor and decrease in the barrier height with increasing the applied substrate bias, while C-V measurements showed that EB deposition also caused a decrease in the barrier height. DLTS studies on the same material in the temperature range of 20 – 350 K showed that at least three electrically active defects are introduced during EB deposition, with energies (0.102 ± 0.004, 0.322 ± 0.014 and 0.637 ± 0.029 eV) within the band gap.

DLTS data was used to construct concentration profiles of these defects as a function of depth below the surface. It was found that the defect concentration increases with increasing substrate bias during the deposition, irrespective of the direction of the applied bias. This may be related to the I-V characteristics of the SBDs. The SBDs investigated by IV measurements showed that GaAs yields SBDs with poorer characteristic. The influence of EB deposition on the device properties of SBDs fabricated on GaAs is presented. These device properties were monitored using a variable temperature I-V and C-V apparatus. In order to have an understanding of the change in electrical properties of these contacts after EB deposition, it is necessary to characterise the EB induced defects. DLTS was used to characterise the defects in terms of their DLTS signature and defect concentration.

(305 words)

Table of contents

Page

CHAPTER 1: INTRODUCTION 1

CHAPTER 2: SEMICONDUCTOR PROPERTIES 3

2.1 General properties of semiconductors 3
2.2 Occupancy of states in the valence and conduction bands 4
2.3 Electrical properties of semiconductor 7
2.3.1 Energy band structure 7
2.3.2 Fermi level 8
2.3.3 Shallow states 8
2.3.4 Deep states 9
2.3.5 Impurities and defects 9
2.3.6 Intrinsic semiconductor 10
2.3.7 Extrinsic semiconductor 10
2.4 General properties of GaAs 11
2.4.1 Growth techniques 12
2.4.1.1 Bulk crystal growth techniques 12
2.4.1.2 Epitaxial growth techniques 13
2.5 Applications of GaAs 14

CHAPTER 3: METAL-SEMICONDUCTOR CONTACTS 17

3.1 Introduction 17
3.2 Schottky barrier contacts 17
3.3 Ohmic contacts 20
3.4 Series resistance 22
3.5 Current-transport mechanisms in SBDs 23

3.6 Characterisation techniques 26
3.6.1 I-V and C-V Measurements 26
3.6.1.1 Current –Voltage Measurements 26
3.6.1.2 Capacitance-Voltage Measurements 28

CHAPTER 4: ION SOLID (SURFACE) INTERACTION 32

4.1 Introduction 32
4.2 Processes leading to damage 33
4.2.1 Ion Energy 34
4.2.2 Mass of Target and Bombarding Ions 34
4.2.3 Angles of Incidence 35
4.2.4 Crystal structure of target 36
4.2.5 Ion Implantation 37
4.3 Energy Loss Mechanisms 37
4.3.1 Electronic Stopping 39
4.3.2 Nuclear Stopping 40
4.4 Range Distribution of Implanted Ions 41
4.5 Doping of Semiconductors 42
4.6 Defect Formation 42
4.7 Thermal Annealing of Defects 44
4.8 TRIM 48

CHAPTER 5: METAL CONTACT DEPOSITION 50

5.1 Metal deposition methods 50
5.1.1 Thickness Monitor 50
5.1.2 Resistive evaporation 51
5.1.3 Electron beam deposition 52
5.2 Sputtering System 54
5.2.1 Sputter Deposition 55
5.2.2 Magnetron Sputter Deposition 56
5.2.2.1 Plasma State 57

5.2.3 DC Glow Discharge 58
5.2.4 RF Glow Discharge 59
5.2.5 Ion Vapour deposition 60
5.2.6 Laser Ablation 62
5.2.7 Ion Beam Sputtering 63

CHAPTER 6: DEEP LEVEL TRANSIENT SPECTROSCOPY 66

6.1 Introduction 66
6.2 Semiconductor junction 67
6.3 Deep states in the bandgap 68
6.4 DLTS measurements 71
6.5 Rate window principle 73
6.6 Parameters determined from DLTS 76
6.7 Defect concentration 78
6.8 DTLS signatures 80

CHAPTER 7: I-V AND C-V EXPERIMENTAL RESULTS 84

7.1 Introduction 84
7.2 Sample preparation 84
7.2.1 Cleaning procedure 84
7.2.2 Ohmic contact fabrication 85
7.2.3 Schottky barrier diode fabrication 86
7.3 Schottky and Material characterisation 86
7.3.1 I-V and C-V results 87
7.4 Summary 100

CHAPTER 8: DLTS EXPERIMENTAL RESULTS 102
8.1 Introduction 102
8.2 Summary 120

CHAPTER 9: CONCLUSIONS 123

CHAPTER 1

INTRODUCTION

GaAs and related alloys have in particular become important in the fabrication of a wide variety of devices such as: light emitting diodes (LED's), solid state lasers, Gunn diodes and high electron mobility transistors (HEMT). An important aspect of the large expansion in the development and production of semiconductor devices has been the demand for more sophisticated techniques for determining the electrical properties of semiconductors.

It has been known for a very long time that, under suitable conditions, defects and impurities can modify in a positive way the properties of semiconductor materials. Defects induced in semiconductor materials during growth and subsequent device fabrication steps such as, ion implantation, ion bombardment, irradiation and plasma-related processing are now mostly considered to be undesirable. Any successful application of defects to tailor the properties of semiconductors, requires an understanding of the properties of defects, such as activation energy, defect concentration and introduction rate.

Defects play a major role in the determination of the electronic properties of a semiconductor, mainly because they interact with free carriers in the form of traps and recombination centres. Their effect is of importance even when the concentrations are very small compared to the free carrier concentration. Defects in the crystal structure of semiconductors exist in the bulk material, at the surface and interface and originate from the material itself, e.g. grown during material growth, or they are produced during the various steps involved in the processing of semiconductor devices, for example, during electron beam deposition.

In the present study a detailed analysis of the Schottky and electrical properties of the GaAs material after the electron beam deposition of Ta metal has been made. (This chapter provides some background information to the main parts of this book).

A general introduction in some of the more important physical and electrical properties of GaAs will be given in chapter 2. In chapter 3, the theory of metal-semiconductor contacts with particular attention on n-GaAs is discussed. Chapter 4 is devoted to the theory of ions interacting with semiconductor surfaces. In chapter 5 the different deposition techniques, which can be used to evaporate metals on semiconductor material are discussed. In chapter 6, the experimental technique (DLTS), as well as certain theoretical aspects are discussed. Chapter 7 gives a layout of the I-V and C-V experimental results. The final chapter, i.e. Chapter 8 gives the DLTS experimental results followed by a review of the conclusions that were drawn from this study.

Chapter 2

Semiconductor Properties

2.1 General semiconductor properties

Semiconductors are material having electrical conductivity intermediate between metals and insulators. This conductivity can be varied by varying temperature, impurity content and by optical excitation. This variation in the electrical properties is the basic property for the use of semiconductors in electronic devices.

Table 2.1: *General properties of some common semiconductors.*

Semicon-ductor	Crystal Structure	E_g (eV) 0 K	300 K	Bandgap Type	Melting-Point (K)	Hall-Mobility(cm^2/V.s) E	H	Ref
GaAs	Cub. Z.B	1.52	1.42	D	1238	8500	400	(2)
Ge	f. c. c	0.74	0.66	I	937	3900	1900	(2)
Si	f. c. c	1.17	1.12	I	1415	1500	450	(4)
GaSb	Cub. Z.B	0.81	0.72	D	712	5000	860	(4)
GaP	Cub. Z.B	2.34	2.26	I	1460	110	75	(6)
AlSb	Cub. Z.B	1.68	1.58	D	1065	200	420	(11)
InAs	Cub. Z.B	0.42	0.36	D	942	33000	460	(9)
InSb	Cub. Z.B	0.23	0.17	D	530	80000	1250	(9)
InP	Cub. Z.B	1.42	1.35	I	1060	4600	150	(11)

I - Indirect and D - Direct band-gap,

E - Electron and H - Holes mobility

To be able to electrically characterize semiconductor materials, an understanding of their basic properties is needed. Electrical conduction in a semiconductor material is facilitated by the motion of carriers in occupied states (electrons in the conduction band or holes in the valance band). The concentration of these electrons and holes can be controlled by the amount of impurities, which are purposely introduced into a semiconductor. Semiconductors are distinguished from other materials by the fact that their atoms are held together by strong directional covalent bonds between nearest neighbor atoms.

2.2 Occupancy of states in the valence and conduction bands

Every solid contains electrons. For the electrical characterization of semiconductor it is, amongst others, necessary to know the response of electrons to an applied electric field. For an intrinsic semiconductor there is just enough electrons to fill all the states in the valence band. The conduction band contains most of the excited electrons from the valence band. To obtain a semiconductor material that is useful for device fabrication, it is necessary to dope the material with specific impurity atoms. In general adding group V element atoms results in extra electrons within the semiconductor yielding an n-type semiconductor material. Similarly, adding group III elements, only three covalent bonds are complete, resulting in holes produced p-type semiconductor material for group IV. The irradiation of semiconductors introduces defects with energy levels in the forbidden band-gap. These defects capture some of the free carriers and thereby change the electrical properties of the semiconductor devices.

The total number of electrons in the conduction band of the semiconductor is given by:

$$n = \int_{E_c}^{E_{top}} N(E)F(E)dE \quad , \tag{2.1}$$

where *N(E)* is the density of states in the conduction band and *F(E)* the probability that a given state is occupied.

E_{top} is the energy at the top of the conduction band and E_c the energy at the bottom of the conduction band. The probability that a state is occupied is given by the Fermi-Dirac distribution function:

$$F(E) = \frac{1}{1 + \exp\left(\frac{E - E_F}{kT}\right)} \tag{2.2}$$

Where k is Boltzmann's constant, T is the absolute temperature, and E_F the Fermi energy. The density of states in the conduction band can be approximated by

$$N(E) = M_c \frac{\sqrt{2}}{\pi^2} \frac{(E - E_c)^{1/2}}{\hbar^3} (m_{de})^{3/2} \tag{2.3}$$

With M_c the number of equivalent minima in the conduction band, $\hbar$ is the reduced Plank's constant and m_{de} the geometric mean of the effective masses along the principal axes of the ellipsoidal energy surface. Using equation (2.2) and (2.3) and evaluating the integral in equation (2.1) gives:

$$n = N_c \frac{2}{\sqrt{\pi}} F_{1/2}\left(\frac{E_F - E_c}{kT}\right) \tag{2.4}$$

N_c is the effective density of states in the conduction band defined by

$$N_c \equiv 2\left(\frac{2\pi m_{de} kT}{h^2}\right)^{3/2} M_c \tag{2.5}$$

and $F_{1/2}(\eta_f)$ is the Fermi-Dirac integral. For the Boltzmann statistics case, i.e. for the Fermi level several kT below E_c in nondegenerate semiconductors, the integral approaches $\pi^{1/2}e^{\eta f}/2$.

Equation (2.4) becomes

$$n = N_c \exp\left(-\frac{E_c - E_F}{kT}\right) \tag{2.6}$$

By similar argument the concentration of holes in the valence band is found to be

$$p = N_v \frac{2}{\sqrt{\pi}} F_{1/2}\left(\frac{E_v - E_F}{kT}\right) \tag{2.7}$$

Where N_v is the effective density of states in the valence band given by:

$$N_v \equiv 2\left(\frac{2\pi m_{dh} kT}{h^2}\right)^{3/2} \tag{2.8}$$

and m_{dh} is the density of state effective mass of the valence band given by:

$$m_{dh} = \left(m_{lh}^{3/2} + m_{hh}^{3/2}\right)^{2/3} \tag{2.9}$$

Where m_{lh} and m_{hh} refer to the "light" and "heavy" holes respectively. As before it follows that:

$$p = N_v \exp\left(-\frac{E_F - E_v}{kT}\right) \tag{2.10}$$

2.3 Electrical properties of semiconductors

In order to electrically characterize semiconductors the following properties are usually of interest: donor density (N_D), acceptor density (N_A), resistivity (ρ), carrier lifetime (τ), and mobility (μ).

The total resistivity ρ, is given as a sum of two contributions

$$\rho = \rho_o + \rho_i \tag{2.11}$$

where ρ_o is due to scattering by impurities and ρ_i is caused by electrons being scattered by phonons. Mobility is a measure of the ease with which the carriers can move under the influence of an electric field, i.e. it is proportional to the inverse of the scattering probability. If the effective density N of the carriers and the resistivity ρ, are known, then the mobility μ, may be calculated from a relation which is a definition of the conductivity σ.

$$\sigma = 1/\rho = e\mu N \tag{2.12}$$

where e is the electronic charge.

2.3.1 Energy band structure

Ever since the application of the band theory of metals to semiconductors, this theory has been successful in explaining the properties of semiconductors. The most important result of the application of quantum mechanics to the description of electrons in a solid is that the allowed energy levels of electrons and holes are grouped into bands. The lowest energy band or valance band (E_v) is completely filled with electrons because of the Pauli exclusion principle. At zero temperature, the upper energy band is normally empty of electrons, because it consists of the unoccupied higher levels in the isolated atom.

The energy region between these two bands is called the forbidden energy gap or so-called band-gap, since no energy levels within the band-gap may exist in a perfect crystal. For example electrons in n-type, which have been promoted to the conduction band (E_c) by the addition of energy from some source, can conduct electricity. The size of the band-gap determines the amount of energy required for this transition. Therefore, depending on the size of this band-gap, a material can be classified as an insulator or semiconductor.

With the aid of optical transmission experiments on semiconductors, a number of workers concluded that semiconductors can further be classified as direct or indirect-gap materials. Values for the energy gap as well as some other general properties of most common semiconductors are indicated in table 2.1

2.3.2 The Fermi level

The Fermi levels for an intrinsic semiconductor lies very close to the middle of the band-gap. When impurity atoms are introduced, the Fermi level must adjust itself to preserve charge neutrality. For an intrinsic semiconductor the number of electrons in the conduction band is equal to the number of holes in the valence band.

The Fermi level for an intrinsic semiconductor is obtained by equating equations (2.6) and (2.10):

$$E_F = \frac{E_c}{2} + \frac{kT}{2}\ln\left(\frac{m_p}{m_n}\right) \tag{2.13}$$

2.3.3 Shallow states

Shallow states are located near the valence band as acceptor states and near the conduction band as donor states.

2.3.4 Deep states

Deep states are classified as those, which are positioned deeper than the shallow level in the band-gap. Deep states tend to be nonradiative recombination centres. Several techniques including capacitance based techniques provide opportunities for the electrical characterisation of these states.

2.3.5 Impurities and defects

The influence of small amounts of impurities present in a semiconductor can drastically influence its electronic properties. This phenomenon forms the basis of semiconductor technology. There are two types of impurities in semiconductors. Firstly, those which are responsible for the conduction and which have shallow energy levels, i.e., energy levels within the band gap close to the conduction or valence band. These are referred to as dopant impurities.

Dopant atoms from elements in a column of the periodic table to the right of the host atom are in general referred to as donors, because they have more unpaired valence electrons than the host atoms and give rise to n-type semiconductors. Those to the left are called acceptors because they can accept electron from the host atoms in order to fulfil local bonding requirements and lead to p-type semiconductor.

The second type of impurity has energy levels, which lie further from the band edges, and usually referred to as deep defects states, traps, recombination centers, generation centers, deep levels or deep impurities. In a neutral semiconductor material, an electron trap is defined to be a defect for which the electron capture is larger than the hole capture rate. In contrast, a recombination center is defined as a defect for which both the electron and hole capture rates are large and comparable in magnitude.

The defects which, are localised with atomic dimension, vacancies i.e. vacant atomic site, and interstitial i.e. extra atom occupying an interstitial site. A Frenkel defect is in principle formed by removing an atom from its lattice site and then placing it in an interstitial position, thus forming a vacancy-interstitial pair. This defect may play an important role in the formation of other defects.

A certain minimum energy must be transmitted to a lattice atom to produce a displacement for the formation of a Frenkel defect.

In terms of their thermal emission properties, these defects can be defined as majority or minority carrier traps. A defect where the rate for thermal emission of a majority carrier is much larger than the rate for thermal emission of a minority carrier is defined as a majority carrier trap. A minority carrier trap has just the opposite definition. From these definitions, it is obvious that an electron trap is a majority carrier trap in n-type material, while a minority carrier trap in p-type material

2.3.6 Intrinsic semiconductor

A perfect crystal structure which contains no chemical impurities and in which no atoms are displaced from their lattice sites is called an intrinsic semiconductor. In such material, there are no charge carriers at 0 K since the valence band is filled with electrons and the conduction band is empty. At higher temperatures, electrons are excited thermally across the band gap to the conduction band. Each electron, which is excited into the conduction band, leaves a hole in the valence band, therefore the number of electrons and holes should be equal.

2.3.7 Extrinsic semiconductor

When a crystal is doped such that the equilibrium carrier concentration of electrons and holes are different from the intrinsic carrier concentration, the material is said to be extrinsic. It is possible to create carriers in semiconductors by introducing impurities into the crystal so that it has a predominance of either electrons or holes. When impurities are introduced into a perfect crystal, additional levels are created within the energy band. An energy level introduced by an impurity near the conduction band is called a donor level and an energy level introduced near the valence band is called an acceptor level.

2.4 General properties of GaAs

GaAs is formed when elements out of group III and group V are combined. It is one of the members of the family of III-V compounds. It is a direct band-gap semiconductor with a smaller effective mass than an indirect band-gap material such as Si. This property provides the electrons in GaAs with a very high mobility, which makes it one of the most important materials for the fabrication of optoelectronic devices. Typical electron mobility values of 8000 cm^2/vs and higher for GaAs are obtained, five times faster than that of Si (1500 cm^2/vs). These mobilities for GaAs increases with a decrease in temperature down to 10 K or if multi-layer supperlattices are grown such as in metal-semiconductor field-effect transistors (MESFET's).

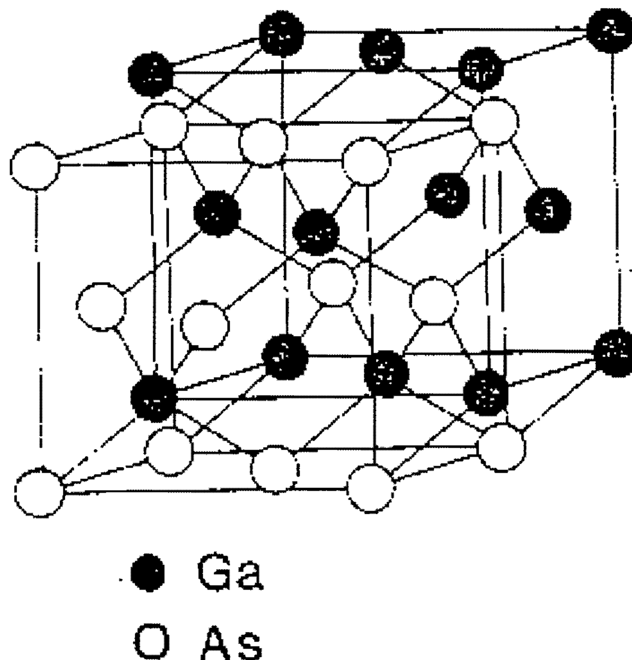

Fig 2.1: *The (atomic) crystal structure of GaAs.*

GaAs is one of the most commonly used materials for fabricating semiconductor devices. Being a compound III-V semiconductor, GaAs has an ionic bonding between Ga and As. Consequently, the nature and reactivity of a GaAs surface depends on its orientation, and therefore, the new defects are known to play an important role in the electronic properties of the semiconductor [11].

The face-center cubic (fcc) or zinc blende type structure of GaAs is illustrated in figure 2.1 with the lattice parameter of the undoped structure, a_o = 4.65 Å.

2.4.1 Growth techniques

The performance and suitability of semiconductor devices critically depends on the state of perfection of the different growth techniques, because the formation of process-induced defects is often closely related to the defect structure present in the as-grown bulk material. GaAs, compared to Si, the crystal growth is more sensitive to thermal gradients and temperature changes during the growth process. These changes normally generate crystal dislocations and other structural defects.

2.4.1.1 Bulk crystal growth techniques

The three most popular methods for bulk growth of GaAs are the:

i) Liquid Encapsulated Czochralski (LEC)

ii) Horizontal Bridgman (HB) or gradient freeze

iii) Czochralski pulling technique

Apart from the fact that their orientations may differ, the crystals grown by these techniques have significantly different defects and impurity densities, and therefore electrical properties. One of the major problems related to these high temperature growth techniques, is the Si contamination which originates from the reactor materials. Depending on the growth conditions, Si can act either as a donor or acceptor and can affect the electrical behavior of the substrate. In the HB process the Si contamination has been suppressed by the deliberate addition of dopants such as O_2, which results in high resistivity GaAs [(6)]. The HB grown crystals further have lower defect densities than LEC crystals.

2.4.1.2 Epitaxial growth techniques for GaAs

The semiconductor device technology of the future demands the fabrication of multi-layered solid-state structures with low defect and impurity concentration. This may be achieved by using one of the following epitaxial growth procedures.

Major epitaxial techniques are:

i) Liquid-Phase epitaxy (LPE)
ii) Vapor-Phase Epitaxy (VPE)
iii) Molecular-Beam Epitaxy (MBE)
iv) Metalorganic Chemical Vapor Deposition (MOCVD)

All of these methods have received considerable attention in the past. The aim is to mention their basic electronic characteristics.

i) In LPE growth of GaAs, the dominant residual donors are due to O_2, which originates from oxides in the Ga starting material. Si and C are the main residual acceptors. The LPE technique is a simple and reliable technique for the growth of a wide range of compound semiconductor materials such as GaAs, AlAs, GaP and GaSb. Hole traps are observed in GaAs grown by this technique.

ii) VPE growth has become one of the popular epitaxial growth techniques of recent years. Its popularity can be attributed to its flexibility in terms of chemical system choices, control of process parameters as well as processing adaptability. The uniformity and high quality of VPE layers are some of its outstanding advantages. The predominant deep center, referred to as EL2, was reported for this technique.

iii) The low temperature (< 500 °C) growth of thin GaAs layers by MBE is now a well-established technique. The n-GaAs grown by MBE was reported with 9 different electron traps with the aid of DLTS. These traps are attributed to the growth parameters [13]. A low concentration of EL2 is observed.

iv) MOCVD has become a very attractive technique for the growth of sophisticated multilayer structures of compound semiconductors. The mobilities of MOCVD grown GaAs are limited by electrical compensation resulting from impurities in both the metal alkyl and hydride sources. With the aid of DLTS it was established that the MOCVD layers have deep level impurities that are controlled by the particular source material, while photoluminescence studies have shown that the primary residual shallow acceptors present were Zn and C. This method also introduces the EL2 defect.

The major disadvantage of LPE is that the surface morphology of the grown layers is inferior to that produced by MBE or VPE and so it introduces difficulties in the subsequent processing of devices. Another is the restricted substrate size that can be used in the sliding boat systems to maintain acceptable uniformity. However, LPE can produce high electrical and optical quality GaAs. MOCVD and MBE are highly attractive because they can be used to grow AlGaAs-GaAs structures.

2.5 Application of GaAs

Metallisation of GaAs has received wide-spread attention in technology, because of its important applications in integrated circuits and infrared detection. GaAs is used in a number of different types of devices.

An application includes photonic and electronic devices. The photonic devices could be divided into three basic groups: (i) the devices that convert electrical energy into optical radiation e.g. LED's and laser diodes, (ii) devices that detect optical signals through electronic processes e.g. photodetectors, and (iii) devices that convert optical radiation into electrical energy e.g. photovoltaic devices or solar cells.

Gallium arsenide is an important material in field-effect transistors, heterojunction bipolar transistors, solar cells and integrated circuits and these components are becoming increasingly important in space applications.

GaAs offers a wider range of operating temperatures and much higher radiation hardness than Si. Integrated circuits fabricated from GaAs by standard processes can withstand temperature from –200 to +200 ^{o}C while operation up to 400 ^{o}C may be possible with special processes.

Gallium arsenate is an important material for devices to be used in space applications, because of its resistance to radiation damage. A number of GaAs semiconductor devices manufactured today must ultimately function in an environment fraught with radiation hazards. The applications of Schottky barrier diode include rectifiers, microwave switches, and mixer circuits, as well as level shifting and electrostatic discharge protection circuits (1,5).

It has also emerged as an optoelectronic material in the early 1960s. Applications of these devices include optical communication between satellites, telecommunication systems and thermal printing systems. High electron mobility transistors (HEMTs) have improved gain and noise performance over an extended frequency range. A further advantage of a HEMT is that it can be incorporated into either monolithic or hybrid microwave and millimeter-wave IC's for space application.

References

(1) F. D. Auret, G. Myburg, S. A. Goodman, L. J. Bredell and W. O. Barnard, Nucl. Instr. and Meth in Phys Res. B **67** (1992) 410.

(2) J. W. Hung, T. F. Kuech, H. Lee, and I. Bhat, Appl. Phys. Lett. **68** (1996) 2392.

(3) G. Myburg, F. D. Auret, W. E. Meyer, C. W. Louw and M. J. van Staden, thin Solid Films. **325** (1998) 181.

(4) B. Goldenberg, J. D. Zock, and R. J. Ulmer, Appl. Phys. Lett. **62** (1993) 381.

(5) M. J. Legodi, F. D. Auret, S. A. Goodman and J. B. Malhrbe, Nucl. Instr. and Meth in Phys Res. B **148** (1999) 441.

(6) M. Rubin, N. Newman, J. S. Chan, T. C. Fu, and J. T. Ross, Appl. Phys. Lett. **64** (1994) 64.

(7) S. A. Goodman, F. D. Auret, M. Ridgway and G. Myburg, Nucl. Instr. and Meth in Phys Res. B **148** (1999) 446.

(8) F. D. Auret, and S. A. Goodman, Appl. Phys. Lett. **73** (1998) 3217.

(9) Heon Lee, and James. S. Harriess, *Journal of Electronic Material*. **27** (1998) 185.

(10) M. J. Legodi, F. D. Auret and S. A. Goodman, Mater Sci and Engin. B **71** (2000) 96.

(11) R. A. Morrow, J. Appl. Phys. **69** (1991) 4306.

(12) M. J. Howes and D. V. Morgan; *Gallium Arsenide, Materials, Devices and Circiuts*. (1985), p481.

(13) D. V. Lang, A. Y. Cho, A. C. Gossard, M. Ilegems, and W. Wiegmann, J. Appl. Phys. **47** (1976) 2558.

(14) S. A. Goodman, F. D. Auret, and W. E. Meyer, J. Appl. Phys. **75** (1994) 1222.

(15) S. A. Goodman, F. D. Auret, and W. E. Meyer; Nucl. Instr. and Meth in Phys. Res. B **90** (1994) 349.

CHAPTER 3:

METAL- SEMICONDUCTOR CONTACTS

3.1 Introduction

The metal-semiconductor contact has received widespread attention in technology because of its important applications in integrated circuits and infrared and ultra-violet detection [1]. This chapter looks at the formation of an energy barrier between a metal and n-type semiconductor and the charge transport over it.

Schottky barrier diodes (SBDs) are the basis for many electronic devices (e.g. detectors). SBDs are also used in the electrical characterisation of defects introduced during semiconductor growth, device processing and also during testing of devices after fabrication. In 1938, Schottky and Mott developed models, which explain current transport across the energy barrier that characterises a metal-semiconductor contact. A brief discussion is given in this chapter.

3.2 Schottky barrier contact

When a metal makes contact with a semiconductor, an energy barrier results at the interface. The electron affinity, χ, of a semiconductor and the work function, Φm, of a metal are important parameters in the formation of Schottky barrier diodes in terms of the Schottky–Mott theory. Figures 3.1 and 3.2 show the energy diagrams for a metal and n-type semiconductor during the formation of a Schottky contact. For

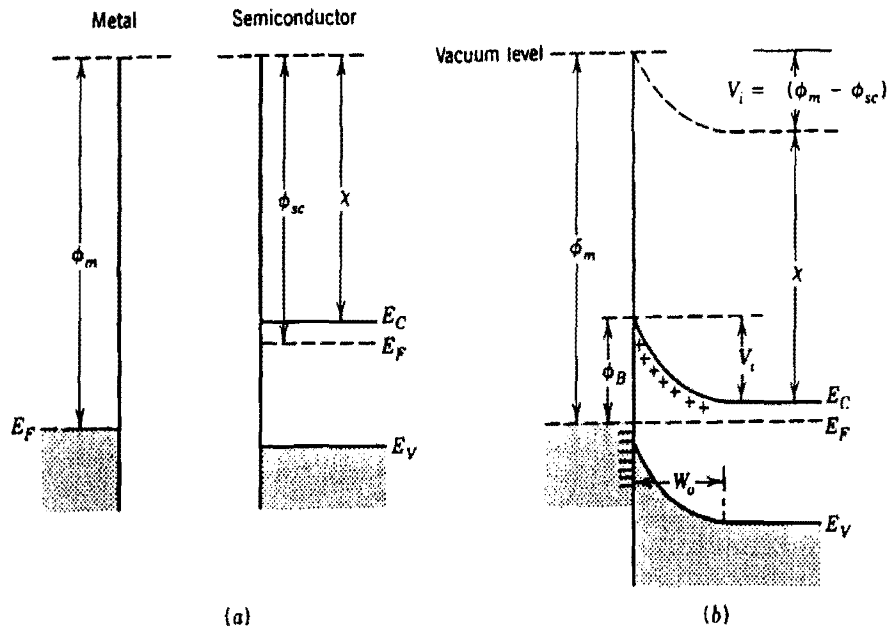

Fig 3.1: *The energy band diagram of a metal-n-type semiconductor with $\phi_m > \phi_{sc}$. (a) Metal and semiconductor isolated from each other (b) after contact (thermal equilibrium).*

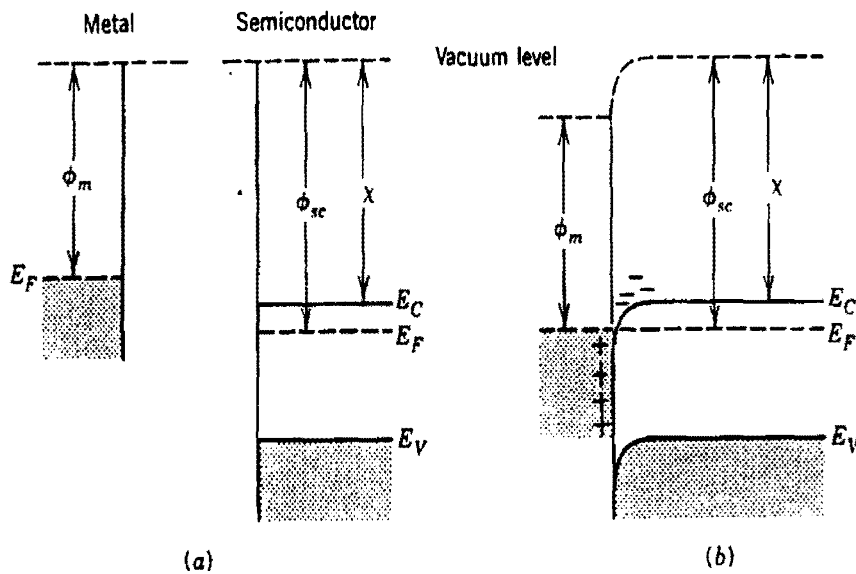

Fig 3.2: *The energy band diagram of a metal-n-type semiconductor with $\phi_m < \phi_{sc}$. (a) Metal and semiconductor isolated from each other (b) after contact (thermal equilibrium).*

According to the Schottky–Mott theory, the barrier arises as a result of the differences in the work functions of the metal and the semiconductor. The work function of a metal, Φm, is the amount of energy required to raise the electron from the Fermi level to an energy state outside the surface of the metal (vacuum level). The work function of a semiconductor material, Φ_s, is given by the difference in energy between the Fermi level and the vacuum level and is thus dependent on the semiconductor doping.

When a metal and semiconductor are brought into contact, the atomic position and the charge distribution of the surfaces will change. Both the metal work function and semiconductor work function has volume and surface contributions. The volume contribution arises because of the crystal lattice's periodic potential, whereas the surface contribution is attributable to any surface dipoles [(8)].

The more important parameter of a semiconductor material is the electron affinity, χ, which is defined as the difference in energy between an electron at rest outside the surface and at the bottom of the conduction band just inside the semiconductor. Φ_s and χ are related by the following equation:

$$\Phi_S = \chi + \xi \qquad (3.1)$$

Where ξ is the energy difference between the conduction band and the Fermi level.

$$\xi = E_c + E_F \qquad (3.2)$$

$$\xi = kT \ln\left[\frac{N_C}{N_D}\right] \quad \text{for n-type} \qquad (3.3)$$

N_C is the effective density of states in the conduction band. N_D is the semiconductor's free carrier concentration, k is the Boltzmann constant and T is the absolute temperature in kelvin.

If the concentration, N_D, of donors is much higher than N_A, acceptors, the effect of the acceptors can be ignored. In such a case the Fermi level moves upward from the middle of the band gap towards the conduction band. Similarly, if the acceptor concentration N_A is dominant, the Fermi level will move downwards towards the valance band.

When a metal is brought into close contact with the semiconductor material, electrons will flow from the semiconductor to the metal due to the differences in their Fermi levels (figures 3.1 and 3.2) until the semiconductor Fermi level coincides with that of the metal. An excess of electrons will thus result in the metal, while the uncompensated positive donor ions are left in the semiconductor.

3.3 Ohmic Contacts

An ohmic contact is considered as a special type of Schottky barrier in which the depletion region is so thin that transport of carriers from the semiconductor to the metal occurs by tunnelling. For ohmic contacts, which are essential for the operation of several device types and measurements of semiconductor characteristics, it is required that its total resistance should be very small compared with the resistance of the semiconductor or device. The barrier heights of the ohmic contact depend directly on the differences between the work function of the metal and the electron affinity of the semiconductor [(3)]. The quality of ohmic contact is greatly influenced by the condition of the semiconductor surface prior to metallisation as well as heat treatment of the material after the contacts have been formed. Some metals used for ohmic contacts require the presence of either "wetting" metallisation below or "capping" metallisation above.

For good metallisation, both ohmic and Schottky contacts require the following:

i. Good adhesion to the semiconductor material
ii. Resistance to wet chemical processing.
iii. Uniform layer.
iv. Reproducibility.
v. Resistance to radiation damage.
vi. Thermally stable

Table 3.1. Gives a summary of some values for specific contact resistivity R_c of ohmic contacts on n- and p- type GaAs.

Table.3.1: *Specific contact resistane values of ohmic contacts on n- and p-type GaAs*

Semiconductor	N_D or N_A (/cm^3)	Metals	Alloy Temp ^oC	Time	R_c (Ωcm^2)	Ref
n-GaAs	3E16	AuGe:Ni	450	100 s	1E-5	(2)
n-GaAs	2E16	AuGe:Ni	440	90 s	6E-5	(1)
n-GaAs	3E16	AuGe:Ni	500	120 s	1E-4	(7)
n-GaAs	-	AuTe:Ni	510	1-5 min	5E-7	(5)
n-GaAs	2E16	Ag:In:Ge	620	120 s	1E-5	(6)
n-GaAs	9E16	AuGe:Ni	390	120 s	6E-7	(8)
n-GaAs	4E14	Au/AuGe/Ni	450	120 s	-	(3)
p-GaAs	4E18	Au:Zn	450	-	4E-5	(4)
p-GaAs	5E18	Au:Zn:Au	400	5 min	8E-6	(10)
p-GaAs	8E14	Mn/Au	450	120	-	(8)
p-GaAs	1E16	Au/Ru	400	120	-	(9)

i 15951984
b15368105

Amongst the various metal deposition techniques, thermal evaporation by resistance, electron beam heating and magnetron sputter deposition are the most widely used techniques for depositing thin metal films on semiconductor surfaces. Resistance heating is applicable to metals having relatively low vaporisation temperatures (< 1500 °C), while electron beam and magnetron sputter deposition are used for evaporating high vaporisation temperature refractory metals. (See chapter 5).

3.4 Series Resistance

The series resistance (R_s) associated with the region between the depletion region and the ohmic contact can be determined from the I-V characteristics. For a large forward current, the voltage drop across R_s cause the actual voltage developed across the barrier region to be less than the voltage applied to the contacts of the diode. A plot of $ln\ I$ vs V, where I is the current flowing through the diode, will then deviate from a straight line as shown in figure 3.3 .

The values of R_s can be obtained by plotting ΔV vs I, where ΔV is the deviation in V for a given I at large forward voltages.

Another way of obtaining the series resistance is to apply a sufficiently large forward bias to obtain a flat band situation, where the depletion region will disappear and the resistance of it become negligible compared with R_s.

UNIVERSITEIT VAN PRETORIA
UNIVERSITY OF PRETORIA
YUNIBESITHI YA PRETORIA

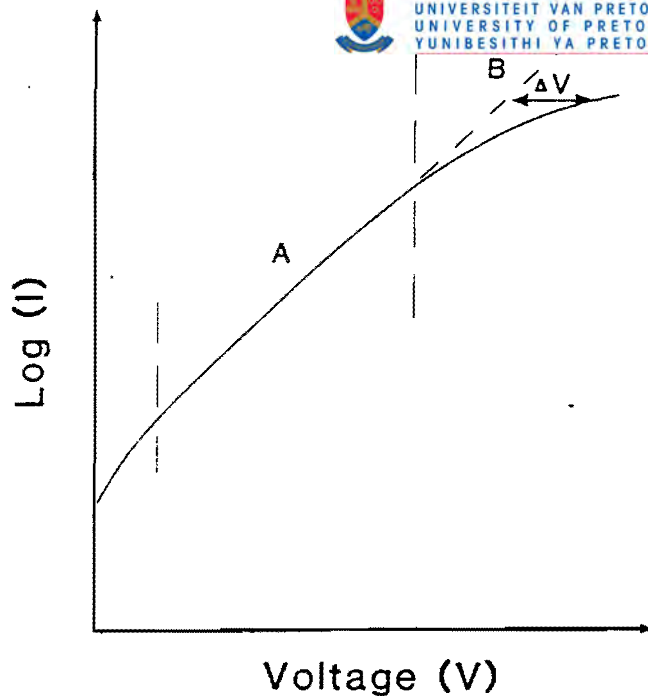

Fig 3.3: *The effect of series resistance as observed by I-V measurements.*

3.5 Current-Transport Mechanisms in SBDs

For Schottky diodes under forward bias, the transport mechanism of electrons across the metal-semiconductor junction can be classified as: emission of electrons from the semiconductor over the top of the barrier into the metal, quantum-mechanical tunnelling through the barrier, recombination in the space charge region, and recombination in the neutral region (hole injection). The inverse processes occur under reverse bias conditions. Diodes for which the mechanism of electrons emitted from the semiconductor, over the top of the barrier into the metal is dominant are called near-ideal, while the three other processes cause departure from this ideal behaviour. Figure 3.4 shows the charge transport processes, which determine the electrical properties of the junction.

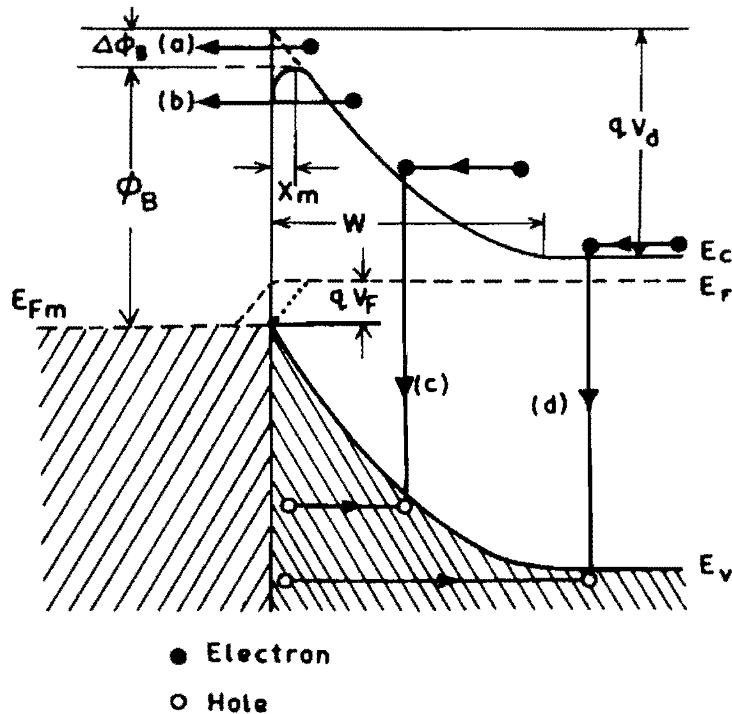

Fig.3.4: *Energy band diagram of a forward biased Schottky junction on n-type semiconductor showing the different current transport processes: (a) thermionic emission, (b) tunnelling through the Schottky barrier, (c) carrier recombination in the depletion region, and (d) carrier recombination in the semiconductor or hole injected from metal into the semiconductor neutral region.*

The Bethe thermionic emission theory [6] made the assumption that the current-limiting process is the actual transfer of electrons over the barrier into the metal, and not diffusion and drift. Under forward bias, the semiconductor Fermi level will be raised relative to the metal's, therefore the barrier height will be lowered correspondingly. The inverse process under reverse bias condition is analogous to thermionic emission from the metal into vacuum but with a barrier height of ϕ_B, replacing the work function ϕ_m.

There are two mechanisms that govern the emission of electrons from the semiconductor over the top of the barrier into the metal.

In the first process, electrons move from the bulk of the semiconductor and across the depletion region of the semiconductor by the mechanisms of drift and diffusion in the electric field of the barrier. At the interface, their emission into the metal is determined by the rate of transfer of electrons across the boundary between the metal and the semiconductor.

Table 3.2. *The I-V barrier height values for different metals to n- and p-type GaAs.*

Metal	ϕ_{bn} (eV)	ϕ_{bp} (eV)	Ref
Ag	0.90	0.50	(14)
Al	0.77	0.61	(14)
Au	0.89	0.50	(13)
Mg	0.63	-	(14)
Cr	0.77	0.62	(11)
Cu	0.96	0.45	(14)
Pt	0.99	-	(12)
Fe	0.83	0.60	(14)
Ni	0.77	0.62	(11)
Pb	0.80	0.52	(13)
Sb	0.91	0.50	(14)
Ti	0.84	-	(12)

According to the diffusion theory, the first of these processes is the most important, whereas according to the thermionic-emission theory the second process is the limiting factor. These processes occur effectively in series.

3.6 Characterisation Techniques

3.6.1 Current-Voltage and Capacitance-Voltage measurements

Current-voltage (I-V) and capacitance-voltage (C-V) measurements are sensitive techniques to determine the effects on the electrical properties of semiconductor devices. The degradation of electrical properties of Schottky diodes can be determined from the changes in leakage current, free carrier concentration and ideality factor.

3.6.1.1 Current-Voltage Measurements

The electron concentration on the semiconductor side of the boundary is given by:

$$n = N_c \exp\left\{\frac{-q(\phi_b - V)}{kT}\right\} \tag{3.4}$$

The motion of electrons over the barrier into the metal is governed by the mechanisms of drift and diffusion. The current density due to electrons passing from the semiconductor into the metal is:

$$J_{sm} = \frac{pqN_c v}{4} \exp\left\{\frac{-q(\phi_b - V)}{kT}\right\} \tag{3.5}$$

where v is the average thermal velocity of the electrons, with p the probability of electrons tunnelling through the insulating layer. There is also a flow of electrons from the metal into the semiconductor. Since the barrier height remains unchanged with applied bias, it follows that:

$$J_{ms} = \frac{pqN_c v}{4} \exp\left(\frac{-q\phi_b}{kT}\right) \tag{3.6}$$

Hence the net current flowing is:

$$J = J_{sm} = J_{ms} \tag{3.7}$$

$$= \frac{pqN_c v}{4} \exp\left(\frac{-q\phi_b}{kT}\right)\left\{\exp\left(\frac{qV}{kT}\right) - 1\right\} \tag{3.8}$$

Assuming that p approaches unity as the insulating layer becomes thinner

$$N_c = 2\left(\frac{2\pi m^* kT}{h^2}\right)^{3/2} \tag{3.9}$$

equation (3.8) yields:

$$J = A^* T^2 \exp\left(\frac{-q\phi_b}{kT}\right)\left\{\exp\left(\frac{qV}{kT}\right) - 1\right\} \tag{3.10}$$

where A^* is the Richardson constant and equal to $4\pi m^* qk^2 / h^3$, k Boltzmann constant, $q\phi_b$ is the Schottky barrier height, T is the absolute temperature, and V is the applied voltage.

The forward I-V characteristic is represented by $I \sim exp(qV/nkT)$, for $V > 3kT/q$. In the reverse direction, the dominant effect is due to the Schottky barrier lowering, or $I_R \approx I_S$, for $V_R > 3kT/q$. Where I_S is the saturation current [2].

In this equation we assumed that barrier height is independent of bias. There are however several reasons why the barrier height may depend on the electric field in the depletion region and hence on the applied bias. Even for a perfect contact, the barrier height is reduced as a result of the image force by an amount $\Delta\phi_{bi}$. Therefore the effective barrier height is:

$$\phi_e = \phi_b - \Delta\phi_{bi} \tag{3.11}$$

In the presence of an interfacial layer, ϕ_b also depends on the bias and therefore the effective barrier height is:

$$\phi_e = \phi_{bo} - (\Delta\phi_{bi})_o + \beta V \tag{3.12}$$

where β is a constant. Equation (3.10) can be written as:

$$J = J_o \exp\left(\frac{qV}{nkT}\right)\left\{1 - \exp\left(\frac{-qV}{kT}\right)\right\} \tag{3.13}$$

where

$$J_o = A^* T^2 \exp\left[\frac{-q\{\phi_{bo} - (\Delta\phi_{bi})_o\}}{kT}\right] \tag{3.14}$$

and

$$\frac{1}{n} = 1 - \beta = 1 - \left(\frac{\partial\phi_e}{\partial V}\right) \tag{3.15}$$

where n is the ideality factor. The current voltage characteristics for non-ideal Schottky diodes with series resistance, R_s, and $V > 3kT/q$, are given by:

$$J = J_o \exp\left[\frac{q(V - IR_s)}{nkT}\right] \tag{3.16}$$

3.6.1.2 Capacitance-Voltage Measurement

The most used capacitor consists of two conducting metal plates separated by an insulating material. A potential energy source connected to the terminals of a capacitor attracts some of the electrons from the top metal plate to the positive terminal of the source. The same number of electrons is repelled by the negative terminal of the source. Hence the top plate charges positive and the bottom plate negative. An increase in the magnitude of the energy source V, allows more work to be done in separating the charges on the metal plate. This results in an increase in the amount of charge Q.

Therefore the amount of charge Q stored is directly proportional to the voltage applied. Thus $Q \propto V$ or $Q = CV$ with C the capacitance or measure of the ability to store charge. The larger the area of the metallic plates A, the more the amount of charge being stored. In addition, the distance between the plates, w, would influence the charge and the permittivity of the material.

Combining these parameters leads to:

$$C = \frac{\varepsilon A}{w} \tag{3.17}$$

In the case of semiconductor materials, in particular Schottky barrier diodes formed by depositing metals onto semiconductor materials, the application of a reverse bias increases the depletion region in the semiconductor. The bias exerts a force on the electrons and they start to move away from the junction. This process will continue until balanced by the electric field formed within the region. Equilibrium will occur and the depletion region will stay constant. A direct analogy with the parallel-plate capacitor is obtained. No free carriers exist within the depletion region and this forms the space between the metal plates. The Schottky contact area becomes the metal plate area. Thus equation (3.17) still applies with w the width of the depletion region, A the area of the contact and ε the dielectric constant of the semiconductor.

The width, W of the depletion region is obtained by integrating Poisson's equation twice, resulting in:

$$W = \sqrt{\frac{2\varepsilon(V_{bi} + V)}{qN_D}} \tag{3.18}$$

Where V is the applied voltage, V_{bi} is the built-in voltage, q the charge on the electron and N_D the density of the ionized donors.

The capacitance is also given by:

$$C = \varepsilon_s \frac{\partial E}{\partial V_r} \quad (3.19)$$

By applying Gauss's theorem to the semiconductor, the electric field can be determined and then it follows that:

$$C = \left(\frac{q\varepsilon_s N_d}{2}\right)^{1/2} \left[V_{bi} + V - \frac{kT}{q}\right]^{-1/2} \quad (3.20)$$

Where V, k, T and q have their usual meanings, N_d is the donor density

From equation (5.17) it follows that when a graph of $1/C^2$ is plotted against the applied voltage, V, a straight line is obtained with a slope of $2/q\varepsilon_s N_d$ were the carrier concentration is determined, if N_D is constant throughout the depletion region. From the intercept on the voltage axis, the barrier height can be determined.

Reference

(1) S. X. Jin, H. P. Wang, M. H. Yuan, H. Z. Somg, H. Wang, W. L. Mao, and G. G. Qin, Appl. Phys. Lett. **62** (1993) 2719.

(2) W.O. Barnard, G. Myburg, F. D. Auret, S. A. Goodman and W. E. Meyer, *Journal of electronic Materials.* **25** (1996) 11.

(3) G. Myburg, PhD Thesis, (1994) 74.

(4) J. Brown, J. Ramer, K. Zheng, L. F. Lester, S. D. Hersee, J. Zolper, Mat. Res Soc. Symp Pro. **49** (1996) 395.

(5) S. Ruvimov, Z. Liliental-Weber, and J. Washburn, Appl. Phys. Lett. **69** (1996) 1231.

(6) C. Uzan-Saguy, J. Salzman, R. Kalish, V. Richter, U. Tish and S. Zamir, Appl. Phys. Lett. **74** (1999) 74.

(7) F. D. Auret, and S. A. Goodman, Appl. Phys. Lett. **74** (1999) 446.

(8) C. D. Wang, L. S. Yu, S. S. Lau, and E. T. Yu, Appl. Phys. Lett. **72** (1998) 121.

(9) E. H. Rhoderick, and R. H. Williams, *In metal-semiconductor contacts*, Clarendon press, Oxford, (1988) 1312.

(10) D. I. Bohme and J. Weber, Phys. Rev B. **47** (1993) 4037.

(11) S. A. Goodman F. D. Auret, G. Muburg, and C. Schutte, Solid State Phenomena. **47** (1996) 391.

(12) F. D. Auret, G. Myburg, L. J. Bredell, W. O. Barnard, and H. W. Kunert; Mater. Sci. Form. **83** (1992) 1499.

(13) F. D. Auret, S. A. Goodman, G. Myburg, and W. E. Meyer, Appl. Phys. A **56** (1993) 547.

(14) W. O. Barnard, G. Myburg, F. D. Auret, S. A. Goodman, and W. E. Meyer; J. of. Elec. Mater. **25** (1996) 1695.

CHAPTER 4:

ION SURFACE INTERACTION

4.1. INTRODUTION

Scientific interest in ion implantation arose in the early 1940's after the first nuclear reactor was developed. During those days, it was assumed that the main area of application of ion implantation would be the doping of compound semiconductors, since diffusion in silicon was already well developed [2]. In general, ion bombardment was considered to have a harmful effect on material properties and the major concern was to avoid it. In 1950's it was realized that the radiation damage might improve certain properties of materials.

Recent development has provided the industrial world with a wide spectrum of technologies, both in the fields of metals and semiconductors. Irradiation produces radical changes in the properties of a solid. Deep level transient spectroscopy (DLTS) is currently the most sensitive technique for studying the electrical properties of radiation induced defects in semiconductors.

Irradiation or bombardment of semiconductor material with energetic particles has been a very active field of research for many years. It primarily focussed on the effect of irradiation on the properties of semiconductors as a function of projectile ion type, energy and dose and identifying the structure, electronic and optical properties of these irradiation induced defects in devices that functioned in radiation environments, for example, near radiation sources or in outer space where they are exposed to cosmic rays and how to remove this damage by annealing.

When designing electronic devices for operation in a radiation environment, it is essential to know the effect of radiation on their characteristics. In radiation environments, there are different types of particles such as electrons, protons, neutrons, alpha particles etc. In outer space, for example electronic devices in satellites are exposed to cosmic radiation, comprising of a variety of high-energy particles, which degrades their performance. In order to evaluate the effect of a radiation environment on the functioning of a device, it is essential to know which particles are involved, the defect introduction rates, and the electronic properties of the defects.

4.2 Physical Process

When the bombarding ions have energies larger then the threshold energy, they result in collision cascades during which the primary ions may become implanted with the ejection of target atoms through near-surface recoil collisions.
Fig.4.1 illustrates the collision of a primary particle with a solid surface and the emission of secondary particle (target atoms).

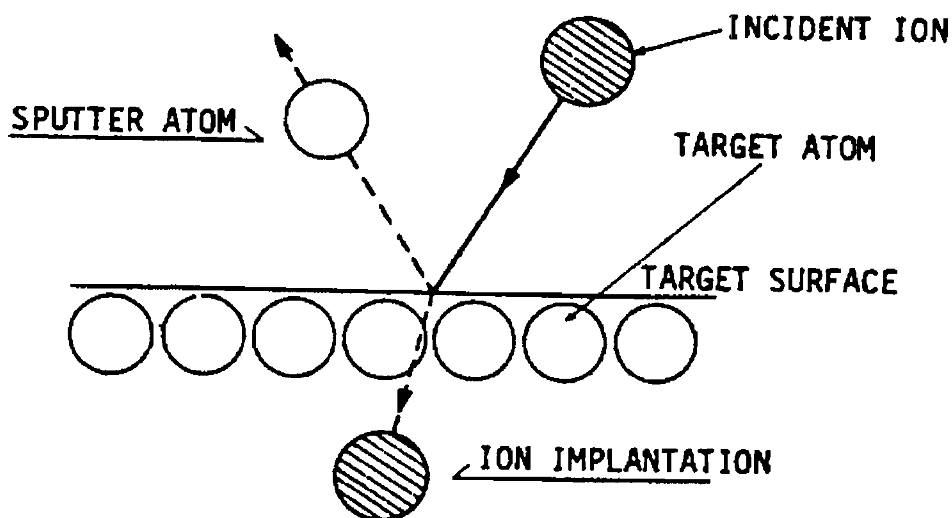

Fig. 4.1. *Illustration of the physical process. The energy transfer between an incident ion and a surface target atom results in the knocked-off of surface atom from the lattice, while the incident ion becomes imbedded below the target surface.*

4.2.1 Ion Energy

The sputter yield increases with ion energy to reach a maximum depending on the stopping power. This is attributed to the increase in collision cascades and their density, which results in increased transport of energy to the surface until the stopping reaches a maximum. Further increases in energy result in the ions becoming imbedded deeper into the target. The process of displacement produced by heavy ions is different from the one produced by electron, neutrons and protons. The ions are ionised in the beginning of their range and then start gaining the electrons in the later part. Therefore it is necessary to consider the energy loss in the different regions separately. At higher energies the moving ion in the solid will lose some or all of its electrons and becomes highly ionised. At this stage in its travel, the main source of energy loss of the moving ion can be neglected and the collisions are of Rutherford type.

As the kinetic energy of the moving ion decreases, its degree of ionisation also decreases. As the moving ion becomes neutral, the energy is lost in collisions with the target atom, this is of hard sphere type. At the high energies, the moving ion directly interacts with the nucleus of the target atom and this interaction is via the Coulomb potential and thus the scattering is of the Rutherford type.

4.2.2 Mass of target and Bombarding ions

For any ion energy larger than the threshold energy, the yield increases with increasing atomic mass of both target atoms and bombarding ions. This is due to the increased nuclear energy deposited to the target lattice, when using heavier targets and incident ions. The nuclear stopping cross-section, S_n, can be written as:

$$S_n(\varepsilon) = 4\pi a Z_1 Z_2 e^2 \frac{M_1}{M_1 + M_2} s_n(\varepsilon) \qquad (4.1)$$

where $S_n(\varepsilon)$ is a universal function, depending on the detailed form adopted for the screened Coulomb interatomic potential. The reduced energy parameter, ε, is given by:

$$\varepsilon = \frac{4\pi\varepsilon_o a M_2}{Z_1 Z_2 e^2 (M_1 + M_2)} E \tag{4.2}$$

where e is the electronic charge, ε_o is the permittivity of free space, a is the screening radius and the remaining variables hold their previously defined meanings [5].

The screening radius ca be expressed as the Thomas-Fermi screening length a_{TF} given by:

$$a_{TF} = \frac{0.8853 a_o}{\left(Z_1^{2/3} + Z_2^{2/3}\right)^{1/2}} \tag{4.3}$$

where a_o=0.529 Å, is the Bohr radius. The projected range of the bombarding ions in the target decreases with increasing target and ion mass numbers.

4.2.3 Angle of Incidence

If the bombarding ions impinge on the target with an angle of incidence θ, then α is given by:

$$\alpha(M_2, M_1, \theta) = \alpha\left(\frac{M_2}{M_1}\right)\cos^{-f}\theta \tag{4.4}$$

where α is for all practical purposes, independent of the ion energy with $f \approx 5.67$ and ($\theta \le 60^o$).

The increase in α, with increasing θ, is due to the increasing density of energy deposited near the target surface.

Alternatively, the range of the bombarding ions in a direction perpendicular to the target surface decreases with increasing θ. Depending on the target-ion combination, the sputter yield reaches a maximum for angles between 60° and 80° (17). For angles of incidence larger than 80°, the atomic interaction between the incident ions and the target atoms decreases so that the sputter yield decreases.

4.2.4 Crystal structure of Target

The atomic interaction, and hence nuclear stopping, between the bombarding ions and target atoms will be larger when the former are incident along a direction normal to a closely packed atomic plane, say (111), compared to a plane with a lower atomic density, e.g. (100). Furthermore, if the bombarding ions are incident along a low crystallographic direction, they penetrate to larger depths below the crystal surface.

The physical effects of energetic particle bombardment on surfaces are dependent on the mass, angle of incidence, energy of the bombarding particles and the atomic mass of the target material. The effects on the surface and the subsurface region of bombardment by energetic species includes:

i) Desorption of weakly bonded surface species,
ii) Ejection of secondary electrons,
iii) Reflection of the energetic species,
iv) Physical sputtering of surface atoms by momentum transfer through collision cascades,
v) Enhanced surface mobilities of atoms on the surface,
vi) Enhanced chemical reaction of adsorbed species on the surface to produce a modified surface.

While in the subsurface the following are taking place:

i) The impinging particles may be physically implanted,
ii) The collision cascades cause displacement of lattice atoms and the creation of lattice defects,
iii) Surface species may be recoiled and implanted into the subsurface lattice,
iv) Mobile species may be trapped at lattice defects,

v) Much of the particle kinetic energy is converted into heat.

When a surface is subjected to bombardment by high-energy ions, some of the particles are reflected as high-energy neutrals. Energetic particle bombardment of surface can also introduce lattice defects. On semiconductors surfaces these defects may act as electron traps when an interface is formed. The formation and heating of lattice defects in the near-surface region increases and react chemically in that region. The implantation of a mobile bombarding species into a surface increases the chemical potential between the surface and the bulk thereby increasing the diffusion rate of mobile species into the bulk of the material.

4.2.5 Ion Implantation

During ion-surface interaction in the linear cascade regime, the incident ions become trapped or implanted inside the substrate. While the ions are slowed down in the semiconductor lattice, host atoms are displaced through energetic recoils and damage is introduced in the crystal lattice. This implantation-induced damage continues as long as the ions have energies larger than the displacement energy, E_d, of the lattice atoms. The amount of damage created depends on the energy deposited per unit volume by the implanted ions, which in turn determines the extent to which the properties of the semiconductor are changed. The two main energy loss mechanisms of energetic particles in a solid target, with some defect reactions are considered in the following discussions.

4.3. Energy Loss Mechanisms

Before considering the range of ions, it is convenient to know the stopping power or specific energy loss, which is equal to:

$$\mathrm{M} = -\frac{dE}{dx} \tag{4.5}$$

where, E, is the ion energy and x is the distance, measured along the direction of incidence of the ions.

The two major processes of energy loss are: elastic Coulomb interactions between the "screened" nuclear charges of ion and target atom and, on the other hand, inelastic interactions of the ion with bound or free target electrons. The screening referred to here arises because a cloud of orbital electrons surrounds the positively charged nucleus. As the approaching ion penetrates this cloud, it experiences an increasing electrostatic repulsion, which deflects its path.

The energy losses due to nuclear and electronic interactions take place in close collisions. In addition, there may be a contribution to the energy loss because of charge exchange between the moving ion and target atom. The total specific energy loss is taken to be the sum of three separable components: nuclear, electronic and charge-exchange.

$$\frac{dE}{dx} = \left(\frac{dE}{dx}\right)_e + \left(\frac{dE}{dx}\right)_{ch} + \left(\frac{dE}{dx}\right)_n \tag{4.6}$$

The two components with ion energy are shown schematically in fig 4.2. It can be seen that both increase with energy.

At the lowest energies, nuclear stopping dominates and is responsible for most of the angular dispersion of an ion beam. At higher energies, electronic collisions are the more important. An ion will have a high probability of being fully stripped of its electrons when moving at velocities greater than the K-shell electron velocity:

$$v = \frac{z_1 e^2}{\hbar} \tag{4.7}$$

4.3.1 Electronic stopping

Interactions with bound or free electrons in the solid results in the process called electronic stopping. The relative effect of the two mechanisms depends on the energy and the masses of the incident particles, as well as the mass of the target

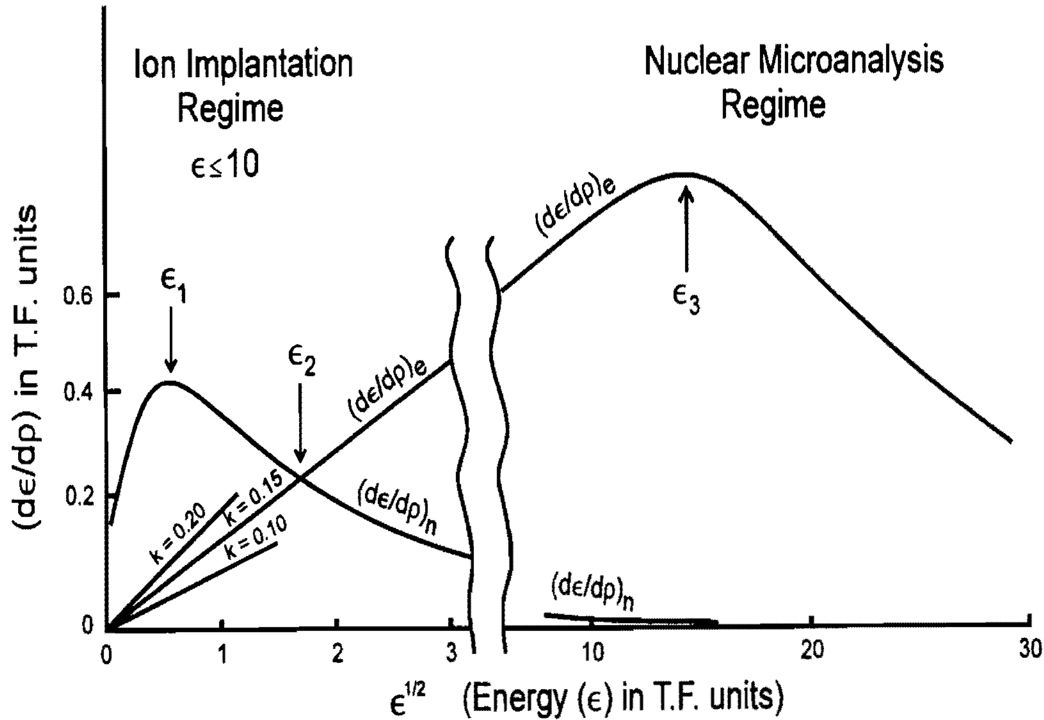

atoms.

Fig.4.2: *Depicts the velocity ($\propto \varepsilon^{1/2}$) dependence of the energy-loss processes, nuclear stopping v = $(d\varepsilon/d\rho)_n$ and electronic stopping $(d\varepsilon/d\rho)_e$, in terms of the reduced energy, ε. The reduced energy, and reduced range $\rho(\varepsilon)$ are dimensionless units and can be expressed in terms of laboratory units of energy, E, and the range, x, as:*

$$\varepsilon = \frac{4\pi\varepsilon_0 a M_2}{Z_1 Z_2 e^2 (M_1 + M_2)} E \tag{4.8}$$

and

$$\rho = N\pi a^2 \frac{4M_1 M_2}{(M_1 + M_2)^2} x \tag{4.9}$$

where M_1 and M_2 and Z_1 and Z_2 are the mass number and atomic numbers of the incident particle and the target atoms, respectively, e is the electronic charge, N is the number of atoms per unit volume, ε_0 is the permittivity of free space and

a is the screening radius, expressed as:

$$a = \frac{0.8853 a_0}{\left(Z_1^{2/3} + Z_2^{2/3}\right)^{1/2}} \quad \text{Å} \qquad (4.10)$$

where $a_o = 0.529$ Å is the Bohr radius.

The reduced energy has two advantages: Nuclear stopping and associated quantities, such as damage production and sputtering, can be approximated by a universal curve for all particle-target combinations, and ion bombardment studies which can be separated into ion implantation and nuclear regimes. In the first regime (ε <10), called the ion implantation regime, both the nuclear and electronic stopping play a significant role. Theoretical treatments are complex in this regime. In the second regime (ε >10), referred to as the nuclear regime, the projectiles have sufficiently high energies to be virtually stripped of all their electrons. In this regime electronic stopping is the dominant energy-loss process. Also, in this regime, the ion trajectory is almost linear, sputtering and collision cascade effects are practically negligible.

Figure 4.2 shows that at low energies, nuclear stopping is the more important process and that it reaches a maximum value (ε_1) and thereafter decreases. It can further be seen from Fig.4.2 that electronic stopping becomes the dominant energy-loss mechanism for (ε_2) and that it increases linearly with velocity up to (ε_3). It should be pointed out that $(d\varepsilon/d\rho)_n$ is only a function of ε (i.e. independent of incident particle type and host atoms).

4.4. Range Distribution of Implanted Ions

When a crystal is irradiated with energetic ions, damage results from the transmission of kinetic energy to the lattice atom through elastic collision. The energy transferred from the bombarding ion to the target atoms is usually sufficient to displace the host atom from its lattice site. Typically, the implanted ion is able to knock-off a target atom from its lattice site if the ion energy is larger than the threshold energy for displacement, E_d, of the host atom. In turn, the displaced atom may displace other atoms, thus creating a cascade of atomic collisions. The size of the collision cascades is governed by nuclear and electrons energy loss processes.

Assuming an amorphous solid, the range distribution can be approximated by a one-dimensional Gaussian distribution having the projected range, R_p, at the mean, and the range straggle, ΔR, as the standard deviation from the mean [11]. The range distribution can be expressed as:

$$N(x) = \exp\left[-\frac{1}{2}\left(\frac{x - R_p}{\Delta R_p}\right)^2\right] \tag{4.11}$$

It can be shown that, if Q_I is the number of implanted ions cm^{-2}, the concentration depth distribution $N(x)$, in atoms cm^{-3}, can be expressed as:

$$N(x) = \frac{Q_1}{(2\pi)^{1/2}\Delta R_p}\exp\left[-\frac{1}{2}\left(\frac{x - R_p}{\Delta R_p}\right)\right] \tag{4.12}$$

A rough estimate of the average concentration N_1(ave) of implanted ions is then given by:

$$N_1(ave) \cong \frac{Q_1}{\Delta x_p} \approx \frac{Q_1}{R_p} \tag{4.13}$$

4.5. Doping of Semiconductors

The doping of semiconductors by an implantation to produce p- and n-type material is today a fundamental routine processing step in device technology. This process involves the introduction of desired dopant atoms into lattice sites in the host material. However, implantation also introduces electrically active defects, which can act either as traps or as recombination centers in semiconductor. Traps reduce the semiconductor free carrier density [6], where as recombination centers introduces a generation-recombination current in Schottky barrier diodes, which lead to inferior rectification properties. Radiation induced defects have also been shown to be particularly harmful during doping by ion implantation.

Later it was realized that the defects introduced during ion implantation could be valuable for device isolation applications, and subsequently there was a shift in emphasis towards optimizing ion implantation induced isolation procedures. In GaAs, for example, particle radiation was found to introduce defects which were effective compensating centers, stable at room temperature, and if present in high enough concentrations, are able to convert doped GaAs into its semi-insulating form [6].

4.6. Defect formation

Defects influence the electronic and optical properties of semiconductors and devices fabricated on them. A thorough understanding of the properties of defects and how they affect the properties of semiconductors are key elements of defect engineering. The introduction of imperfections into a perfect crystal disrupts the periodic structure and thus alters the properties of the material. There are two main types of defects, which the particle irradiation can introduce in a semiconductor [1]. Firstly, point defects, which are localised with atomic dimensions. They are often referred to as primary irradiation induced defects and are introduced by electron irradiation. Secondly, extended defects, where the disorder extends beyond the volume of one or two atoms (dislocations or line defects) [4]. They are usually introduced when irradiating with heavier particles (for example alpha particles).

Complex defects are formed when there is association between the intrinsic or extrinsic and interstitial or substitutional defects. For instance, a Frenkel pair forms when a vacancy interacts with a close (self-) interstitial, while two vacancies on neighbouring lattice sites form a divacancy.

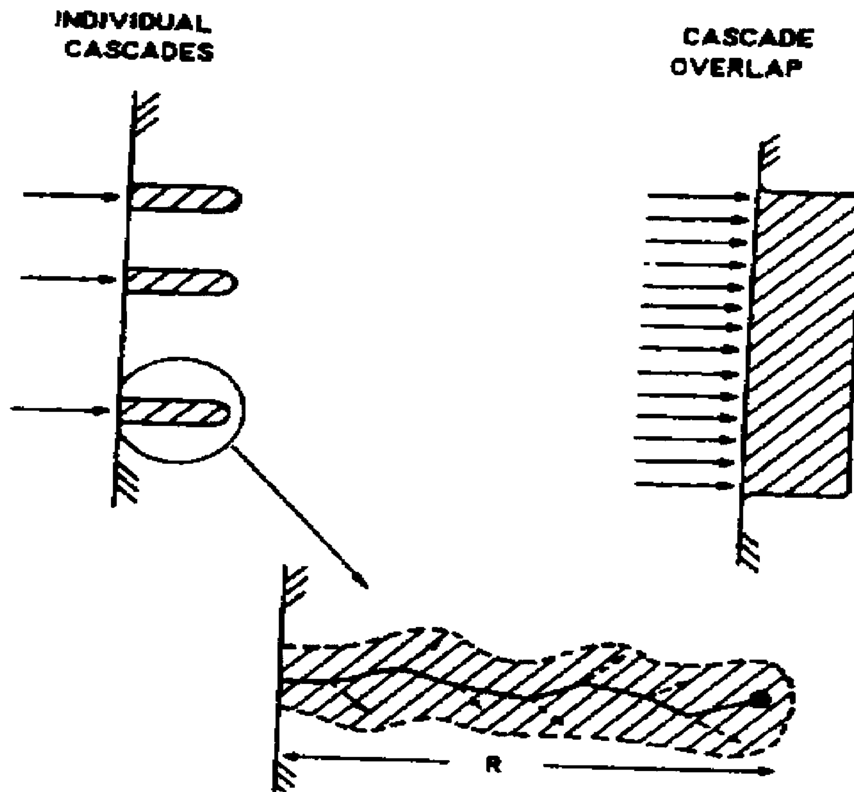

Fig.4.3: *Collision cascade schematic illustrating separated individual collision cascades and the results of their overlap.*

In compound semiconductors, each sublattice has its own vacancy, interstitial, and substitutional or interstitial impurity. An atom of one sublattice placed in the other sublattice from an antisite defect. Point defects should by definition imply a localised lattice perturbation, which might involve the local atom or atomic site and a few neighbours. The electronic perturbation associated with the geometrical perturbation described can extend to larger distances.

When energetic particles strike a solid, defects may form in the following manner. An incident atom collides with a lattice atom and transfers its energy to the recoil atom. During the transfer of sufficient energy, a vacancy is formed and the recoil atom collides with other atoms and displaces them, if it transfers sufficient energy. The recoil atoms will come to rest, usually in interstitial positions, some might come to rest in a vacancy. Clusters or cascades [11], normally result when the recoil atoms have much higher energies than the displacement energy, E_d, for a particular crystal and lattice orientation.

4.7. Thermal annealing of defects

During implantation, ions come to rest at random positions in the crystal lattice and change the periodicity of the material. Therefore it is possible, by a suitable heat treatment (annealing) to restore the crystal lattice. With the aid of isochronal and isothermal annealing, various annealing stages have been identified for GaAs. During isochronal annealing an irradiated sample is annealed at different temperatures for a fixed time, while isothermal annealing is done at a specific temperature but for different time-periods.

During annealing, defects react to reduce their concentration to that associated with thermal equilibrium in a material [9]. In reducing the defect concentration in the solid material, the thermodynamic driving forces may employ the following processes [10]. Migration to sinks or defects may recombine with their counterparts, for example vacancies combining with interstitials. Formation of defect complexes: when simple defects combine with themselves or with impurities or when the complexes dissociate.

Each of these processes is characterised by its activation energy, because the annealing kinetics of defects at a temperature, T, can be linked to the dominant process involved in the annealing. Information on the distribution of sinks involved in the annealing process can also be extracted from the kinetics. Thus knowledge of the annealing kinetics can provide information on the defect concentration, and their nature.

Consider N defects per unit volume, which diffuse to sinks. An initial random distribution of sinks and defects is assumed. The number of defects per unit volume which disappear in the sinks per given time is proportional to the number of defects present at the particular time, t, and is given by the equation

$$\frac{dN}{dt} = -KN^{\alpha} \tag{4.14}$$

with K being the rate constant and α the order of the annealing reaction.
Upon integrating equation (4.14) for $\alpha = 1$, we find that the defect concentration decays exponentially as:

$$N(t) = N_o \exp(-Kt) \tag{4.15}$$

where N_o is the initial defect concentration. To visualise the rate constant, K, we assume a random distribution of "immobile" vacancies and mobile interstitials. K arises from an interstitial vibrating in the crystal at a frequency K_o and approaching periodically an energy barrier E_m for migration to the vacancy. If the probability that the interstitial has sufficient energy to surmounts the barrier E_m then the reaction rate, K, is the probability that the interstitial has sufficient energy times the frequency of approach to the energy barrier, and is given by:

$$K = K_o \exp(-E_m / kT) \tag{4.16}$$

In practice K_o is approximately equal to kT/h with h being Planck's constant. kT/h is roughly the frequency of the most numerous phonons present in the lattice, and these phonons dominate the vibration.

With particle irradiation, vacancies and interstitials are created in pairs with vacancies situated in the neighbourhood of where they are created. Recombination of these defects occurs through the diffusion of the species, and the kinetics of the annealing reaction reflects the distribution in distance of the pairs [12].This distribution, can also be described by a correlation factor γ, as in figure 4.4. R_{pq} is the distance between two pairs: p and q, and r_p is the distance between two element of a pair. The correlation factor γ is given by:

$$\gamma = \frac{R_{pq}}{r_p} \tag{4.17}$$

It can be seen from equation (4.17) and figure 4.4, that, when γ is large, the vacancy-interstitial pairs are together and interact with one another. These are "close-pairs" of the first order, with the activation energy governing the reaction being the barrier separating the pair. For small γ (γ ≈ 1), the elements making up the pairs are not bound, and are randomly distributed with the kinetics of the second order. In this case, energy barrier is the activation energy of the migrating species. The random distribution of interstitials and vacancies results in the rate equation:

$$\frac{dN_I}{dt} = \frac{dN_V}{dt} = -KN_I N_V \tag{4.18}$$

with subscripts I and V depicting interstitial and vacancies respectively. Assuming that $N_I = N_V$, the above equation reduces to the second order rate equation:

$$\frac{dN_I}{dt} = -KN_I^2 \tag{4.19}$$

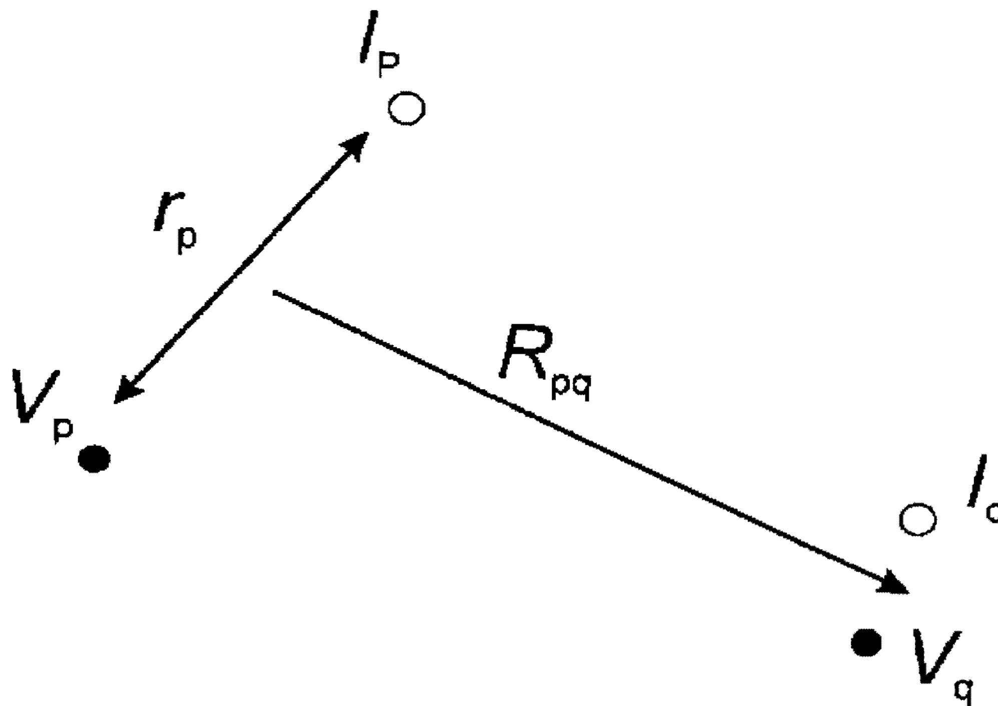

Fig. 4.4: *A representation of a pair distribution. The filled and empty circles represent vacancies and interstitials respectively* [(6)].

The following procedure is mostly adopted to identify annealing mechanisms:

i) After annealing for t seconds at a specific temperature T, the change in defect concentration (ΔN) is plotted as a function of annealing time t.

ii) The slope in (i), represents the reaction rate K at that particular temperature T.

iii) The procedures in (i) and (ii) are repeated for a number of temperatures in the defect's transitional region.

Then the slope of a plot of reaction rate K with $1/T$ gives the activation energy for the reaction. For first order reactions, $ln(K)$ vs $1/T$ yield a straight line, while for second order reactions, a straight line will be given by a plot of $1/K$ vs $1/T$.

The reaction rate, K, is in general related to the enthalpy ΔH through

$$K = K_0 \exp(-\Delta H / kT) \tag{4.20}$$

with the value of K_O being dependent upon the entropy, ΔS, associated with the defect migration process and the number of jumps, N_j before the defect is annihilated. If v_O represents the lattice frequency, the exponential pre-factor, K_O, is given by:

$$K_O = \frac{v_O}{N_j} \exp(-\Delta S / k) \qquad (4.21)$$

In practice, the entropy is ignored and the experimentally determined enthalpy (ΔH) can be considered as the activation energy of the barrier, ΔE, to the respective reactions. For example, the barrier to the migration or some defect species or dissociation of a defect complex. Thus, the experimentally determined value of K_O provides information on the physical nature of the reaction.

Thermal annealing studies play an important role in helping to identify the structure of defects. The reason for this is defect characterisation techniques such as Deep level transient spectroscopy (DLTS) and photoluminescence (PL), cannot be used to identify the structure of defects. The only way to match a defect whose structure has been identified by electron paramagnetic resonance (EPR) to one identified by DLTS or PL, is through thermal annealing studies.

4.8 TRIM

In this review, emphasis is often placed on methods to calculate or predict the effects of ion bombardment of compound semiconductors. For this purpose, relatively simple methods of calculation are used. One of the most versatile and accurate programs is the TRIM Monte Carlo program [7], which simulates bombardment in an amorphous or random solid. This program is often used to compare its predictions to experimental results. Computer simulations of implant profiles can be produced using the TRIM (TRansport of Ion in Matter). It should be remembered that TRIM assumes the target to be amorphous. The amount of energy deposited into energetic recoils and the total number of vacancies produced for given ion-target interactions can also be simulated using TRIM.

References

(1) S. A. Goodman, F. D. Auret, M. du Plessis and W. E. Meyer, Semicond. Sci. Technol. **14** (1999) 127.

(2) Heier Ryssel and Ingolf Ruge, *Ion Implantation.* (1986) 54.

(3) S. A. Goodman, F. D. Auret and W.E. Weyer, Nucl Instr and Meth in Phys Res. B **90** (1994).

(4) F. D. Auret, S. A. Goodman, G. Myburg and W. O. Barnard, J. Appl. Phys. **74** (1993).

(5) S. Wasa and J. Hayakawa, *in handbook of Sputter deposition: Principles, Technology and Applications*, Noyes Publications, New Jersy. (1991) 96.

(6) F. D. Auret, S. A. Goodman, R. M. Erasmus, W. E. Meyer, and G. Myburg, Nucl Instr and Meth in Phys Res. B **106** (1995) 323.

(7) C.Uzan-Saguy, J. Salzman, R. Kalish, V. Richter, U. Tish and S. Zamir, Appl. Phys. Lett. **74** (1999) 17.

(8) W. Eckstein, *In computer simulation of ion-solid interactions*, Springer Ser. Mat. Sci. **10** (1991).

(9) F. D. Auret, S. A. Goodman, G. Myburg and W. E. Meyer, Appl. Phys. A. **56** (1993) 547.

(10) D. I. Bohme and J. Weber, Phys. Rev. B **47** (1993) 4037.

(11) J. W. Corbett, Solid State Physics, suppl, *Electron Radiation Damage in Semiconductors and Metals*, Academic Press, New York. (1966) 642.

(12) D. Pons and J. C. Bourgoin, Phys. Rev. Lett. **47** (1981) 1293.

(13) J. A. Davies, MRS Bulleting. **26** (1992).

(14) R. S. Averback and Mai Ghaly, Nucl. Instr, and Meth. In Phys. Res B **127** (1997) 1.

(15) K. Thommen, Radiat. Effects. **2** (1970) 201.

(16) J. W. Mayer and S. S. Lau *in Electronic Materials Science*, Macmillan Publishing Company, New York. (1990).

(17) H. H. Anrson, and H. L. Bang: *Sputter by particle Bombardment I, Ed.* R.Behrisch, Springer verlag, Berlin. (1981) 202.

CHAPTER 5:

TECHNIQUES

5.1 Metal Deposition Method

There are several ways of depositing metal contacts onto semiconductors. The simplest method is resistive evaporation where metals are heated in a wire crucible or boat. It was found that this method introduces no defects in GaAs and yielded the highest quality Schottky barrier diodes. In the case of electron beam evaporation, stray electrons cause the defects in the semiconductor.

Thin films are widely used for making electronic devices, optical coatings and decorative parts. Thin films are also necessary for the development of optical devices. They are fabricated by the deposition of particles on the substrate. The particles may be atoms, molecules, and atomic ions, ionised fragments of molecules, or grains of material, both charged and uncharged. In a vacuum the particle moves from its source to the substrate surface with a very low probability of collision with residual gas molecules. The preparation of surfaces prior to thin film deposition is often of key importance for obtaining good adhesion and other required properties of the interface. In vacuum evaporation, the following physical factors must be considered: the cleanliness of the vacuum, the methods of heating the evaporant, for outgassing the evaporant, for cleaning the substrate surface and the method for ensuring film uniformity.

5.1.1 Thickness Monitor

Both the resistive and electron beam evaporations use a thickness monitor to measure thin film thickness. A technique based on the oscillating frequency of a quartz crystal is a sensitive technique used to monitor film thickness during deposition. A quartz crystal is mounted within a sensor head, which supplies both electrical contact cooling and mechanical support. A sensor head is supported by two liquid feedthroughs for cooling water and electrical contact wire. It is usually placed adjacent to the substrate in the vacuum environment, to receive an equivalent amount of the deposited material.

The central region of the quartz is fully plated on both sides with silver or gold, which are suitable for adhesion of most materials one might wish to monitor. It is this region which oscillates and is the only part that need to be exposed to the deposition source. The external hardware of the quartz monitor consists of an oscillator circuit and frequency counting electronics. These systems will convert frequency shift to equivalent film thickness and deposited rate. The user supplies the density and the z-ratio of the material.

Since quartz is a piezoelectric material, it responds to applied voltages with mechanical motion. If a free running RF voltage is applied to the crystal, it will respond by oscillating at its natural resonant frequency. When a thin film is deposited on vibrating quartz, a shift in frequency occurs, which is linearly proportional to the mass deposited. The resonant frequency is also dependent on various degrees of the temperature, pressure, and stresses presented by the deposited films.

The temperature of the monitor increases upon exposure to the incoming deposition material, however, temperature is controlled by allowing the sensor head to be cooled during deposition. The stress induced frequency shift and gas pressure effects are negligible in the majority of vapour deposition conditions. The resonant frequency decreases whenever material is deposited.

5.1.2 Resistive Evaporation

Resistive evaporation is the simplest method, where metals are heated in a wire crucible or boat. The heart of the evaporation system is the resistance heated refractory metal source. The source is the evaporant heater, a container, and the most probable cause of failure. The selection of a suitable source is the critical decision. A source is selected to meet the following requirements: evaporant compatibility, capacity, and power availability.

Boats or holders are made of a refractory metal that can be heated by passing a current through it; for example, tungsten, tantalum, platinum, and graphite are preferred boat materials. Boats are available in an endless range of sizes and shapes.

UNIVERSITEIT VAN PRETORIA
UNIVERSITY OF PRETORIA
YUNIBESITHI YA PRETORIA

Many materials contain absorbed gases and volatile impurities. For this reason a shutter is usually placed between the evaporation source and the substrate to protect the substrate surface contamination during preheating of the source. The shutter is swung open when the experimenter is satisfied that the impurities in the vapour stream have been reduced to a tolerable level.

5.1.3 Electron Beam Deposition

Electron beam evaporation is very popular for the deposition of metals on semiconductors, especially due to its ability to evaporate high melting point metals such as titanium under vacuum conditions. Furthermore the system yields a controllable deposition rate, which can be varied from fractions to tens of Å/s, the electron beam evaporation source is a thermal evaporator as is a resistance-heated source. In electron beam evaporation, the heating energy is supplied to the top of the evaporant by the kinetic energy of a high-energy electron beam and the evaporant is contained in a water-cooled cavity or hearth. The evaporants contained in a water-cooled hearth, do not react with the hearth. Heating by the electron beam allows attainment of temperature limited by radiation and conduction to the hearth.

In the case of electron beam evaporation, the defects in the semiconductor are caused by stray electrons from the filament which are not completely focused on the metal target being evaporated (3). Although these electrons do not have high enough energies to cause atomic displacement in the semiconductor lattice, they facilitate the formation of electrically active defects with energy levels in the semiconductor band gap (5). These defects levels acts as "stepping stones" for carriers and lead to carrier conduction mechanisms other than thermionic emission, thereby resulting in a poor rectification quality of Schottky diodes. This problem can be solved by using a shield, which prevents the stray electrons from impinging on the semiconductor. SBDs fabricated using this shield had rectification properties near identical to those of the high quality resistively deposited SBDs (3,4).

The electron beam is magnetically directed onto a small spot on the evaporant material, hence the contact with the hearth is too cool for chemical reaction. The main disadvantage of this type of source is that the substrate and coating film are bombarded by electrons and energetic ions. In addition the electron beam source emits a modest flux of soft X-rays. These emissions from the source, although small, can damage sensitive devices.

The texture of the evaporation material affects the evaporabilty of the target materials. Materials that are good thermal conductors and melt well below evaporation temperature, can be evaporated from any form of raw material. All other materials are difficult to evaporate from anything but as hot pressed pieces. Most materials when heated as powders or granules form a localised hot spot of a very small volume. The following points are recommended for successful deposition of thin films from an electron beam evaporation source, (i) selection of evaporant surface form with a largest possible volume. One should avoid evaporating powdered or granular materials, (ii) use a largest hearth volume, (iii) use the largest beam spot area possible but still attain the required deposition rate, (iv) increase the spot size if increasing the power causes instability and (v) continues sweep e-beam over surface.

The core of an electron beam source is the hearth assembly, upon which the electron gun and magnetic lens are mounted. The water-cooled hearth, containing the evaporant, also serves as the mounting base for the entire gun. The gun hearth must make excellent electric contact to the vacuum chamber base because the high voltage flows through it. The electron gun consists of a pair of filament holding blocks and a coil filament mounted on ceramic insulators and positioned about 2 mm from a grounded anode. The filament cavity (cathode) and the anode configuration are designed for the case of beam extraction. The molybdenum or tungsten is usually the material of choice.

A magnetic field of a few hundred gauss is required to bent the electron beam from the electron gun through 270^0 and focus it upon the evaporant. The magnetic circuit consists of a pair of soft iron side plates with adjustable beam formers and two magnets, an electromagnet and a permanent magnet in parallel. The field of the permanent magnet is chosen such that the beam is positioned within the hearth and the parallel electromagnet is used to increase and decrease the main magnetic field for longitudinal beam position control. Like the cathode cavity, the magnetic lens is designed to focus the beam to about 0.5 cm diameter at a nearly vertical angle of incidence upon the evaporant charge. All the permanent and electromagnets in an evaporation source must be embedded within the water-cooled hearth because of the high temperature.

5.2 Sputtering System

Sputtering system consists of a target (a plate of the material to be deposited or the material from which a film is to be synthesized) connected to a negative voltage supply (dc or RF), the substrate holder facing the target. This substrate holder may be grounded, floating biased, heated, cooled or some combination of these. A gas is introduced to provide a medium in which a glow discharge can be initiated and maintained. The most common sputtering gas is argon (Ar).

When the glow discharge is started, positive ions strike the target plate and remove target atoms by momentum transfer, and these condense into thin films. There are in addition, other particles, and radiation produced at the target, which may affect film properties. In sputter deposition, surfaces subjected to ion bombardment face numerous events. These include: (i) secondary electron emission, (ii) secondary positive or negative emission, (iii) emission of radiation (photons, x-rays), (iv) reflection of incident particles, (v) heating, (vi) chemical dissociation or reaction, (vii) crystallographic changes, (viii) backscattering etc.

Sputtering yield is defined as the number of atoms ejected from a target surface per incident ion. In the energy range of practical interest for sputtering processes (10 – 5000 eV), the yield increases with incident ion energy and with the mass of the incident ion. The sputtering yield determines the erosion rate of sputtering targets.

Sputtering is one of the most commonly used methods for the deposition of the thin films. This method is widely used in semiconductors, photovoltaics, recording and automotive industries. In this method high melting point materials like ceramics and refractory metals, which are difficult to deposit by other evaporative techniques, are easily deposited. There are several types of sputtering, namely, dc glow discharge, RF sputtering, magnetron, and ion beam sputtering. Dc glow discharge sputtering is limited to the sputtering of conductive targets. RF sputtering is used for any targets and substrates regardless of its conductivity and the RF source is needed to sputter insulating targets.

When using a sputtering system, one of the major problems is the incorporation of the sputtering gas in the film, especially when there is ion bombardment of the film. This affects the stoichiometry and the adhesion of films. Compressive stresses may be generated in the films because of the energetic species arriving at the substrate.

5.2.1 Sputter Deposition

Metallisation of semiconductors is a critical processing step during device fabrication. Sputter deposition is frequently employed for this purpose, because it facilitates the stoichiometric deposition of compounds, controllable deposition of high melting point metals and it yields very high deposition rates. In addition, sputter deposited layers exhibit better adhesion compared with layers deposited by other methods. However, due to the energetic particles involved, sputter deposition is damaging on an atomic scale and causes lattice disorder at and below the semiconductor surface.

During sputter deposition, a metal target is bombarded with Ar ions and the sputtered metal atoms are deposited on the semiconductor surface. Sputter deposition, which is widely used for its ability to stoichiometrically deposit compounds, also introduces a larger number of different electrically active defects in semiconductors [6]. These defects result in a drastic decrease in barrier height of SBDs on n-type semiconductor and an increase in barrier height of SBDs on p-type semiconductors. It was found that it is possible to minimize the damage introduced by the selection appropriated deposition parameters, for example, temperature.

During sputter deposition of thin metal films onto a semiconductor, the metal target is connected to the to electrode (cathode) to which a negative dc bias, $-V_b$, is applied, while the substrate is placed on the grounded anode. The positive Ar ions are accelerated across and they bombard the target.

5.2.2 Magnetron Sputter Deposition

Magnetron systems are widely being used to deposit thin metal films and for high rate sputter etching. In both processes the exposed semiconductor surface is subjected to energetic plasma particles which introduce damage in the lattice. Consequently, the structural, electrical and optical properties of semiconductors are altered. These changes are reflected in the performance of devices fabricated on the processed semiconductor. The extent to which the structural, electrical and optical properties of the semiconductor is changed, depends critically on the plasma conditions. i.e. on the ion species, ion energy, plasma pressures and time of exposure.

There are three types of magnetron sputtering which are widely used for thin film deposition namely, conical, cylindrical and planar magnetron sputtering. In magnetron sputtering, the substrate is connected as an anode. The substrate will be sufficiently biased to ensure that ions and electrons arrive at the substrate. Within the cathode target, permanent magnets are embedded such that the resultant magnetic field is several hundred gauss. The glow discharge is concentrated in the high magnetic field region; thus a circular cathode glow is obtained, which cause an erosion area.

The surface of the cathode is non-uniform due to the circular cathode glow. This shortens the actual lifetime of the cathode target. Water is used to cool the target down. When a dc voltage is applied, say 1000V, the electrons on the cathode electrode (target) will be accelerated towards the anode and gain energy in this process. Since the substrate is biased or grounded with respect to the target, then the electrons will travel towards the substrate and the probability of these electrons to ionize the sputtering gas will be less. The magnetic field causes spiral motion of the electrons, which will increase gas ionization. The target will then be sputtered.

When the strength of the magnetic field is several hundred gauss, then the positive space charge mode is dominant in the sputtering discharge. In this mode the glow discharge is concentrated in the high magnetic filed region, thus a circular cathode glow is observed.

5.2.2.1 Plasma State

Plasma is regarded as a gas containing charged and neutral species, including, electrons, positive ions, negative ions, atoms, and molecules. Because electrons have a much higher mobility, any surface in contact with the plasma will develop a floating potential, $-v_f$, with respect to the plasma. Plasmas are initiated and maintained by applying an electric potential i.e. dc or ac or a combination of both across the neutral gas. An important parameter of a plasma is the degree of ionisation, which is the fraction of the original neutral species, which have become ionised. In steady state, the state of ionisation must be equal to the rate at which charged particles are lost from the plasma volume through recombination and diffusion or convection to the boundary.

The presence of a relatively large population of neutral species will dominate the behavior of the type of plasma. To form and sustain plasma requires some energy source to produce the required ionization. The substrate carrier and magnetic field in the weak field regions, which surround a substrate plays a major role in determining the nature of a plasma, which is in contact with the substrate. This affects the properties of the product, which is formed.

5.2.3 DC Glow Discharge

A glow discharge is a low-pressure gas with a high impedance dc power supply. When a voltage is applied, a very small current flows. This is due to the presence of a small number of ions and electrons resulting form a variety of sources. Fig.5.1 is the illustration of a dc glow discharge voltage versus current density characteristics.

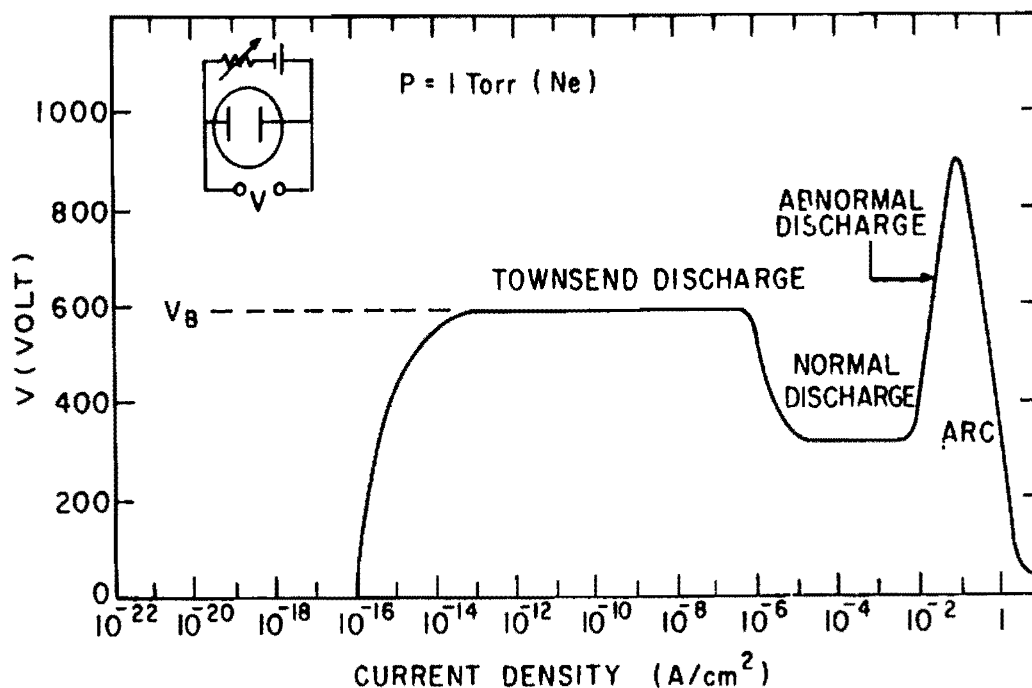

Fig.5.1 The formation of a dc glow discharge [8].

Initially, the current is nearly constant because all of the charges present are moving. As the voltage is increased, sufficient energy imparted to the charged particles so that they produce more charged particles by collisions with the electrodes and with neutral gas atoms. As more charge is created, current increases steadily, but the output impedance of the power supply limits the voltage. This region is known as the Townsend discharge. Eventually, an avalanche occurs. Ions strike the cathode and release secondary electrons, which form more ions by collision with neutral gas atoms. These ions are accelerated towards the cathode to produce more electrons that in turn produce more ions. When the numbers of electrons generated are sufficient to produce enough ions to regenerate the same number of electrons, then the discharge is self-sustaining. The gas begins to glow, the voltage drops and the current rises abruptly. At this point, the mode is called the "normal glow". After the bombardment covers the whole cathode surface, further increases in power produce both increased voltage and current density in the discharge. This region is the "abnormal glow". The output impedance of the power supply limits the voltage, and the low-voltage high current discharge is formed.

Crucial to the formation of an abnormal glow is the breakdown voltage, V_B, see figure 5.1. This voltage is mainly dependent upon the mean-free path of the secondary electrons and the distance between the anode and cathode.

5.2.4 RF Glow Discharge

As the frequency of an applied ac signal is increases above 50 kHz, two important effects occur. Firstly, electrons oscillating in the glow space acquire sufficient energy to cause ionization, thus reducing the dependence of the discharge on secondary electrons and lowering the breakdown voltage. Secondly, the electrodes are no longer required to be electrical conductors, since rf voltages can be coupled through any kind of impedance.

At typical RF frequencies used for sputtering (5-30 MHz), most of the ions are immobile and one would expect negligible ion bombardment of the electrodes. In fact this is not the case. If one or both of the electrodes is coupled to the RF generator through a series capacitor, a negative voltage will develop on the electrode. Owing to the difference in mobility between electrons and ions. Upon application of a RF voltage through the capacitor, a high initial electron current flows to the electrode, on the second half of the cycle, only a relatively small ion current can flow. Since no charge can be transferred through the capacitor, the voltage on the electrode surface must be self- bias negatively until the net current is zero. These results in the negative potential, then the average dc value of this potential is nearly equal to the peak voltage applied.

To obtain sputtering from only one electrode in an rf system, it has been shown that the electrode which is to be the sputtering target must be an insulator or must be capacitively coupled to the rf generator and that the area of that electrode must be small compared to that of the directly coupled electrode. The ratio of the voltage between the glow space and the small capacitively coupled electrode (V_c) to the voltage between the glow space and the large directly coupled electrode (V_d) is

$$\frac{V_c}{V_d} = \left(\frac{A_d}{A_c}\right)^4 \tag{5.1}$$

where A_d and A_c are the areas of the directly and capacitively coupled electrodes, respectively.

5.2.5 Ion Vapour Deposition

Ion vapour deposition or ion plating is the name given to a class of ion assisted physical vapour deposition processes. In this process both the substrate and the growing film are subjected to energetic ions to cause changes in the formation process and the properties of the deposited film.

The application for ion plating or ion vapour deposition extend to the areas where adhesion is poor. Many coating requirements, which are not met because of poor adhesion, can be met with ion vapour deposition. These include coating of metals, e.g. TiN.

A large vacuum chamber containing rotating or planetary substrate holders is used. The chamber is equipped with a pumping system, Ar gas pressure control, and gauging. Because of the energy deposited in the film and plasma, the vacuum chamber walls should be water-cooled. The cathode in ion plating, the substrate acts as the target in a sputtering system. As a result, there are two deposition processes occurring simultaneously. The substrate is sputtered and the evaporant is deposited. The film is grown to the extent that the deposition rate exceeds the sputtering rate. The capability of ion plating is that sputtering before deposition cleans the substrate

The deposition takes place in a plasma environment. Plasma is a gaseous medium, which contains enough ions and electrons to be electrically conductive. Energy is introduced into the plasma by acceleration of electrons in a DC or RF biasing. These Ar^{+} and Ar^{++} ions are then fragment by collisions. The depositing species usually traverse the plasma before condensing on the substrate; in so doing some of the species are fragmented or ionised in the plasma. In addition to ionisation and excitation by electron-atom collisions, the atoms or molecules may be excited or ionised by collisions with excited metastable species in the plasma. The amount of modification will depend on the mass, energy and flux of the bombarding species. The adhesion of a deposited film to a surface depends on the deformation. The energetic particle bombardment prior to and during the initial stage of film formation may enhance adhesion by changing the surface chemistry.

Most commonly used sources for ion vapour depositions are resistance or induction heated thermal evaporation. The energetic particles used for bombarding surface and growing films are gaseous ions and arise from, (i) biasing (dc or rf) the surface in contact with the plasma, (ii) extraction of ions from a confined plasma and accelerating them to the substrate.

The energy of the ion deposition heats the deposition chamber and tooling, driving off the absorbed gasses and contaminants. These gases contaminate the plasma and react with the film. The heat deposited on the chamber and tooling requires water-cooling.

5.2.6 Laser Ablation

Laser ablation (decomposition) is defined as a method of ejecting atoms or clusters from the target due to focused laser irradiation and deposition onto the substrate. (Film deposition by laser ablation is carried out by irradiation of the target by a focused laser beam). Various kinds of pulsed lasers are often used, such as ArF, KrF, XeCl and UV lasers. When choosing the laser, two parameters are important, i.e., the wavelength and pulse width. A suitable or good pulsed laser is the one with short wavelength and short pulse width. The wavelength influences the absorption coefficient of the target material.

The laser ablation technique is of great importance in sophisticated material and device research in laboratories and a small-scale production of high cost-performance devices. During deposition, the target is often rotated to eliminate changes in composition. For the growth of multilayer structures, the target is often exchanged. The target and substrate are arranged as a parallel configuration so as to achieve a symmetric distribution of thicknesses on the substrate. In order to guide the laser light into the deposition chamber an incident window should always be transparent to the incoming laser light. Synthesised quartz is the preferred window material. Oxygen or an inert gas is introduced for eliminating unintentional deposition on the window. In the preparation of the film, it is important to control the plume in order to obtain high quality films. Plume is a luminous cloud, which is normal to the target. The optimum laser fluence for film preparation depends on the substrate-target spacing and the gas pressure.

Target preparation is important for film growth. The target morphology affects the surface morphology of the films. A fresh target surface is preferred because after prolonged irradiation of the target, its composition at the ablated surface often deviates from the original stoichiometric one, especially in ablation with a low fluence. An advantage of laser ablation for the preparation of high-Tc films is stoichiometric deposition including oxygen. In order to achieve the stoichiometry, a high oxygen pressure during deposition is important. Another advantage of laser ablation is the high deposition rate. The disadvantages of this technique are droplet formation on the deposited film, the limitation on large area deposition and the high cost of the excimer laser.

The characteristics of laser ablation are,

- Material with high melting points can be deposited
- Almost no contamination is present
- Films can be prepared in an oxidation environment with relatively high pressure because of the absence of a heater or filament in the deposition chamber.

The target composition is transferred to the film, leading to stoichiometric deposition. A large number of droplets of submicron size are often seen on the surface of the deposited films.

5.2.7 Ion Beam Sputtering

Ion beam sputtering is used for deposition of thin films of metals and insulators. The sputtering offers the advantage of easily and independently controlling the ion flux and ion energy. In the ion beam sputtering system the incident ions are generated at the ion source. The target is bombarded by the ion beam in a sputtering chamber separated from the ion source.

There are several types of ion beam sources developed for use in thin film applications, namely, Penning ion source, Kaufmanns ion source, Duoplasmation and hollow anode or hollow cathode glow discharge ion source. The most commonly used source is Penning and Kaufmanns ion sources.

A Penning ion source has a cylindrical anode and two enclosing cathodes. A magnetic field is applied parallel to the anode. Plasma is created by applying several hundred volts between cathode and anode in the presence of an operating gas e.g. Ar. The electrons from the plasma move towards the anode and due to the magnetic field, they form a helical path and increase the ionization of the gas. Ions are then attracted towards the cathode and bombard the cathode, producing more secondary electrons, which cause further ionization of the gas. An aperture in the anode or cathode is used to extract ions into a beam.

The Kaufmanns ion source has a plasma chamber within the ion source with a hot filament cathode. The source can either be physically located inside a deposition chamber or in a differentially pumped separate chamber. The cathode is a thermionic filament. A low pressure and a discharge voltage of approximately 50 V can be utilized in this source. The ions in this source are created by magnetically enhanced low-voltage discharge. A magnetic field is applied to increase the path length of the electrons. Ions created in the source can be accelerated by means of multi-aperture grids.

In this source an ion beam with large current can be obtained by the application of a low extraction voltage e.g. for Ar, an ion current of 50mA can be obtained by applying extraction voltage of less than 2 kV. Duoplasmation is used to generate a high intensity narrow ion beam. The plasma is created and confined both by electric and magnetic fields. Glow discharge ion sources use parallel plate glow discharge for the creation of ions while the hollow anode or hollow cathode glow discharge ion source involves extraction of the beam through a hole in the electrode plates. In ion beam sputter deposition, the distance between the substrate and the target and the potential of these in the vacuum chamber can be arbitrarily selected. However, it is important to design the layout of the substrate and target so that reflected incident ions, neutrals, and secondary electrons do not affect the deposition on the substrate. In order to satisfy these conditions, one should understand the backscattering characteristic of the incident ion beam and those of the particles sputtered at the target (e.g. atoms and ions), their angular distribution and energy distributions.

References

(1) L. S. Yu, Q. Z. Liu, Q. J. Xing, D. J. Qiao, and S. S. Lai, J. Appl. Phys. **84** (1998) 132.

(2) S. M. Sze, *Physics of Semiconductor devices.* (1981) 279.

(3) G. Myburg and F. D. Auret, J. Appl. Phys. **71** (1992) 6172.

(4) F. D. Auret, W. O. Barnard, W. E. Meyer and G. Myburg, *Thin Solid films.* **13** (1993) 235.

(5) F. D. Auret, L. J. Bredell, G. Myburg and W. O. Barnard, Japan, J. Appl. Phys, **30** (1991) 8.

(6) F. D. Auret, S.A. Goodman, G. Myburg and W. E. Meyer, J. Vac. sci. Technology. B **10** (1992) 2336.

(7) E. H. Rhoderick and R. H. Williams, *Metal-semiconductor Contacts.* Sec. ed Clarendon Press Oxford (1988) 75.

(8) S. M. Rossnagel, J. J. Cuomo and W. D. Westwood, *Handbook of plasma processing technology.* (1989) 135.

CHAPTER 6

DEEP LEVEL TRANSIENT SPECTROSCOPY

6.1 INTRODUCTION

The study of the electrical properties of semiconductors by means of transient capacitance methods is a well-established technique in experimental physics. The technique used in this study to observe the electrical properties of defects was the deep level transient spectroscopy (DLTS) method, pioneered by D. V. Lang. in 1974[4]. The scope of this chapter is to give a brief background to the DLTS method and to show how it leads to the determination of the properties of a deep level defect.

The spectroscopic nature of DLTS allows independent studies of different defect species in the semiconductor. Furthermore, because DLTS is a space charge related technique, it facilitates control of the charge states of defects in the space charge region, which enables charge state dependent processes to be studied. DLTS is further attractive because it can be used to characterise defects using various kinds of space charge based devices. This includes simple Schottky barrier diodes (SBDs), as well as device structures with higher degrees of complexity. The sensitivity of DLTS for detecting defects in concentrations as low as 10^{10} cm^{-3} is superior to any other electrical characterisation technique.

Since its introduction, DLTS has become a widely accepted technique to determine the electronic properties of defects in semiconductors. It has been applied to study growth-induced defects, impurities, radiation-induced defects and metastable defects in various semiconductors.

6.2 Semiconductor junction

In order to perform a DLTS measurement, a rectifying junction, such as a p-n junction or a Schottky barrier is required. Defects in a semiconductor are analyzed by probing the space-charge layer, also referred to as the depletion region. The width, W, of the depletion region of a SBD or p^+-n junction varies with the applied voltage according to:

$$W = \sqrt{\frac{2\varepsilon(V_{bi} + V)}{qN}} \tag{6.1}$$

where ε is the dielectric constant of the depleted semiconductor, V_{bi} is the build-in voltage of the junction, V is the externally applied voltage, q is the charge of an electron, and N is the density of the ionized impurity due to dopants and other imperfections. The junction capacitance due to the depletion layer is:

$$C = \frac{\varepsilon A}{W} = A\sqrt{\frac{q\varepsilon N}{2(V_{bi} + V)}} \tag{6.2}$$

where A is the area of the junction. It is clear that if N changes in the depletion region, W and C will also change and the junction capacitance will be a direct measure of the total charge. If the concentration of electrons or holes trapped at deep levels is changed by the thermal or optical emission of carriers to the conduction or valance bands, this change can be monitored by measuring the variation of the junction capacitance at constant applied voltage. The variation in junction capacitance because of temperature dependent variation of N forms the basis of capacitance-based DLTS.

6.3 Deep states in the band-gap

A deep state may be defined as an electronic energy state introduced within the band-gap of a semiconductor as a result of the presence of a lattice defect or impurity. Since deep states are positioned deeper in the energy gap than shallow levels, they are more difficult to ionise.

Deep levels are found to be present in all semiconductors and can affect the electrical and optical properties of the semiconductor. Deep levels are often referred to traps, recombination centres and generation centres. In a neutral semiconducting material, an electron trap can be defined as a defect for which the electron capture rate C_n is much larger that the hole capture rate C_p, and defined as a recombination centre if both the electron and hole capture rates are large, i.e. $C_n \sim C_p$. The electron and hole capture rates are given by the following expressions, respectively:

$$C_n = \sigma_n \langle V_n \rangle n \tag{6.3}$$

and

$$C_p = \sigma_p \langle V_p \rangle p \tag{6.4}$$

where n and p are the concentration of electrons and holes, σ_n and σ_p are the electron and hole capture cross-section and $\langle V_n \rangle$ the average thermal velocity of electrons given by:

$$\langle V_n \rangle \equiv \sqrt{\langle V_n^2 \rangle} \tag{6.5}$$

$$\langle V_n \rangle = \sqrt{\frac{3kT}{m_e^*}} \tag{6.6}$$

where m_e^* is electron effective mass, k is Boltzmann's constant and T is the absolute temperature. An analogous expression holds for holes.

Thermal emission rates are proportional to a Boltzmann's factor exp($-\Delta E/kT$), where ΔE is the depth of the trap from the band edge to which the carrier is emitted. The emission rate of an electron is given by:

$$e_n = \frac{\sigma_n \langle V_n \rangle N_c}{g} \exp\left[\frac{-\Delta E}{kT}\right] \tag{6.7}$$

where $\Delta E = E_C - E_T$ with E_C and E_T the energies of the conduction band and the trap respectively, N_C is the effective density of state in the conduction band, g is the degeneracy of the defect level an T is the absolute temperature. The quantity $\langle V_n \rangle N_C$ varies as T^2, and therefore, if e_n can be measured as a function of temperature, an Arrehenius plot of e_n/T^2 versus $1/T$ will yield the activation energy. The analogous expression holds for hole emission to the valence band.

The electron and hole capture cross-sections are generally temperature dependent. There are relevant mechanisms (the Auger effect and multiphonon emission) in discussing non-radiation capture processes that are accompanied by a large lattice relaxation. Multiphonon emission is the most successful in accounting for the temperature dependence of the capture cross sections of numerous defects. The capture cross-section takes the form:

$$\sigma = \sigma_\infty \exp\left(\frac{\Delta E_\sigma}{kT}\right) \tag{6.8}$$

where ΔE_σ is the thermal activation energy of the capture cross-section. This leads to a more general expression for the thermal emission rate of electron to the conduction band:

$$e_n = \frac{\sigma_n \langle V_n \rangle N_c}{g} \exp\left[\frac{-\Delta E + \Delta E_\sigma}{kT}\right] \tag{6.9}$$

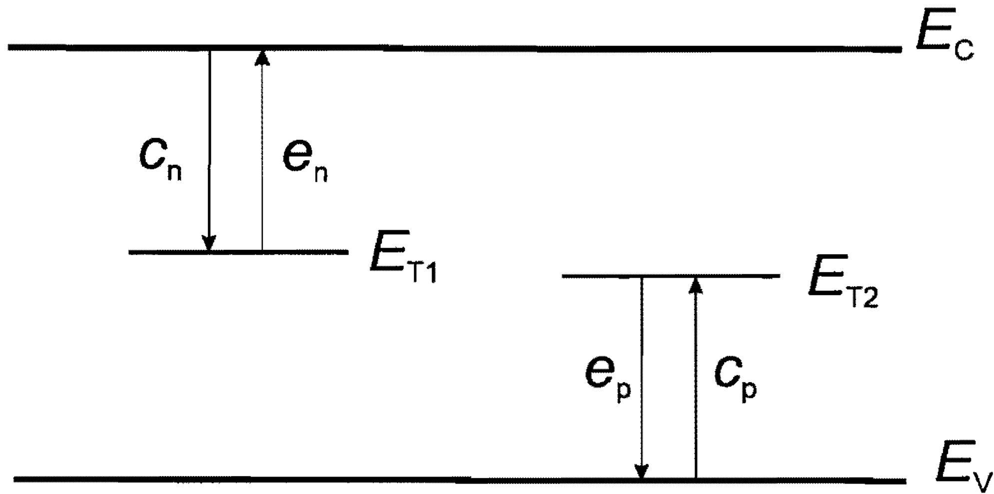

Fig.6.1: *The thermal emission and capture processes at deep levels.*

The thermal activation energy for emission of the electron to the conduction band, $E_T = \Delta E + \Delta E_\sigma$, determined from an Arrhenius plot, therefore, has two components: the energy difference between the trap level and the bottom of the conduction band, ΔE, and the thermal activation energy of the capture cross-section, ΔE_σ. The activation energy for thermal emission is the most commonly used parameter to characterise a deep level. However, the physical parameter ΔE in equations (6.7) and (6.9) is the Gibbs free energy:

$$\Delta E = E_C - E_T \equiv \Delta H - T\Delta S \qquad (6.10)$$

where ΔH and ΔS are the changes in enthalpy and entropy, due to the change in charge state of the defect. When combining equations (6.7) and (6.10), it follows that:

$$e_n = \frac{\sigma_n \langle V_n \rangle N_C}{g} \exp\left[\frac{\Delta S}{k}\right] \exp\left[\frac{-\Delta H}{kT}\right] \qquad (6.11)$$

Therefore, the slope of an Arrehenius plot yields the enthalpy of the deep level, and not the free energy, which can only be determined from optical measurements.

However, from equation (6.10) it can be seen that the activation energy obtained from the slope of an Arrehenius plot is equal to the free energy obtained at T = 0 K. Therefore, for temperatures greater than 0 K, the trap position can only be determined accurately if the temperature dependence of the band gap is known.

6.4 DLTS measurements

Consider the origin of a capacitance transient due to a majority carrier trap where (a) to (d) schematically show the change states of the defect level at various times before and after the transient.

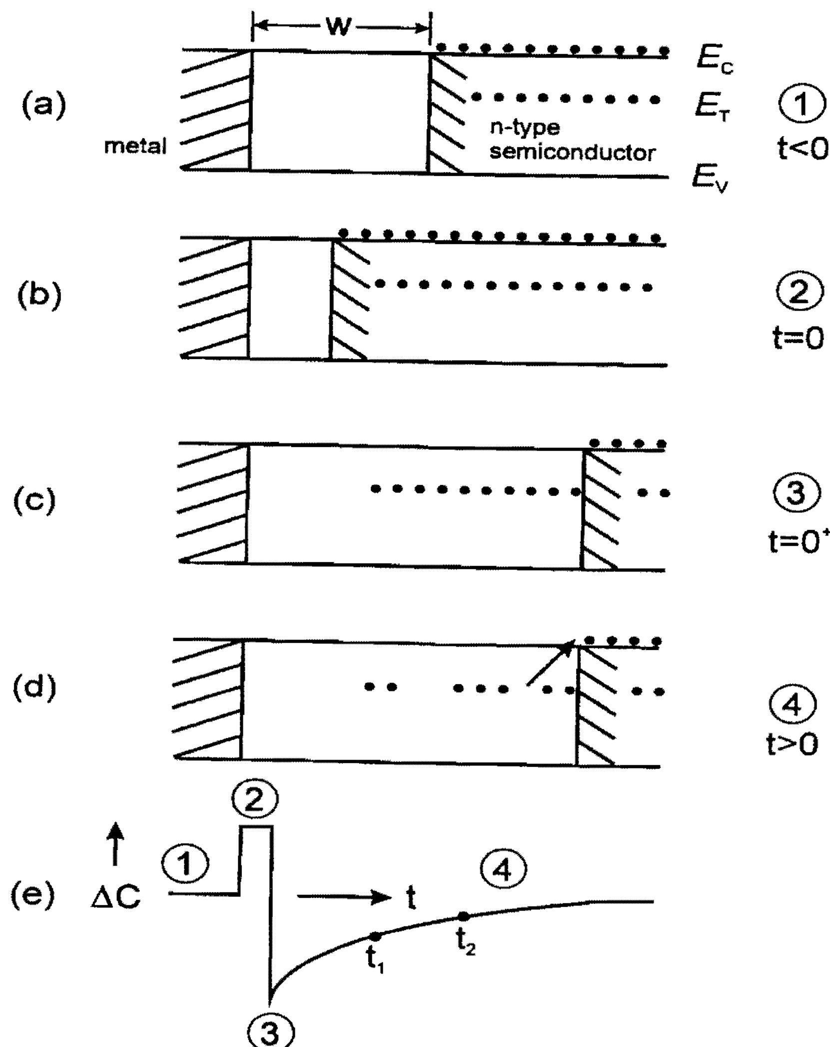

Fig 6.2: *Capacitance transient due to a majority carrier trap in a p^+-n diode. The schematics show the charge states of the defect level and the width of the space charge region at various times before and during the transient.*

In the space charge region of a reverse-biased semiconductor junction, electronic transitions consist entirely of emission processes, since no carriers are available for capture, thus junction capacitance response may be interpreted in terms of emission rates. Since states within the space charge region have no possibility of being filled by capture processes, emission processes can only be observed following the forced introduction of carriers which are to be captured. This is accomplished by pulsing the junction bias. Figure 6.2, illustrates this pulsing sequence schematically, and shows the accompanying capacitance transient that results from the emission processes.

Initially the junction is under reverse bias, V_r, to establish space charge dominant conditions. The space charge region (a) is empty, since no carriers are available for capture. Reducing the reverse bias will collapse the space charge region making majority carriers available for capture; this process is illustrated in (b), then (c) illustrates the increase in width of the space-charge layer when the reverse bias is re-established. This excess charge in the space-charge region may be transferred to the conduction band through the emission process as shown in (d). It can be seen that due to the collapse of the space-charge region when the reverse bias is reduced, there is an increase in the junction capacitance. (e) shows the steps (1-4) as described above being shown in terms of the sample capacitance versus time.

The junction capacitance is reduced when the reverse bias is re-established. This reduction in the capacitance, where the capacitance is much lower than the equilibrium value, is due to the capture of some of the carriers. However, as the trapped carriers are emitted to the conduction band, there is an increase in the capacitance transient. This transient response of the capacitance due to the emission of carriers is the fundamental process from which the trap properties are derived in the DLTS experiment.

Since the emission processes are exponential, the capacitance transient shows exponential decay. The characteristic decay time constant (τ) of this transient is related to the emission rate e_n by:

$$e_n = \frac{1}{\tau} \tag{6.12}$$

Each defect state may be studied independently through its unique activation energy for carrier emission and its cross section for carrier capture.

6.5 Rate window principle

The basic idea underling the DLTS technique is the rate window concept [4]. If we consider a series of repetitive bias pulses applied to the sample we obtain a signal that consist of a series of transients with a constant repetition rate as is shown in figure 6.3. Should the temperature be varied, the time constant of the transients varies exponentially with *1/T*.

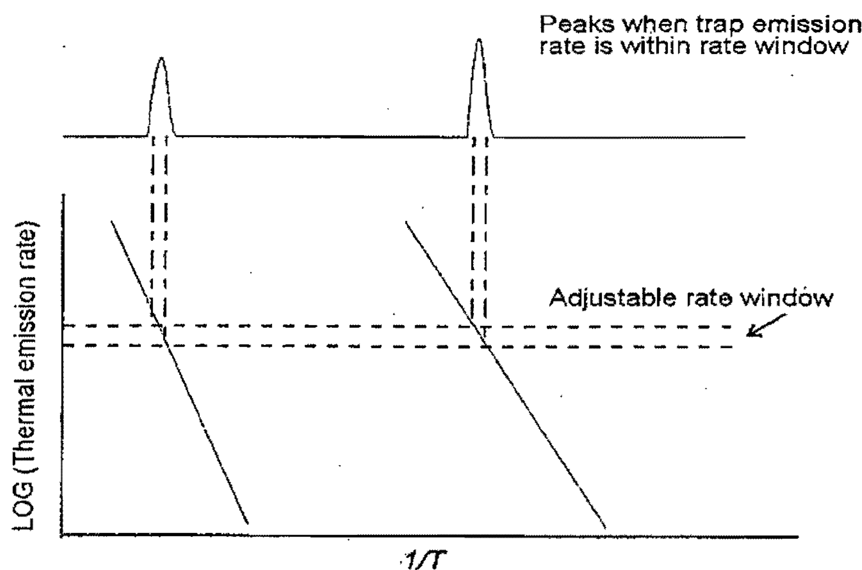

Fig 6.3: *A diagram indicating how a rate window produces a peak when the decay rate of the input signal corresponds to the rate selected by the window* [4].

There are several ways in which the DLTS rate window rate concept may be achieved in practice. One of the methods employed is a lock-in amplifier (LIA). A repetitive capacitance transient signal can be Fourier-analyzed into its frequency components. This is made possible by the use of a weighting function. As the decay time-constant changes with the sample temperature, the fundamental signal component goes through a maximum at a temperature where the reciprocal of the decay time constant approximates the lock-in frequency. This constitutes a rate window.

In the lock-in method, the rate is set by the choice of lock-in frequency. A disadvantage of the lock-in method is that the instrument overloads during the filling pulse due to a very large pulse recovery transient. The problem may be overcome by gating off a portion of the transient as is shown in figure 6.4. This signal is held at a constant value with a sample-and-hold device [8], for the duration of the pulse t_p, and the capacitance meter response time t_d.

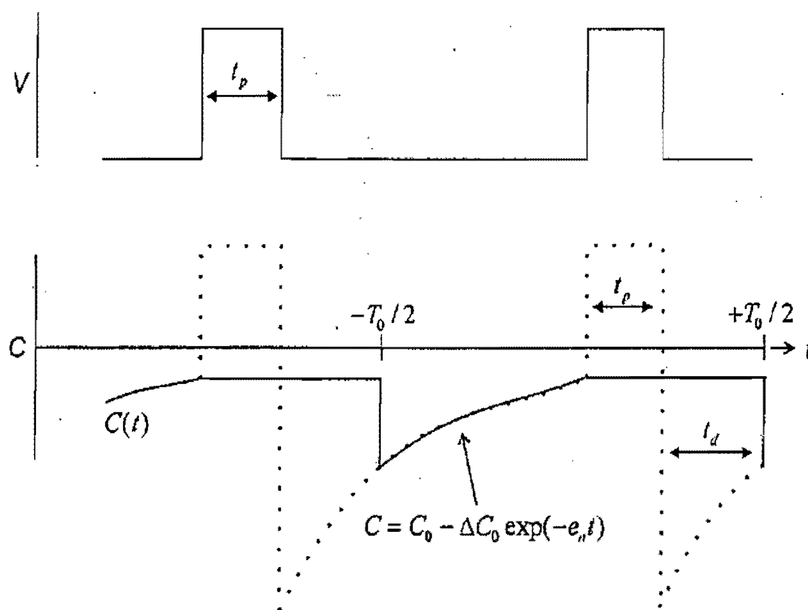

Fig 6.4: *Top figure shows pulsing sequence for DLTS picture. Bottom picture, signal held constant for the duration of the pulse t_p and the capacitance meter response time t_d* [4].

As is shown in the figure 6.4, the transient entering the LIA starts at $t = t_d + t_p$. After registering the first transient signal, the LIA calculates the integral of the product of the incoming signal with the cosine weighting function, producing the first Fourier component.

To calculate the first Fourier component of the cosine waveform, the input signal to the LIA is written as [5]:

$$f(t) = \begin{Bmatrix} A\exp(-e_n t) \\ -\frac{T_o}{2} \leq t \geq \frac{T_o}{2} \end{Bmatrix} \tag{6.13}$$

where it is assumed that the DLTS transient signal is purely exponential with a decay time constant:

$$\tau = \frac{1}{e_n} \tag{6.14}$$

and amplitude A.

The Fourier expansion of this function over the interval $-T_o/2 < t \leq T_o/2$ is:

$$f(t) = \frac{a_o}{2} + \sum_{n=1}^{\infty}\left[a_n \cos\left(\frac{2\pi nt}{T_o}\right) + b_n \sin\left(\frac{2\pi nt}{T_o}\right)\right] \tag{6.15}$$

and the Fourier coefficients are given by:

$$a_n = \left(\frac{2}{T_o}\right)\int_{-\frac{T_o}{2}}^{\frac{T_o}{2}} f(t)\cos\left(\frac{2\pi nt}{T_o}\right)dt \tag{6.16}$$

and

$$b_n = \left(\frac{2}{T_o}\right)\int_{-\frac{T_o}{2}}^{\frac{T_o}{2}} f(t)\sin\left(\frac{2\pi nt}{T_o}\right)dt \tag{6.17}$$

For the first Fourier components equations (6.15) and (6.17) together yield [5]:

$$b_1 = \frac{\pi a_1}{w} = \frac{4\pi A\left(1 - e^{-w}\right)}{w^2 + 4\pi^2} \tag{6.18}$$

where $w = T_c/\tau$.

a_1 and b_1 depend only on the transient decay time constant τ. During a DLTS temperature scan, the defect's emission rates e_n changes with temperature. Therefore a_1 and b_1 also change and have a maximum where

$$\frac{db_1}{d\tau} = o \quad \text{and} \quad \frac{da_1}{d\tau} = o \tag{6.19}$$

By applying these conditions and solving for e_n we obtain [5].

$$\frac{1}{e_n} = \frac{0.4243}{f} \tag{6.20}$$

6.6 Parameters determined from DLTS

A complete analysis of DLTS data yields the defect concentration, activation energy, capture cross-section and depth distribution of the defect.
The electron emission rate can be determined from the time dependence of the capacitance transient. The density of occupied traps at time t after removing the filling pulse is:

$$N(t) = N_T \exp(-e_n t) \tag{6.21}$$

where e_n is the thermal emission rate and N_T is the trap concentration.

From equation (6.7) and (6.12) it can be shown that the change in trap a population gives rise to a corresponding changes in diode capacitance, which is time dependent, and if $N_T << N_D$ can be expressed as:

$$C(t) = C_O - \Delta C_O \exp(-e_n t) \tag{6.22}$$

where C_o is the equilibrium reverse bias capacitance and ΔC_o the change in capacitance directly after removal of the filling pulse.

The procedure for determining the energy level, E_T, and capture cross-section, σ_n, of a defect is to extract e_n from the transient, $C(t)$, in equation (6.22) at several temperatures and then use equation (6.7) to obtain E_T and σ_n. The key step in this process is to obtain e_n from the transient for which several analogue and digital methods are used. DLTS experiments were performed using boxcar averages or lock-in amplifiers to analyzer the transient resulting from the application of a repetitive bias pulse sequence. For both these methods, DLTS proceeds by scanning the sample temperature and feeding the repetitive thermal emission transient, which varies with temperature, into the analyzer (boxcar or lock-in amplifier). A DLTS spectrum is obtained by plotting the output signal of the analyzer versus temperature. The resulting signal is a maximum when the thermal emission rate matches the "rate window" of the analyzer. Each peak on the DLTS spectrum is indicative of an energy level with a specific E_T and σ_n.

In our study of the emission of electrons, we need to consider the effect of electric field. It plays a cardinal role in the depletion region because it affects the accurate determination of defect concentration and the DLTS signatures. Since the region outside the depletion region is neutral, we can make use of Gauss's law to determine the electric field. This law simply states that the product of the electric field and an area surrounding it, is directly proportional to the electric charge.
Thus:

$$EA = \frac{q}{\varepsilon_O} \tag{6.23}$$

with q the sum of electric charges enclosed within the surface A. The differential form of Gauss' law is :

$$\nabla . E = \frac{1}{\varepsilon_o} \rho \tag{6.24}$$

Furthermore, in a pure electrostatic field, E may be expressed as minus the gradient of the potential φ

$$E = -\nabla \varphi \tag{6.25}$$

combining these two equations we obtain Poisson' equation

$$\nabla . \nabla \varphi = -\frac{\rho}{\varepsilon_o} \tag{6.26}$$

6.7 Defect concentration

A defect property that is important when characterizing defects is the defect concentration (N_T). This property is required in order to assess the extent to which a particular defect can alter the properties of the semiconductor. One of the simplest methods of obtaining the majority carrier defect concentration as proposed by Lang [4], is to monitor the capacitance change ($\Delta C/C$) where $\Delta C << C$, using the largest possible majority carrier pulse (i.e., all defects in the space-charge region are filled). N_T could be calculated from:

$$N_T = 2\left(\frac{\Delta C}{C}\right)(N_D - N_A), \tag{6.27}$$

where (N_D – N_A) is the net concentration that is approximated to the donor concentration when $N_D >> N_A$ and ΔC is the change in capacitance after removing the pulse. Equation (6.27) is used when the material to be measured is a thin film, but results in errors on the determination of a deep level concentration for the case where the deep level acts as a major carrier trap. The lambda factor, λ, is introduced to derive a correction formula to extract the true deep level concentration from the experimental DLTS results.

In the depletion layer electrons are depleted from the layer. The electronic states at the deep level are empty in the layer. The depletion layer width, x, is related to the high frequency junction capacitance by $C = \varepsilon A/x$ and λ is obtained as:

$$\lambda = \left\{ \frac{2\varepsilon\left(E_T - E_f\right)}{q^2 N_D} \right\}^{1/2} \tag{6.28}$$

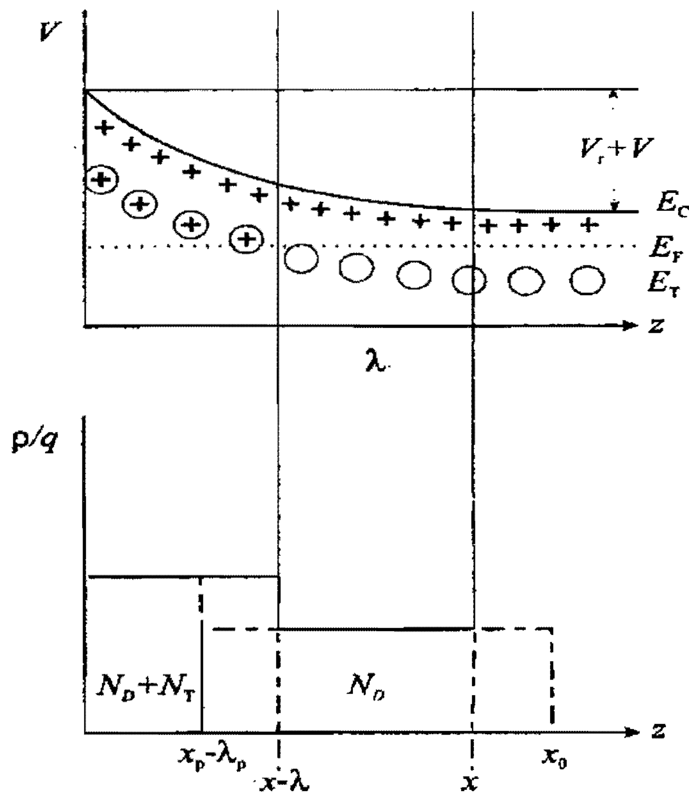

Fig 6.5: *Energy band diagram for a Schottky barrier with corresponding charge distribution.*

Zohta and Watanabe used the fixed bias variable pulse together with the edge region correction proposed to determine defect concentrations. The fixed bias variable pulse technique relies on the change in depletion width when the majority carrier pulse, V_p, is changed by a small increment.

The depletion region within a distance, $x = w - \lambda$, below the metal-semiconductor interface can be probed by applying successively larger increments of V_p till the flat-band condition is reached. Taking into account the influence of carriers in the edge region an accurate determination of the deep level concentration can be made using [2]:

$$N_T = 2\left(\frac{\Delta C}{C}\right)N_D\left[\left(\frac{x-\lambda}{x}\right)^2 - \left(\frac{x_p-\lambda_p}{x}\right)^2\right]^{-1} \tag{6.30}$$

where λ and λ_p are the widths of the edge region before and after applying the filling pulse, x and x_p are the depletion region widths before and after pulsing.

It must be pointed out that the sensitivity of the junction to trapped charge varies linearly from zero at the junction ($x = 0$) to a maximum at the edge of the depletion region ($x = w$). Therefore, DLTS cannot be used to accurately measure the trap concentrations close to or at the metal-semiconductor interface.

6.8 DLTS signatures

The DLTS signature is the combination of the capture cross section (σ) and activated energy (E_T). By substituting expressions for σ_n, $\langle v_n \rangle$, and N_c in the equation:

$$e_n = \frac{\sigma_n \langle v_n \rangle N_c}{g}\exp\left(\frac{-E_T}{kT}\right) \tag{6.31}$$

We obtain:

$$e_n = \sigma_n\sqrt{\frac{3kT}{m_e^*}}\,2M_c\left(\frac{2\pi m_e^* kT}{h^2}\right)e^{\frac{-E_T}{kT}} \tag{6.32}$$

$$e_n = 9.8 M_c m_e^* \sigma_n k^2 T^2 \left(\frac{\pi}{h^2} \right)^{3/2} e^{\frac{-E_T}{kT}} \tag{6.33}$$

which forms the basis for the construction of an Arrhenius plot from:

$$\ln \frac{e_n}{T^2} = \ln \left[9.8 M_c m_e^* k^2 \left(\frac{\pi}{h^2} \right)^{3/2} \right] \sigma_n - \frac{E_T}{k} \left(\frac{1}{T} \right) \tag{6.34}$$

From (6.34) is it clear that an Arrhenius plot, i.e., a plot of $ln\ (e_n / T^2)$ versus $1/T$, will yield the activation energy from the slope and capture cross section from the $ln\ (e_n / T^2)$ axis intercept (figure 6.5).

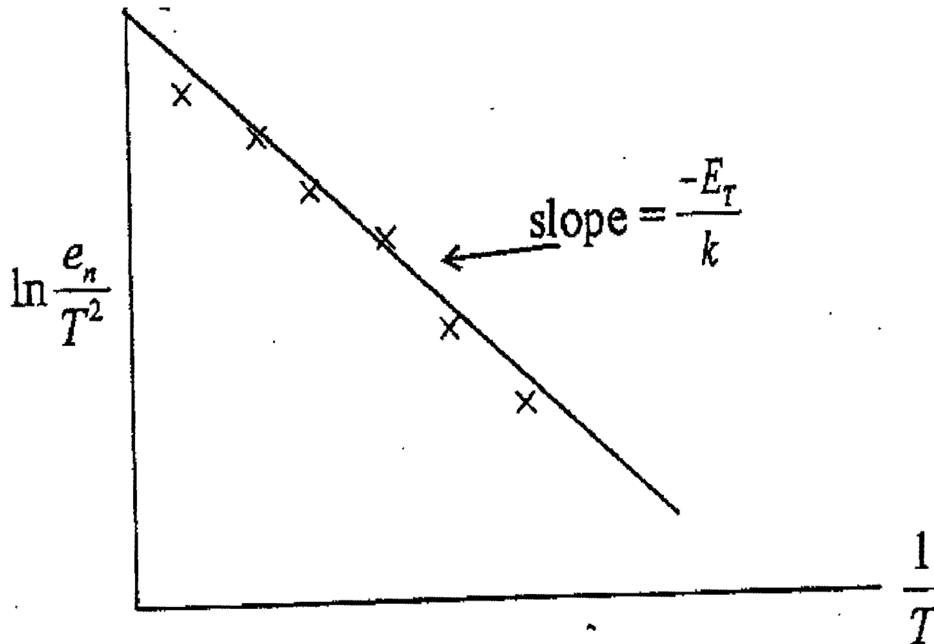

Fig 6.6: *Arrhenius plot drawn from DTLS spectra at various frequencies.*

By using the following equation:

$$c_n = \sigma_n \langle v_n \rangle n \quad (6.35)$$

where n is the free carrier density, the capture rate, C_n, can be determined.

In ploting the Arrehenius graph, several data points are needed. This can be obtained by scanning the sample with different frequencies, typically in the range 1-200 Hz. Since the DLTS peak positions are frequency dependent and shift in temperature, different sets of (e_n, T) points are obtained.

The spectroscopic nature of DLTS allows independent studies of defects in the semiconductor. Furthermore, because DLTS is a space charge related technique, it facilitates control of the charge state of defects in the space charge region, which enables charge state dependent processes to be studied. DLTS is further attractive because it can be used to characterize defects using various kinds of space charge based devices. This includes simple Schottky barrier diodes (SBDs), as well as device structures with higher degrees of complexity. Finally, sensitivity of DLTS for detecting defects in concentrations of 10^{10} cm^{-3} is superior to any other electrical characterization technique. Since its introduction, DLTS has become a widely accepted technique to determine the electronic properties of defects in semiconductors. It has been applied to study growth-induced defects, impurities, radiation-induced defects, and metastable defects in various semiconductors. DLTS technique was used in chapter 8 to determine the electrical properties of metallisation induced defects in n-GaAs. It should be pointed out that DLTS in itself cannot directly provide the structure of a defect. This has to be obtained by structure-sensitive techniques, such as electron paramagnetic resonance (EPR) or local vibrational mode (LVM) spectroscopy. However, structural defect identification via DLTS is possible by comparing defect properties, e.g. annealing kinetics, which can be measured by DLTS as well as by structure-sensitive techniques.

Reference

(1) Q.Y. Ma, M. T. Schnidt, X. Wu, H. L. Evans, and E. S Yang J. Appl. Phys. **64** (1988) 2469.

(2) Yasuhito Zohta and Miyoko Oku Watanabe, J. Appl. Phys. **53** (1982) 1809.

(3) F.D. Auret and M. Nel, Meas. Sci. Techn. **2** (1991) 623.

(4) D. V. Lang, J. Appl. Phys. **45** (1974) 3014.

(5) F. D. Auret, Rev. Sci. Instrum. **57** (1986) 1597.

(6) J. L. Benton, *Journal of Crystal Growth.* **106** (1990) 132.

(7) H. Lefevre and Schulz, Appl. Phys. Lett. **12** (1977) 45.

(8) G. L. Miller, D. C. Lang and L. C. Kimerling, Rev. Mater. Sci. **7** (1977) 377.

(9) A. Wang and C. T. Sah, J. Appl. Phys. **55** (1984) 565.

(10) H. G. Grimmeiss, E. Janzen and B. Skaratam, J. Appl. Phys. **51** (1980) 3740.

(11) S. A Goodman, F. D. Auret and E. Meyer, Jpn. J. Appl. Phys. **33** (1994) 1949.

CHAPTER 7

I-V and C-V RESULTS

7.1 Introduction

This chapter deals with the electrical characterisation of the damage caused during the electron beam (EB) deposition of Ta. We used a Schottky contact system as contact structure for the electrical characterization of the samples after processing. It has been found that electron beam (EB) deposition creates damage at and below the semiconductor surface [(1)]. Current-voltage (I-V) and capacitance-voltage (C-V) measurements were used to evaluate the characteristics of EB deposited Schottky barrier diodes (SBDs) and to compare these properties to those of resistive deposited contacts. Using deep level transient spectroscopy (DLTS), the defects introduced during deposition were characterised.

7.2 Sample Preparation.

n-Type GaAs with a free carrier concentration of $2\times10^{16}/\ cm^3$, grown by metalorganic vapour phase epitaxy (MOVPE), was used to investigate EB deposition induced defects.

7.2.1 Cleaning Procedure.

The samples were subjected to the following treatment prior to metallisation. The wet chemical cleaning consists of a degreasing step in boiling trichloroethylene (TCE), a rinse in boiling isopropanol and thorough rinses in 18 MΩ cm de-ionised water. A solution of H_2O:NH_4OH:H_2O_2 in the ratio 100:3:1 was employed for chemical etching. The oxide present on the semiconductor was stripped off by immersion of the sample in a solution of H_2O:HCl (1:1), then followed a thorough rinses in de-ionised water. Finally, samples were blown dry with nitrogen gas. This

method was recommended to obtain contacts with a low contact resistance and high quality SBDs with low leakage current (2).

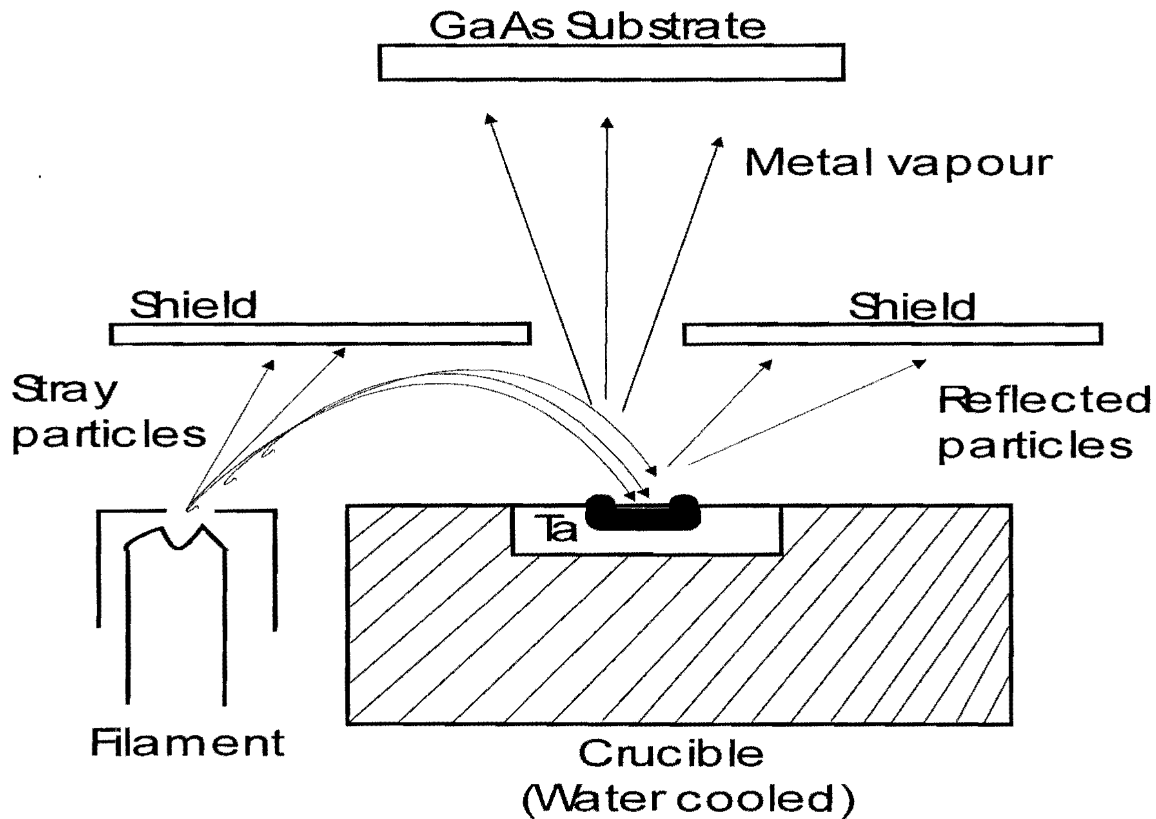

Fig 7.1: *Schematic diagram of an electron beam evaporation system fitted with a shield to minimise substrate damage by stray electrons.*

7.2.2 Ohmic Contact Fabrication.

Immediately after cleaning, the samples were placed into the electron beam deposition system. Once a pressure of 1.5 $\times10^{-6}$ Pa was reached, appropriate metals were evaporated on the backside of the n^+ substrate. The metal layers were as follows: Ni/AuGe/Au (100Å/ 2500Å/ 2500Å) .The thicknesses of layers were monitored with an Inficon XTC thin film thickness and rate monitor. The samples were then annealed in a furnace for 2 minutes at 450 °C under Ar gas atmosphere.

7.2.3 Schottky Barrier diode Fabrication.

Before fabricating the SBD, samples were again cleaned following the procedure in 7.2.1. Ta metal was electron-beam deposited through a metal contact mask to give "dots" 0.76 mm in diameter and 1000 Å thick. The metal shield in the EB system (Fig 7.1) was used to protect the sample from energetic electrons originating at the filament during the electron-beam deposition. The quality of the Schottky contact was established by conducting room temperature I-V and C-V measurements on the samples after metallisation.

7.3 Material Characterisation

I-V and C-V measurements (Fig 7.2) were carried out prior to DLTS studies. The theory of this technique is discussed in section 3.6.1. All measurements were performed in the temperature range 297.0 - 300.0 K, and each data point were read three times and averaged.

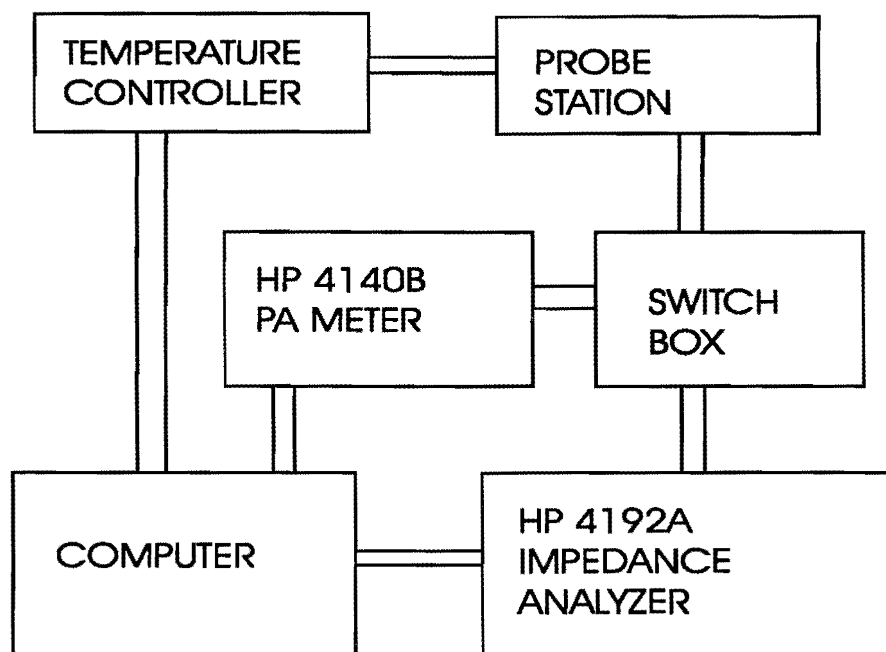

Fig 7.2: *Set-up of the measurement system used for I-V and C-V characteristics.*

7.3.1 I-V and C-V Results

An HP 4140B picco-ammeter was used to carry out the capacitance measurements. The capacitance response to a voltage was measured. The free carrier concentration N_D was found from the slope of $1/C^2$ against V, and the built-in potential was determined from the intercept on the V axis.

During I-V and C-V measurements, the samples were screened from light and electro-magnetic noise by enclosing them in a dark metal box. The most important characteristics obtained were; the series resistance (R_s), the barrier height (ϕ_b), the ideality factor (n), and the leakage current (I_r). The results were obtained by analysing the I-V data under the assumption that the dominant current transport mechanism is thermionic emission. According to the thermionic emission theory, the J-V characteristics for $V > 3kT/q$ are given by the modified equation:

$$J = J_o \exp\left(\frac{qV}{nkT}\right)$$

where J is the current density and J_o the saturation current density which is given by

$$J_o = A^{**}T^2 \exp\left[\frac{-q(\varphi_b - \Delta\varphi_{bi})}{kT}\right]$$

with $\varphi_e = \varphi_b - \Delta\varphi_{bi}$ is the effective barrier height, $\Delta\varphi_{bi}$ the image-force lowering of the barrier φ_b, A^{**} the effective Richardson constant, and T the absolute temperature of the metal/semiconductor junction.

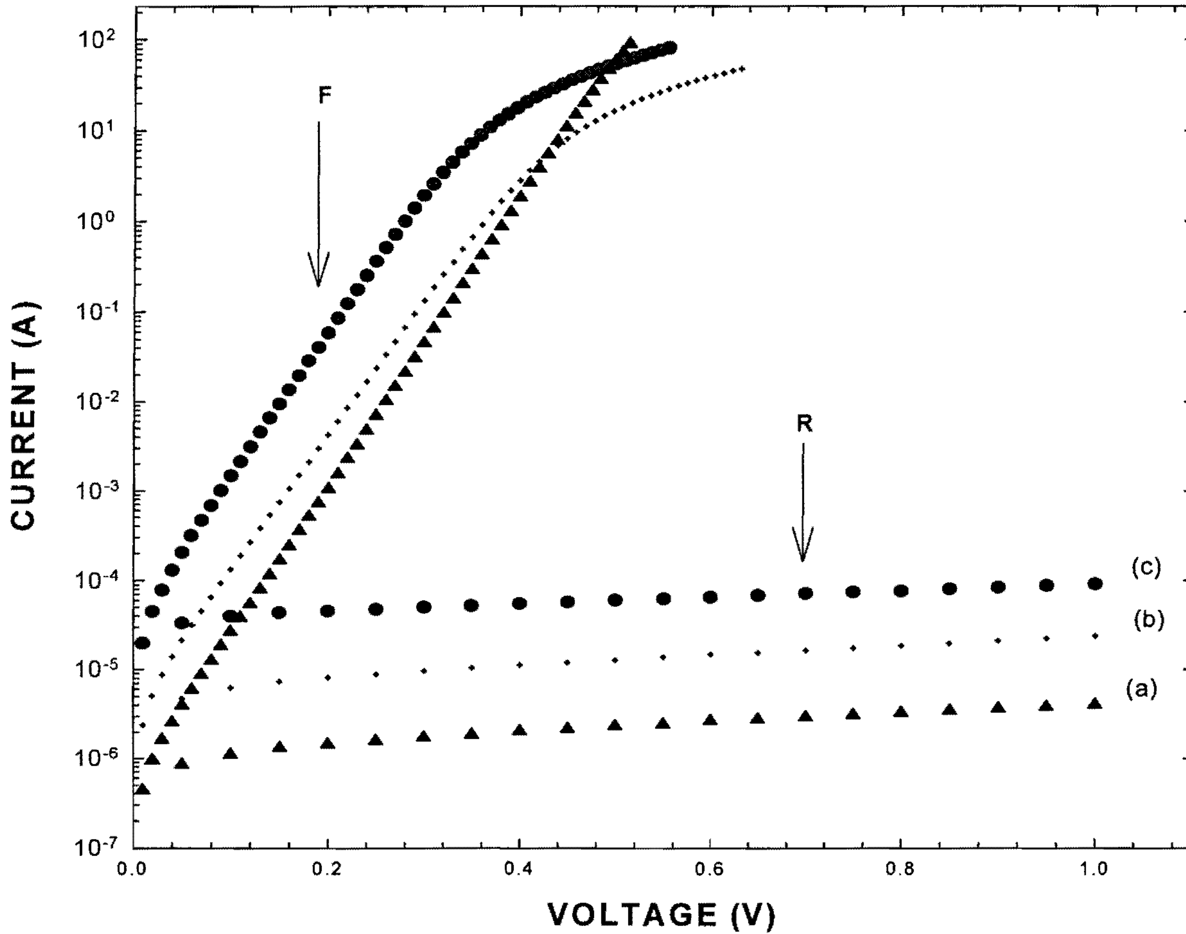

Fig 7.3: *I-V characteristics of control sample, Ni SBDs, curve (a). Curves (b) and (c) are for Ta with and without an electron shields respectively, on the same material.*

Assuming that dominant current transport mechanism in resistive evaporation SBDs is therminonic emission, it was found that the control diode (curve (a)) in Fig. 7.3 had an ideality factor, n, of 1.03 and a barrier height, ϕ_b, of 0.84 and 0.91 eV for I-V and C-V respectively, which are in good agreement with those reported in the literature [4].

The deposition of Ta SBDs using the EB deposition system was compared with the deposition of Ni SBDs fabricated by using resistive evaporation, which is believed not to introduce any defects and also its potential to evaporated ~1600 °C for Ni. This metal was chosen because of having the same barrier height as Ta. The most important parameter under investigation in Fig 7.3 was the reverse leakage current. From this investigation it was seen that the reverse leakage current exhibited a strong dependence on the EB deposited without shielding the substrate. Curve (a) is a representative of Ni SBDs with reverse leakage current at 1.0 V of 3.9×10^{-6} A. IV curves (b) and (c) are representative of Ta SBDs deposited with and without shielding the substrate. Comparing curve (b) and (c), it is clear that shielding the GaAs from the stray electrons lead to improved diode quality. This can be explained by the fact that the GaAs is exposed to energetic particles originating at, amongst others at a region close to the filament. When shielding the substrate from stray particles, the exposure of the surface to energetic particles originating at the filament is minimal and thus the defect concentration is low. On the other hand, when depositing without shielding the GaAs from the stray particles, the total particle dose on the GaAs is higher and therefore more defects are introduced which in turn cause poorer I-V characteristics. A detailed investigation has shown that when the electrons strike the molten metal, x-rays of various energies are produced as well as electrons backscattering from the molten metal target will reach the substrate [7].

Table 7.1: *Summary of I-V and C-V measurements of Ni SBDs deposited by resistive evaporation and Ta SBDs deposited by electron beam deposition, with and without shielding the substrate, using the same material.*

	Resistive Evaporation	Electron Beam Deposition	
		With Shield	Without Shield
n	1.03 ± 0.01	1.05 ± 0.01	1.06 ± 0.01
ϕ^{I-V} (eV)	0.84	0.78	0.77
ϕ^{C-V} (eV)	0.91	0.88	0.86

One of the most important parameters of SBDs is the rectification characteristics. Table 7.1 is a summary of properties of Ta and Ni SBDs fabricated on the same GaAs materials. Ta SBDs, which were EB-deposited with and without shielding the substrate were compared with Ni SBDs deposited by resistive evaporation. The increase in the ideality factor from 1.03 to 1.06, accompanied by a corresponding decrease in the barrier height from 0.84 eV to 0.77 eV for I-V measurement and 0.91 eV to 0.86 eV for C-V measurement were observed. It is evident that the barrier height of EB deposited Ta SBDs are lower than the SBDs which were resistively deposited. This is the result of stray electrons originating at the filament, causing damage at and close to the semiconductor interface. From this table it is clear that Ta SBDs deposited without shielding the substrate, show large deviations from ideality. A value of n larger than one reflects the excess current due to thermionic-field emission, field emission, edge leakage and recombination generation over to thermionic emission.

Since all the diodes investigated were manufactured on the same material which was subjected to the same chemical cleaning before metallisation (thus, eliminating the possibility of surface contamination), the deviation of n from unity observed here points to the introduction of electrically active defects during EB evaporation. It was clear that the shielding of the substrate from stray particles originating at the filament introduces less damage to the substrate as it has been observed in Fig. 7.3. During biasing of the substrate, a shield was used to screen the substrate from stray particles.

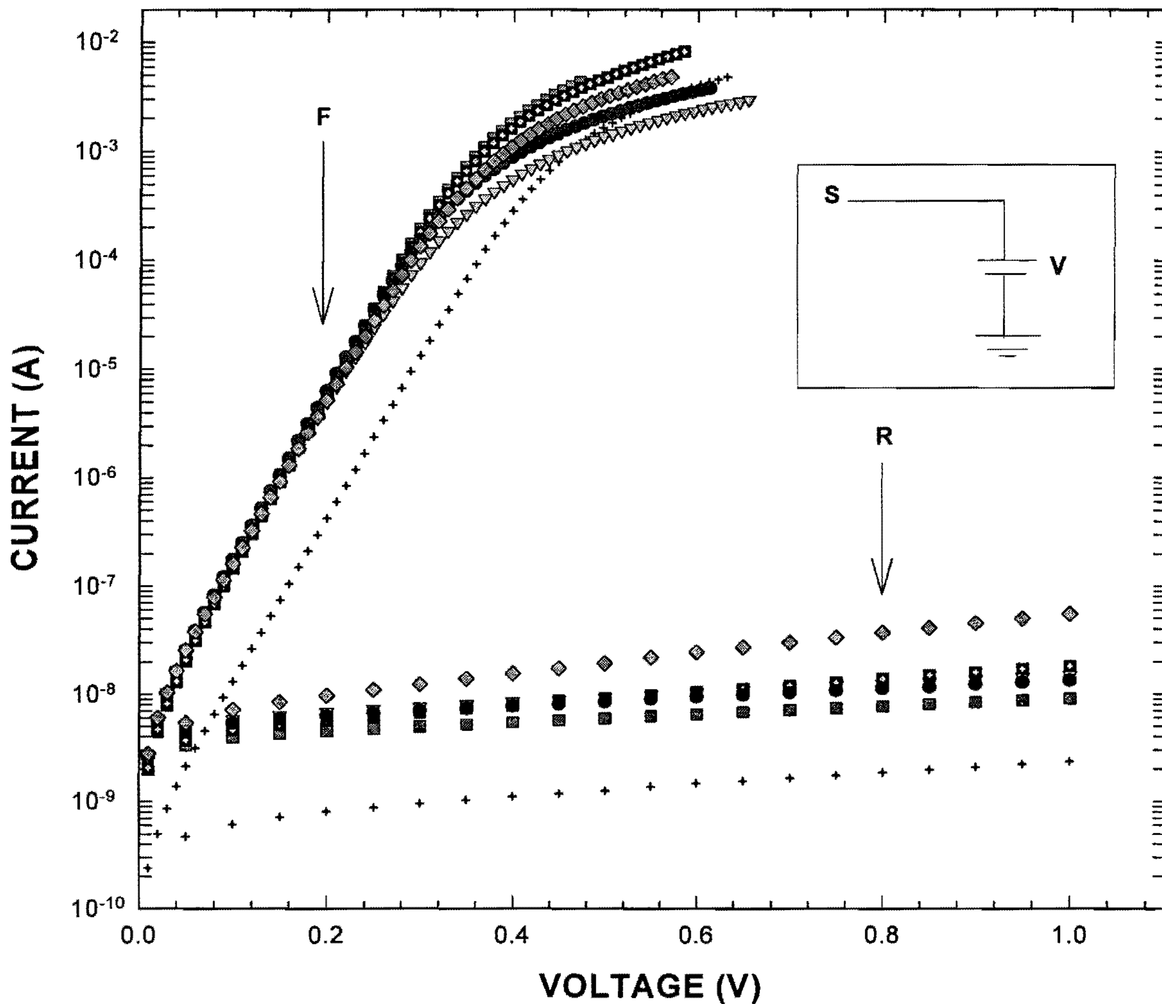

Fig 7.4: *Forward (F) and reverse (R)* current-voltage *(I-V) characteristics of Ta SBDs fabricated on n-GaAs by EB deposition with an electron shield in position at applied positive voltage to the sample (S) (+: 0 V; ✪: 100 V; ●: 500 V; ▲: 1000 V; ▼: 1500 V; ◆: 2000 V)*

Fig 7.4 is representative of the I-V characteristics of Ta SBDs fabricated with shielding the substrate from stray electrons. A plot shows a trend of the Schottky diode I-V characteristics towards non-ideality with increasing applied voltage from 0 V to 2000 V irrespective of the direction of applied voltage (i.e. positive or negative). However, from inspection of Fig 7.4, where the I-V characteristic of EB deposited SBDs without shielding the substrate, it can be seen that there is deviation from linearity in the forward bias region of the I-V curves, especially in the low voltage region, which proves that other current mechanisms contributes to the leakage current.

The current obtained at 1.0 V reverse bias increases from 8.9×10^{-8} A to 4.2×10^{-7} A with increasing an applied positive voltage on the substrate from 0 V to 2000 V respectively. The shift in the current indicates the damage in the material, although it cannot give the extend of the damage. Recombination generation is speculated to be dominant.

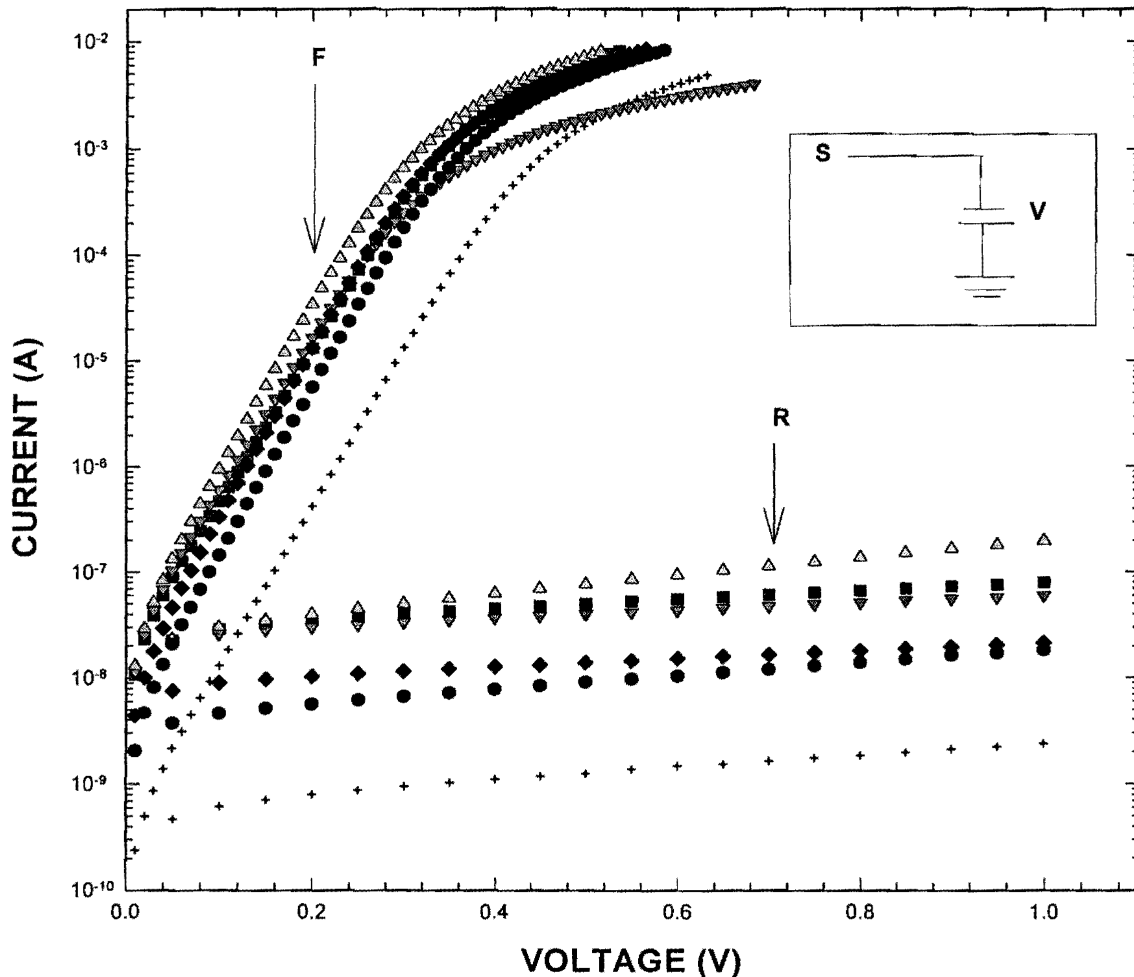

Fig 7.5: *Forward (F) and reverse (R)* current-voltage *(I-V) characteristics of Ta SBDs fabricated on n-GaAs by EB deposition with an electron shield in position at applied negative voltages to the sample (S) (+: 0 V; ●: 100 V; ◆: 500 V; ▼: 1000 V; ✪: 1500 V; ▲: 2000 V)*

Comparison of Fig 7.4 and Fig 7.5 indicates that more damage was introduced when a negative voltage was applied to the sample. The current transport mechanism across the metal-semiconductor junction is no longer purely thermionic in nature.

Current transport through other mechanisms as listed in section 3.3 have increased. Fig 7.5 is a representative of the I-V characteristics of Ta SBDs fabricated with shielding the substrate from stray particles during the negative biasing of the substrate (GaAs). The applied voltage was ranging from 0 V to -2000 V. The effect of the applied voltage was clearly observed. In Fig. 7.5 a similar trend as obtained in Fig. 7.4 were observed. At 1.0 V reverse bias, the current increases from 9.0×10^{-8} A to 3.0×10^{-7} A. The effect of EB deposition on the I-V measurement is shown in Fig. 7.4 and Fig. 7.5, which are representative of the I-V characteristics of Ta SBDs fabricated during the positive and negative biasing of the substrate. The current at 1.0 V reverse bias for the extreme applied negative voltage (2000 V) was found to be 2.0×10^{-8} A, while for the extreme applied negative voltage (-2000 V) was found to be 3.0×10^{-7} A.

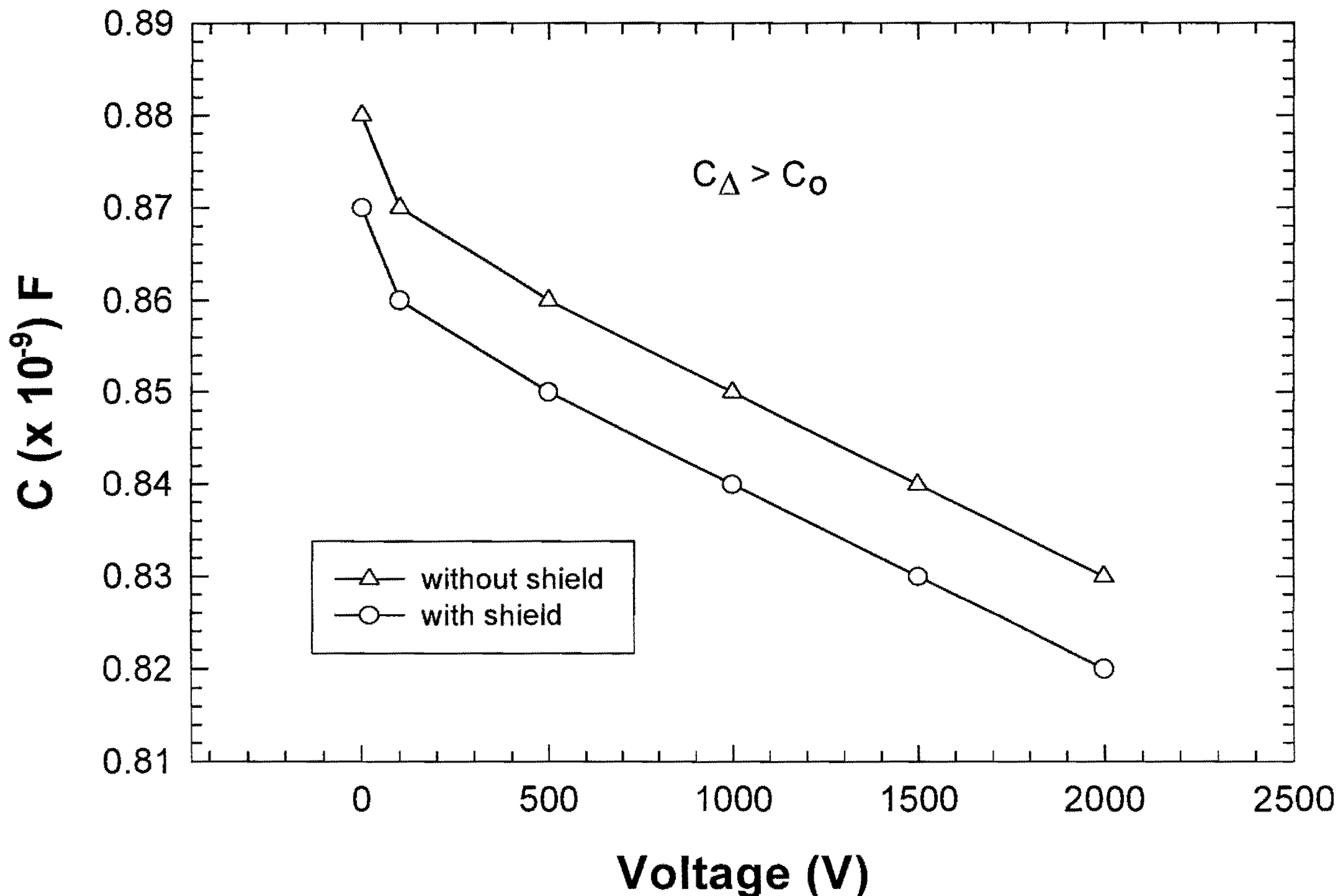

Fig 7.6: *The capacitance as a function of positive applied substrate voltage. The error bars is as the same as the size of the symbol.*

Fig 7.6 and Fig 7.7 illustrate the inverse square of the capacitance as a function of positive and negative applied sample voltage respectively. Diodes fabricated with and without shielding the substrate from stray particles were compared. For control purpose, the shield was removed. It was observed that the capacitance of the diode fabricated without shielding was higher compared to diodes fabricated with shielding. The capacitance was seen to increase with increasing the positive applied voltage on the substrate for both shielding and without shielding the substrate. From the slope and the intercept of the graph, the free carrier concentration, N_D and the build-in potential of the material were determined.

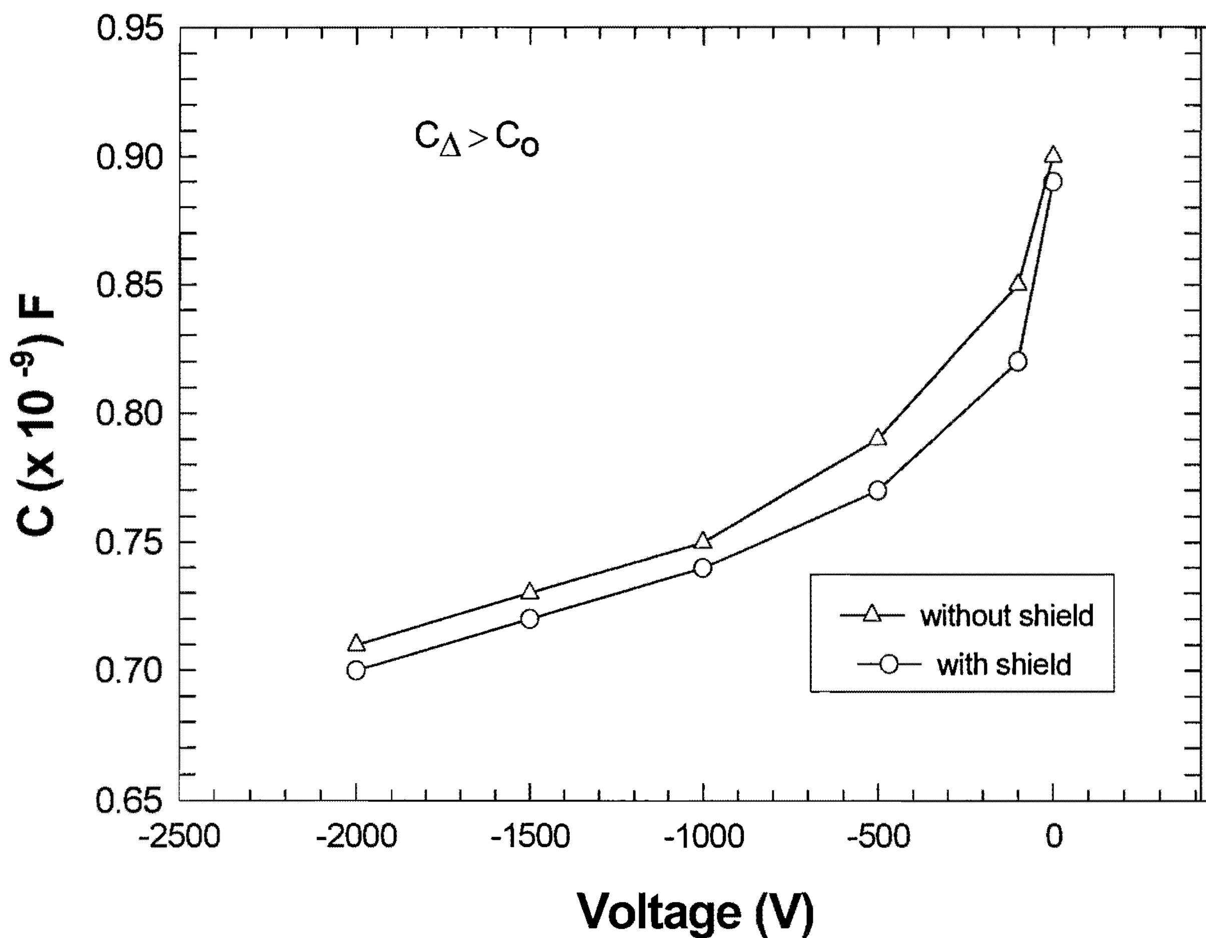

Fig 7.7: *The capacitance as a function of negative applied voltage. The error bars is as the same as the size of the symbol.*

From both Fig 7.6 and Fig 7.7 one could observe that the capacitance obtained from the diodes fabricated without shielding the substrate was found to be greater than the diodes fabricated during the shielding of the substrate.

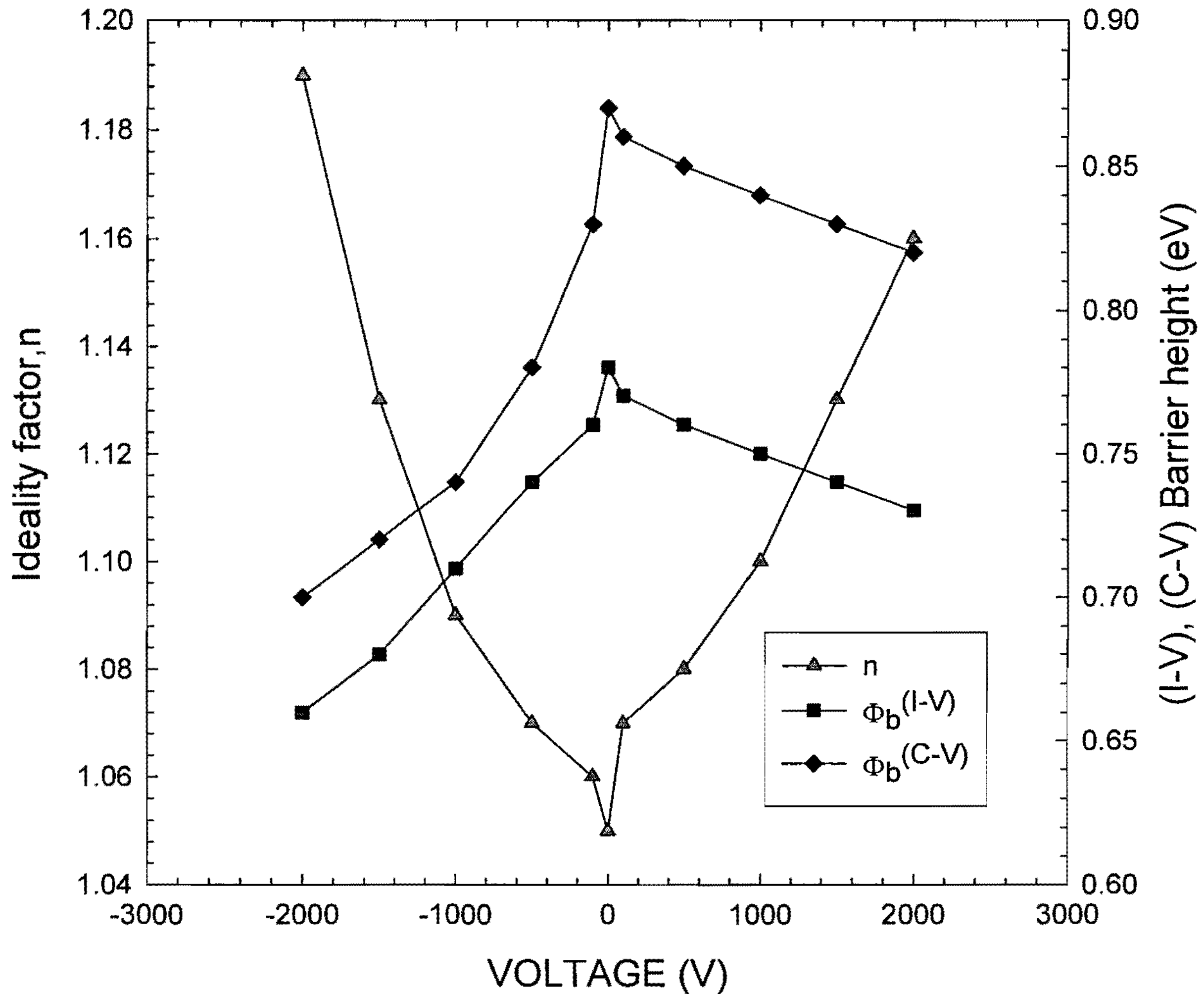

Fig 7.8: *The barrier height, ϕ^{IV}, ϕ^{CV} and ideality factor, n, of Ta Schottky barrier contacts as functions of applied substrate voltage, deposited with shielding the substrate. The error bars is as the same as the size of the symbol.*

Fig 7.8 depicts the barrier heights, ϕ^{I-V}, ϕ^{C-V} and the ideality factor, n, as a function of the applied voltage on the substrate. These parameters were extracted from the I-V and C-V characteristics of a metal-semiconductor contact. The ideality factor was observed to increase from 1.05 to 1.18 and from 1.05 to 1.17. When the negative and positive voltages were applied to the sample, respectively, the barrier heights followed the same trends i.e. decrease with applied voltages. One might argue that the use of higher voltage (irrespective of the polarity used) leads to the increased defect concentration.

To account for the origin of particles, the following gases were identified in the chamber: H, H_2, C, N, O, OH, H_2O, CO, N_2, CO_2, and C_xH_y. Positive ions are: H, H_2, and negative ions are: O, OH, C and C_xH_y. These particles also reach the substrate. It is clear from Fig 7.8 and Fig 7.10 (deposited with and without shielding the substrate respectively) that ϕ(I-V) is less than ϕ(C-V). The difference between ϕ(I-V) and ϕ(C-V) during the negative applied voltage to the substrate was observed to be less as compared to the differences during the positive applied voltage to the substrate. During the negative applied voltage to the substrate, the damage is suspected to be from electrons, H, H_2 and Ta^+. On the other hand the damage observed during the positive applied voltage to the sample is due to the accelerated electrons, OH^-, N^-, CO^-, $H_xH_y^-$ and carbon ions to the substrate. The value of the ideality factor, n, was found to be larger than one, which reflects the excess current due to recombination generation over to thermionic emission. The deviation of n from unity observed here points to the introduction of electrically active defects during EB deposition.

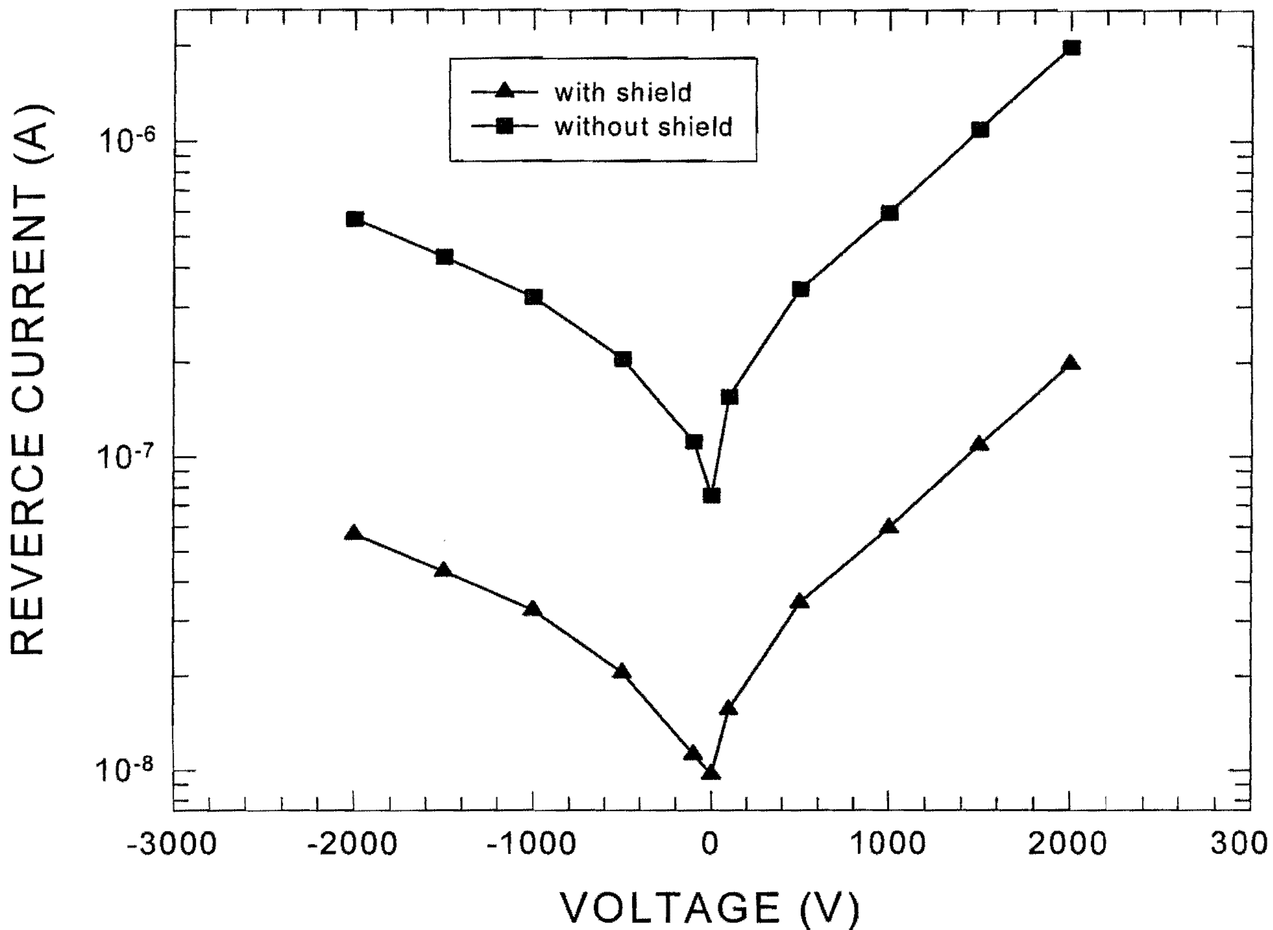

Fig 7.9: *The reverse current as a function of applied substrate voltage for SBDs deposited with and without shielding the substrate. The error bars is as the same as the size of the symbol.*

The applied positive voltage resulted in a significant difference between the I-V and C-V barrier heights. On the other hand, the applied negative voltage resulted in a small difference between the I-V and C-V barrier heights. We therefore argue that this deviation from ideality of the SBDs when exposed to stray particles is due to the defects caused by the stray electrons and other particles during deposition. Fig 7.9 depicts the reverse current (Ir) measured at 1.0 V plotted as a function of applied voltage to the substrate. It can be seen that there is a linear change on both the applied positive voltage and the applied negative voltage. A high reverse leakage current was obtained as the applied voltage was increased.

It is speculated that the experimentally measure current values are not solely due to only thermionic-emission but a combination with other current transport mechanisms, especially recombination generation.

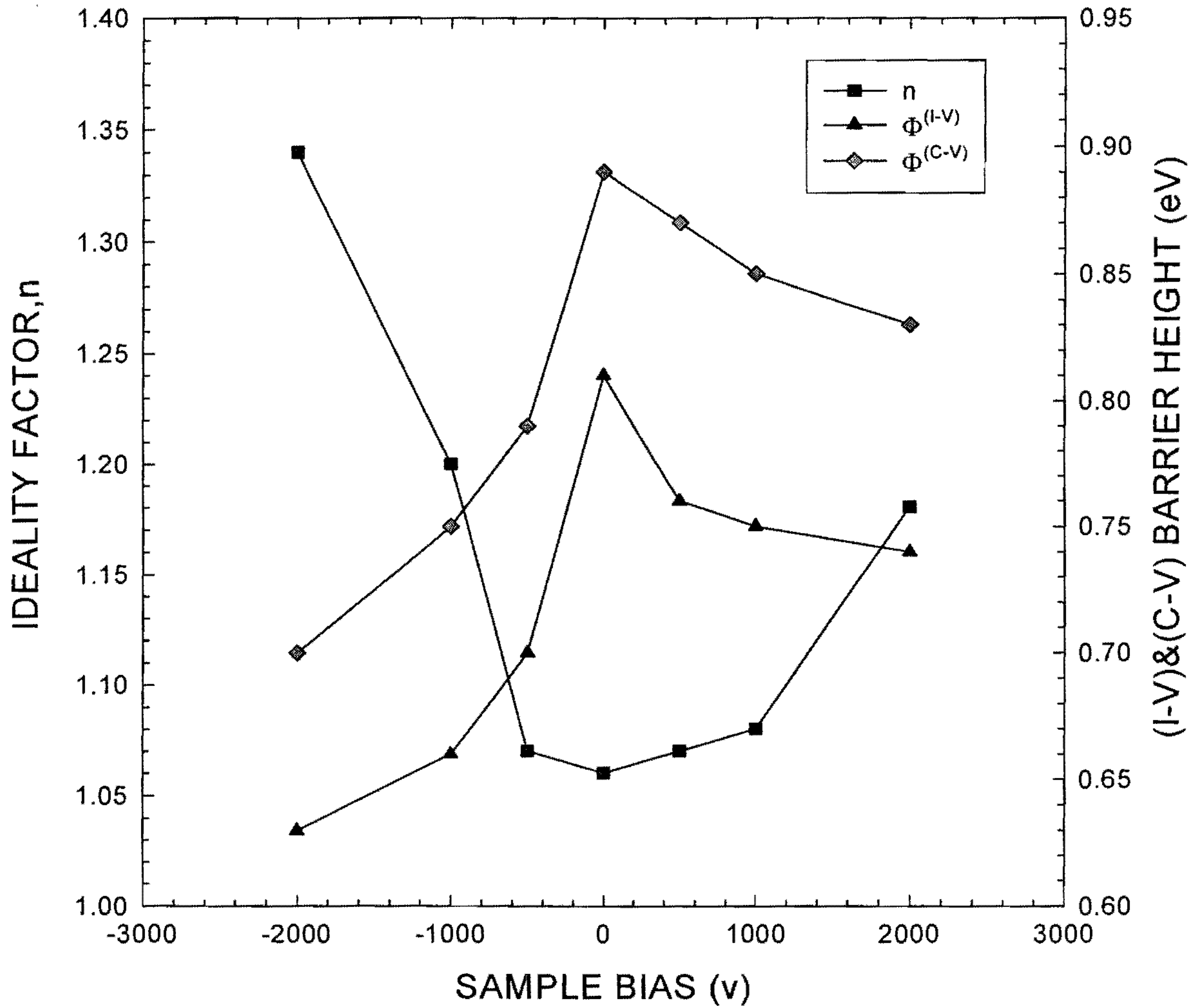

Fig 7.10: *The barrier height, ϕ^{IV}, ϕ^{CV} and ideality factor, n, of Ta Schottky barrier contacts as functions of applied substrate voltage, deposited without shielding the substrate. The error bars is as the same as the size of the symbol.*

For control purpose Fig 7.10 was plotted, which shows the Schottky barrier contacts of Ta deposited without shielding the substrate. Fig 7.10 represents the I-V, C-V barrier heights, and ideality factor as a function of applied sample voltages. The ideality factor was observed to increase from 1.06 to 1.34 and from 1.06 to 1.18, when the negative and the positive voltages are applied to the sample, respectively.

The barrier heights decreased with increasing applied voltages, positive or negative. More damage was observed in this figure as compared to Fig 7.7.

7.4 SUMMARY

To summarise, Fig 7.3 contains the data of Schottky barrier heights of Ta on n-type GaAs. These values were determined by the current-voltage and capacitance-voltage techniques. The quality of the diodes that were used in this study is shown also in Fig 7.3 in terms of the ideality factor.

The effect of EB deposition at different applied (positive and negative) substrate voltages on GaAs may thus be summarised as follows: It was found that after DLTS measurements defect concentration increases as the applied voltage during deposition increases, irrespective of the direction of the applied voltage. The degree of nonideality of the SBD investigated by I-V measurements showed the same behaviour with increasing applied voltage, that is, at higher applied substrate voltage, GaAs yielded SBDs with poorer characteristics. The deviation of ideality factor, n, from unity observed here reflects the excess current due to recombination generation over to thermionic-emission.

Reference

(1) S. A. Goodman, F. D. Auret, G. Myburg, and C. Schutte; Solid State Phenomena. **47** (1996) 391.

(2) R. E. Williams; Gallium Arsenide Processing Techniques (Artech House 1984) 85.

(3) S. A. Goodman, F. D. Auret, and G. Myburg, Semicond. Sci. techol. **7** (1992) 1241.

(4) W. O Barnard, G. Myburg, F. D. Auret, S. A. Goodman, and W. E. Meyer; J. of. Elect. Mater. **25** (1996) 1695.

(5) F. D. Auret, G. Myburg, S. A. Goodman, L. J. Bredell, and W. O Barnard; Nucl. Instr, and Meth in Phys. Res. B **67** (1992) 410.

(6) F. D. Auret, S. A. Goodman, Y. Leclerc, G. Myburg, and C. Schutte; Mater. Sci. and Techn. **13** (1997) 945.

(7) F. D. Auret, S. A. Goodman, G. Myburg, and W. E. Meyer; Appl. Phys. A **56** (1993) 547.

CHAPTER 8:

DLTS RESULTS

8.1 INTRODUCTION

In this chapter, the DLTS results obtained after depositing Ta SBDs at various applied voltages on GaAs will be discussed. As will be shown below, the DLTS spectra indicate that defects with energy levels in the GaAs band gap were introduced during EB deposition. Metallisation induced defects were characterized by DLTS using a two-phase lock-in amplifier based system to analyze the transient [1], in the temperature range from 20 to 350 K. Defects concentration profiling was done by using a constant reverse bias and varying a filling pulse V_p with an increment of 0.2 V stating at 1.2 V and T_p = 0.2 ms.

A full discussion of the theory of DLTS was given in chapter 6, while chapter 2 describes the Schottky junction that was used as a contact structure. After establishing the integrity of the Schottky contacts on the sample by I-V and C-V measurements, DLTS scans were recorded to establish if there were any deep levels in the samples. The quality of a rectifying device depends on the amount of imperfections (impurities and defects) at the metal-semiconductor interface, as well as in the depletion region of the diode.

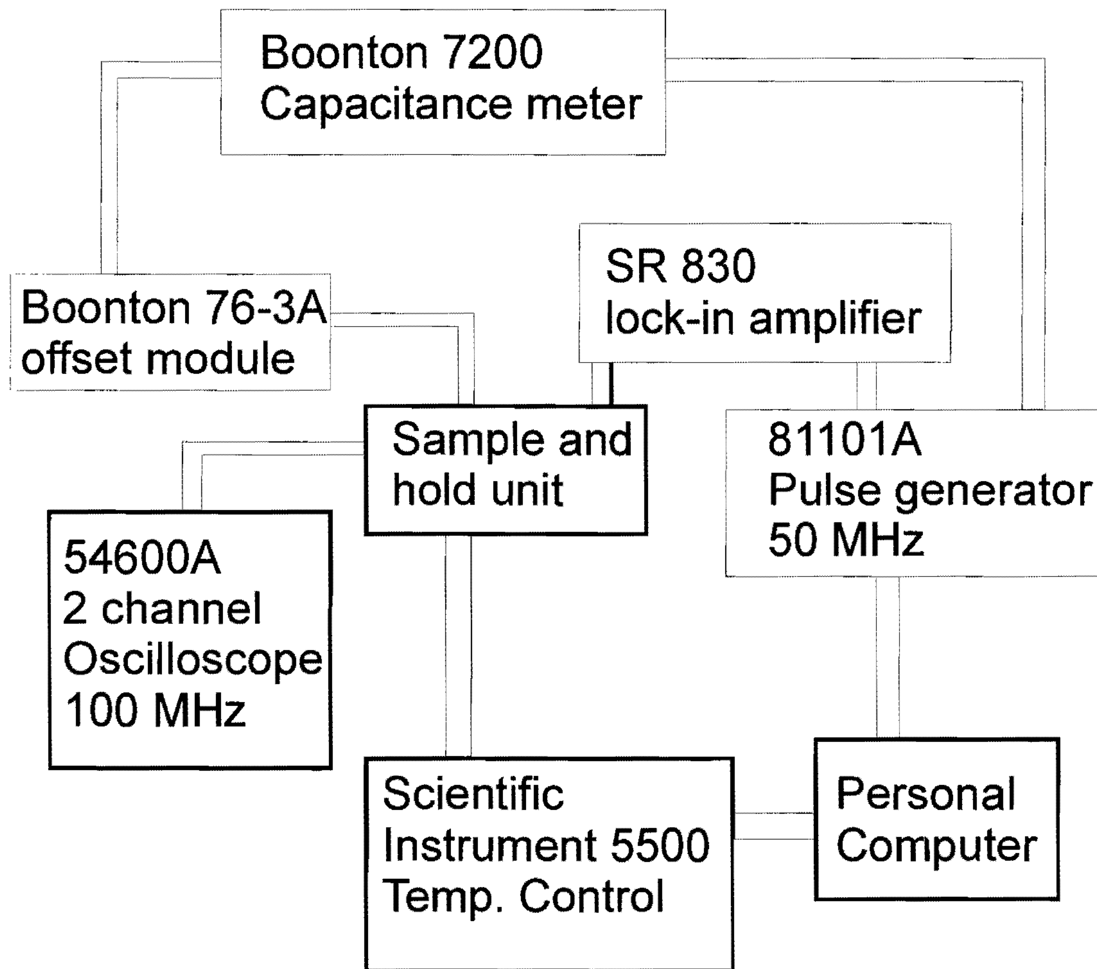

Fig 8.1 *Block diagram of lock-in-amplifier-based DLTS system.*

A lock-in amplifier-based (LIA) deep level transient spectroscopy (DLTS) system comprised of a SR 830 LIA, a Boonton 7200 capacitance meter and a cryostat with temperature controller, was employed to detect and characterize defects introduced during EB deposition of Ta. The DLTS spectra were acquired at a rate of 4 $K.min^{-1}$ in both temperature directions to eliminate any peak temperature discrepancies due to uneven cooling or heating. DLTS has the advantage of being a very sensitive measuring technique, in part because of the repetitive nature of the data collection and signal averaging. Next we discuss the DLTS results obtained from diodes fabricated on GaAs surface that were exposed to different positive and negative voltages. From the DLTS pulse parameters required to detect those defects, it was estimated that they were located within the first micron below the surface.

The defect concentration referred to in the discussion below is the average concentration in the region probed by DLTS.

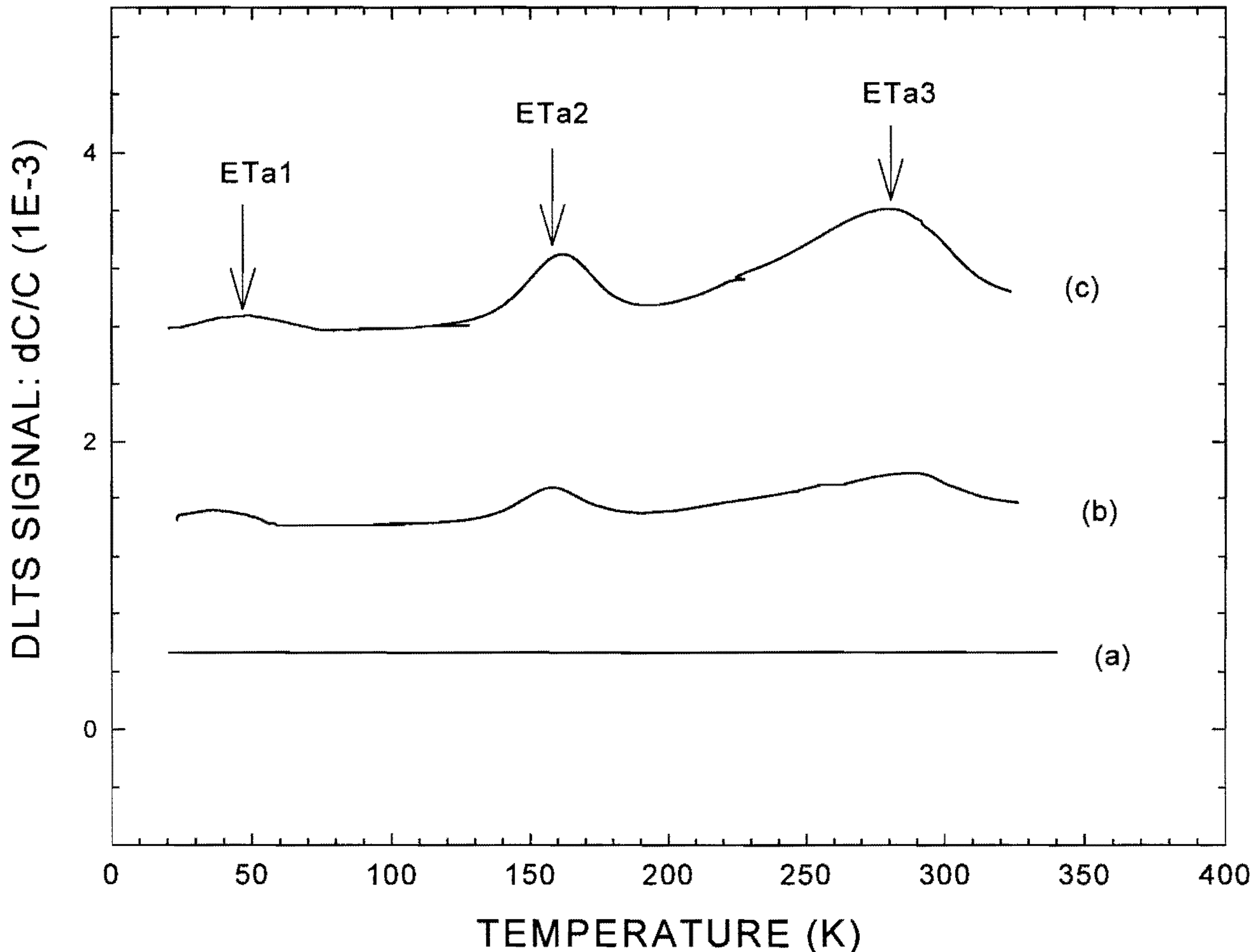

Fig 8.2 *DLTS spectra of Ta SBDs EB deposited on n-GaAs with and without shielding the substrate from stray electrons originating at the filament (curve (b) and (c)) respectively, as well as Ni SBDs (curve (a)) deposited by resistive evaporation on the same material. All spectra were recorded at a lock-in amplifier frequency of 46 Hz, a quiescent bias of V_r = 1.0 V and a filling pulse of V_p = 1.2 V.*

In Fig 8.2 DLTS spectra for EB deposition as well as for the control sample are presented. Curve (a) is a representative of a Ni SBDs deposited by resistive evaporation. From this spectrum, no defects were detected by DLTS in the material

used for this study. Curves (b) and (c) are representative of a Ta SBDs deposited by EB system on the same GaAs material.

In these curves [(b) and (c)], three defects ETa1, ETa2 and ETa3 are present. These defects were not detected in resistively deposited Ni SBDs fabricated on the same material. This is because resistive evaporation of metals does not introduce defects [(6)]. Three defects introduced during EB deposition indicates that the electron shielding used in curve (b) did not provide a complete shielding from stray particles, but that was effective enough to ensure that EB induced defect with concentration less than those unshielded diodes curve (c). Alternatively, it may also be argued that these defects were introduced by particles scattered towards the sample from areas in the vacuum chamber other than the filament areas. Primary electrons scattered from the molten Ta and secondary electrons generated in the Ta due to interaction with electrons in the electron-beam and electrons of Ta. Curve (c) is representative of Ta SBDs, which were EB deposited without the electron shield. The relative heights of the DLTS peaks in each curve on the graph are not the same, indicating that the defect concentrations are different. When the peak heights of curve (b) and (c) were compared, it was found that the peaks in (c) are higher than the corresponding peaks observed in (b). In curve (c), ETa3 was observed to have a broad peak.

From Fig 8.2, the use of a shield was observed to be effective enough to ensure that EB induced defects has concentration less than those fabricated without the shield. The remainder of this study was based on the use of shield.

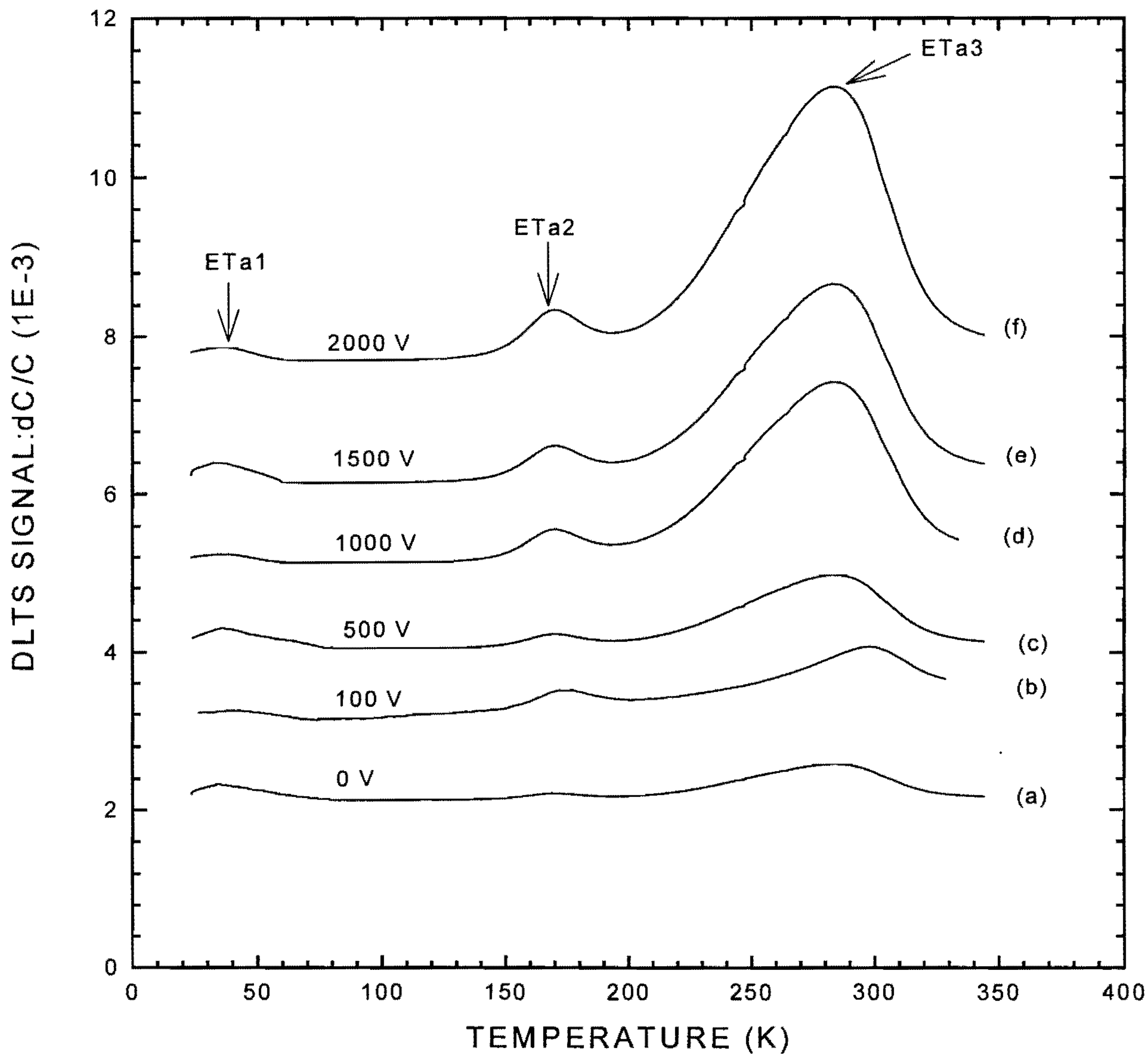

Fig 8.3 *DLTS spectra of a Ta SBD deposited on n-GaAs by EB deposition with shielding stray electrons originating at the filament, for different applied positive voltages (from 0 V to 2000 V), curve (a) to curve (f) respectively. The spectra were all recorded at a lock-in amplifier frequency of 46 Hz, a reverse bias of V_r = 1.0 V and the filling pulse of V_p = 1.2 V.*

Fig 8.3 depicts the DLTS spectra after EB deposition of Ta during the positive biasing of the sample. The sample was shielded from stray particles originating at the filament. At least three defects ETa1, ETa2, and ETa3 were observed. The defect concentrations were seen to increase with increasing the applied voltage. However, ETa3 become broader, while ETa1 and ETa2 have narrow peaks, respectively. The full width at half maximum (FWHM) for ETa3 measured at the applied voltages, 1000 V, 1500 V and 2000 V, showed an increase in FWHM values.

The defects observed in Fig 8.3 were profiled. DLTS depth profiling was performed by recording spectra at fixed $V_r = 1.0$ V but incrementing V_p in small steps from one scan to the next. The approach of Zohta et al [11] was then used to obtain the defect concentration as a function of depth below the interface. The depth profile of these EB deposition induced defect have been obtained by the DLTS depth profiling technique described in chapter 6 of this book. It can be seen from Fig (8.4), (8.5) and (8.6) that the defect concentrations were increased with increasing the applied positive voltage.

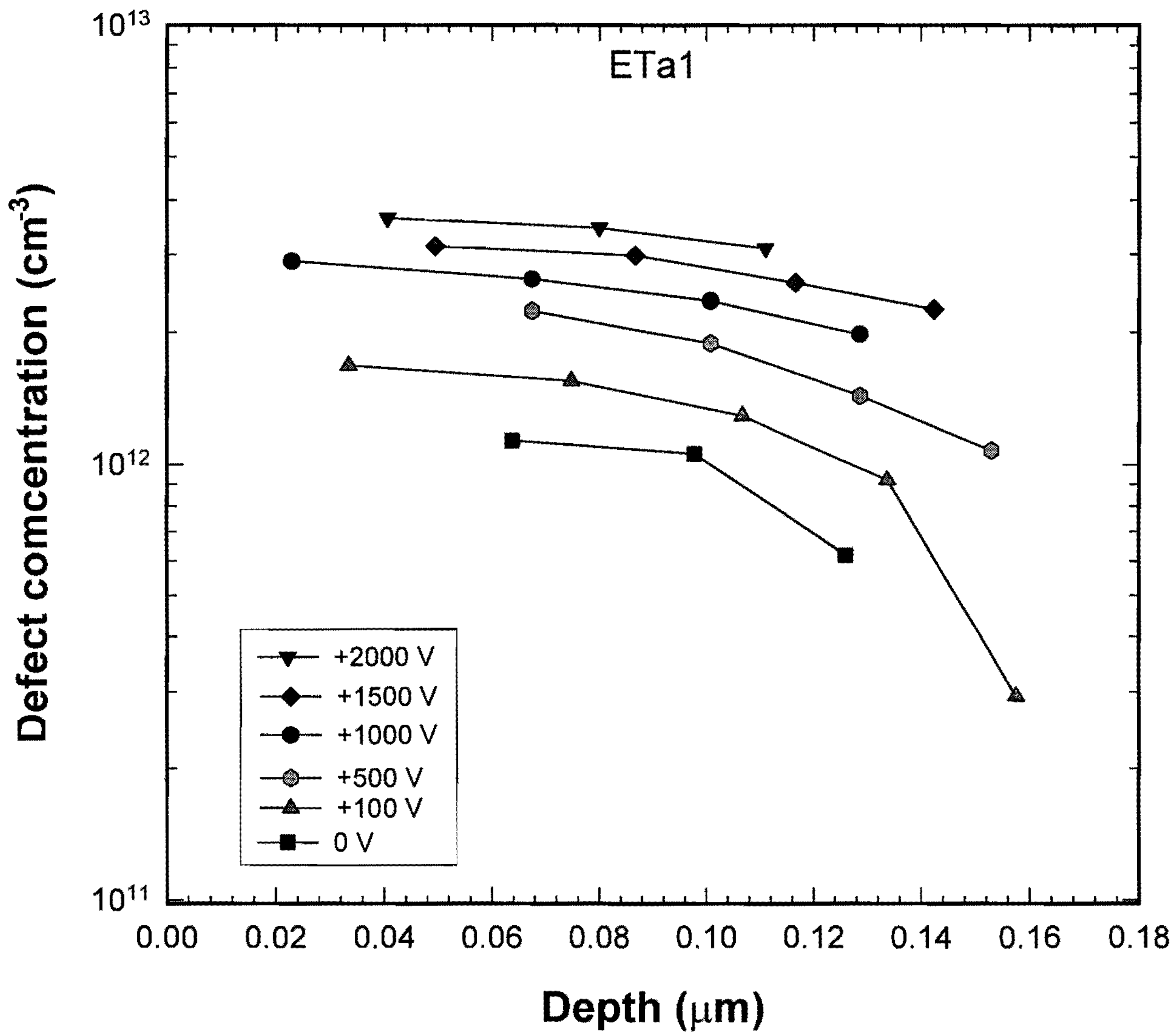

Fig 8.4 *Depth profiles (constructed from DLTS measurements) of the ETa1 defect introduced in n-GaAs during Ta Schottky contacts formation, during the positive applied voltage.*

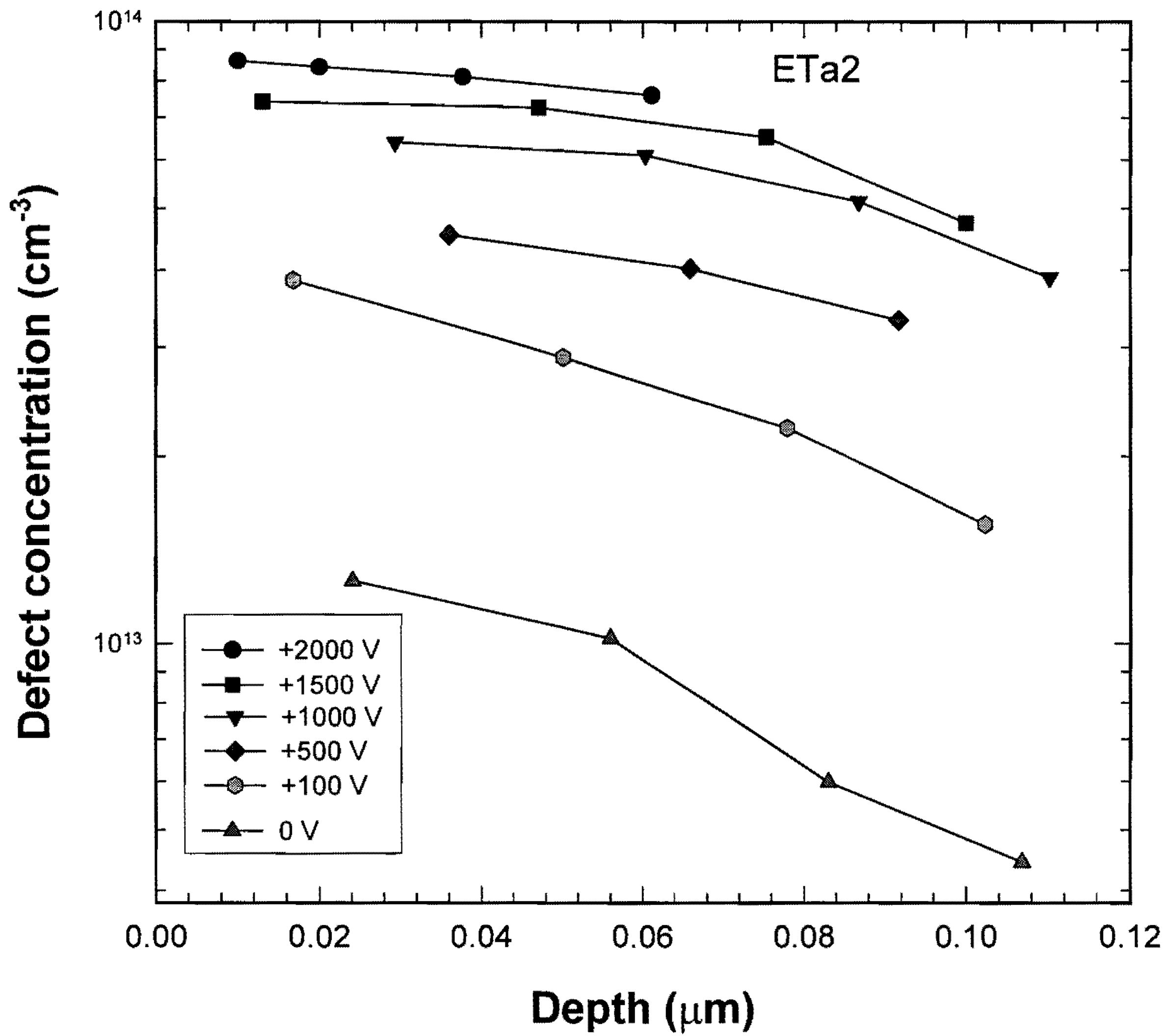

Fig 8.5 *Depth profiles (constructed from DLTS measurements) of the ETa2 defects introduced in n-GaAs Ta Schottky contacts formed during the positive applied voltage.*

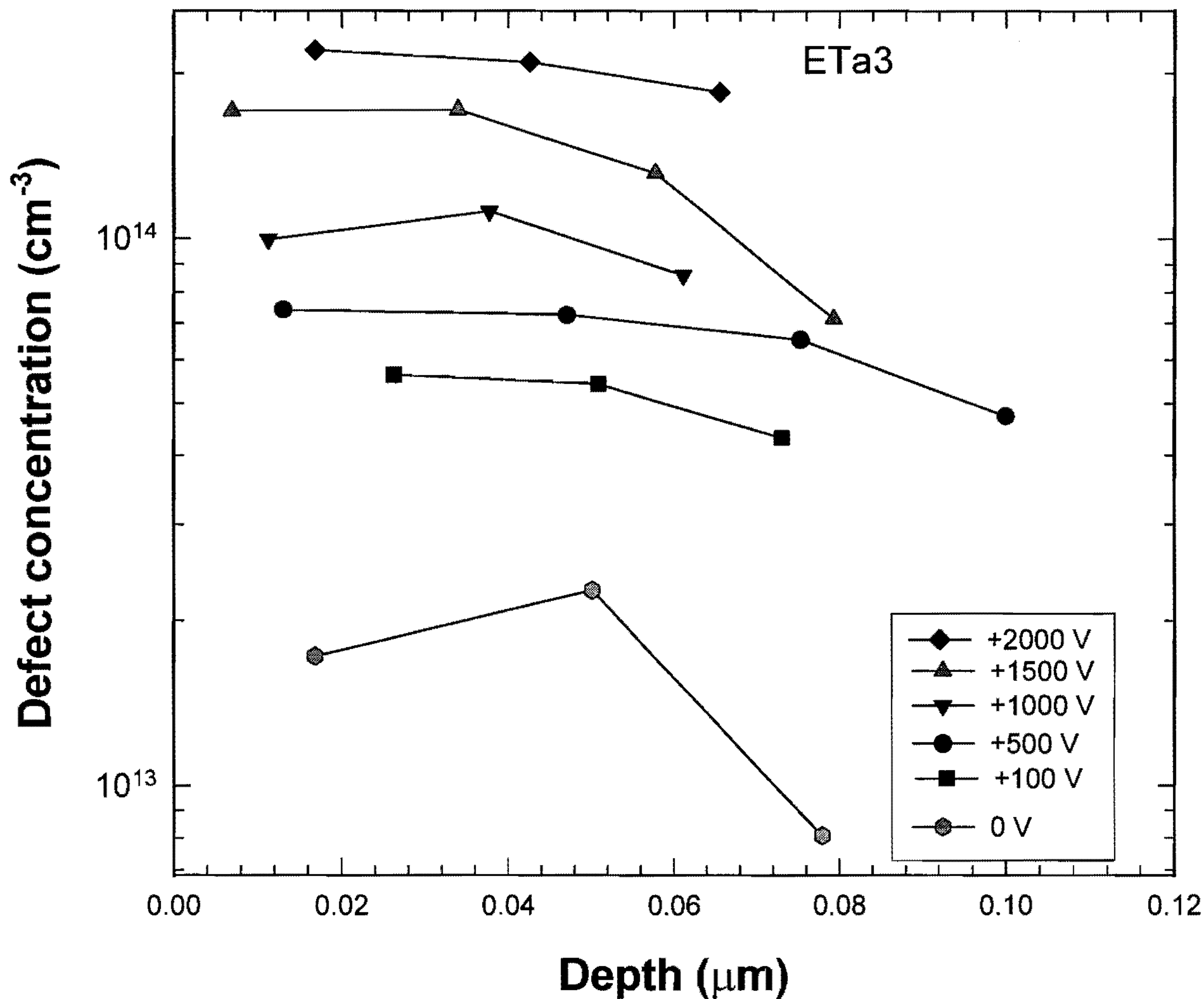

Fig 8.6 *Depth profiles (constructed from DLTS measurements) of the ETa3 defect introduced in n-GaAs during Ta Schottky contacts formed during the applied positive voltage.*

Three defects ETa1, ETa2 and ETa3, which were observed after EB deposition of Ta, were profiled. Figures 8.4, 8.5 and 8.6 show their depth profiles in the case of applied positive substrate voltage. From the depth profiles in both figures, some important observation can be made. (i) In all GaAs samples, the ETa2 and ETa3 appeared to be closer to the interface than the ETa1, implying that they are physically different. (ii) The maximum concentration of ETa3 increased slightly during the increase in the applied positive voltage.

(iii) Maximum concentration of ETa3 decreased during the increase in the applied negative voltage. (iv) It can be seen that the defect concentration decreased as we move into the substrate.

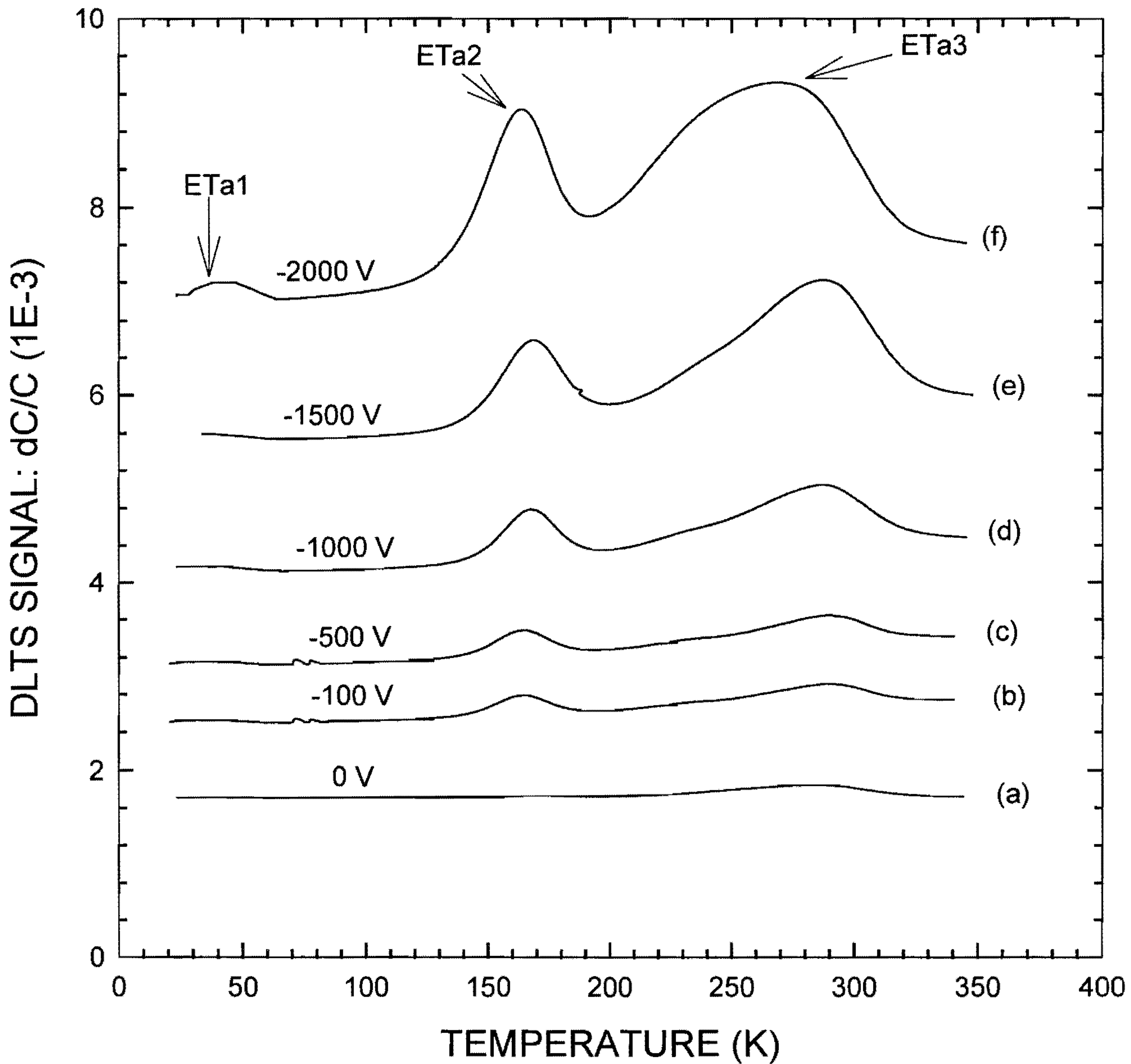

Fig 8.7 *DLTS spectra of a Ta SBD deposited on n-GaAs by EB deposition with shielding stray electrons originating at the filament, for different applied negative voltages (from 0 V to -2000 V), curve (a) to curve (f) respectively. The spectra were all recorded at a lock-in amplifier frequency of 46 Hz, a reverse bias of* $V_r = 1.0$ V *and the filling pulse of* $V_p = 1.2$ V.

Fig 8.7 is representative of the DLTS spectra after EB deposition of Ta during the negative biasing of the sample. The sample was also shielded from the stray particles originating at the filament. During the negative biasing of the sample at least three defects were introduced (ETa1, ETa2, and ETa3). The defect concentrations were seen to increase with the increasing the applied negative voltage. However ETa3 become broader as compared to Fig 8.3. The peak height of ETa2 was observed to increase and becoming sharper as the applied voltage increases. The FWHM for ETa2 measured at the applied voltages, -1000 V, -1500 V, and -2000 V were observed to increase by a factor of 0.1. The FWHM for ETa3 was observed to increase by a factor of 0.4. This factor is more than the value obtained for the same defect (ETa3) in Fig 8.3.

From DLTS spectra, Fig 8.3 and Fig 8.7 (DLTS spectra of a Ta SBDs for different applied positive and negative voltages respectively) it can be seen that the relative concentrations of defects formed during EB deposition depends on the applied voltages. In order to explain the origin of EB deposition induced defects observed here, we consider what happens to the GaAs during metallisation. The heavy energetic Ta particles (ions or atoms) impinge on the sample. As the voltage were applied to the sample, different ions can be expected to reach the GaAs samples. The metal-ions do not penetrate deep into the semiconductor but can transfer enough energy to cause displacement damage at and within several atomic layers below the GaAs surface. Electrons can penetrate much deeper but cannot transfer enough energy via elastic collisions to cause displacement damage [(7)].

The defects observed in Fig 8.7 were profiled. The defect concentration distribution below the metal-GaAs interface was calculated. To minimize the problem associated with field assisted emission, spectra recorded by increasing V_p in steps of 1.0 V were subtracted from each other so that information of only a narrow spatial region, instead of that corresponding to the full pulse height is analyzed. The depth profiles thus obtained for all EB deposition indicated that the concentrations decrease into the substrate.

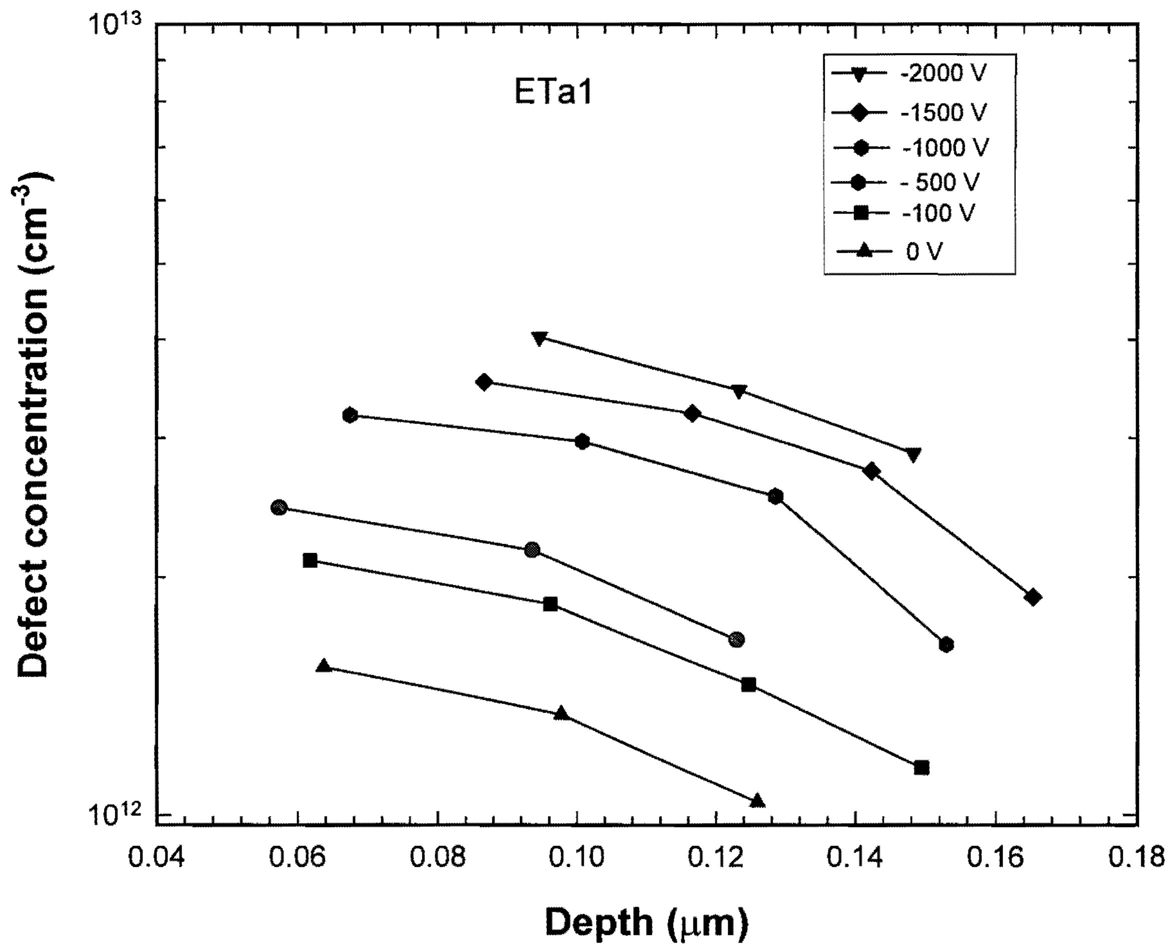

Fig 8.8 *Depth profiles (constructed from DLTS measurements) of the ETa1 defect introduced in n-GaAs during Ta Schottky contacts formed during negative applied voltage*

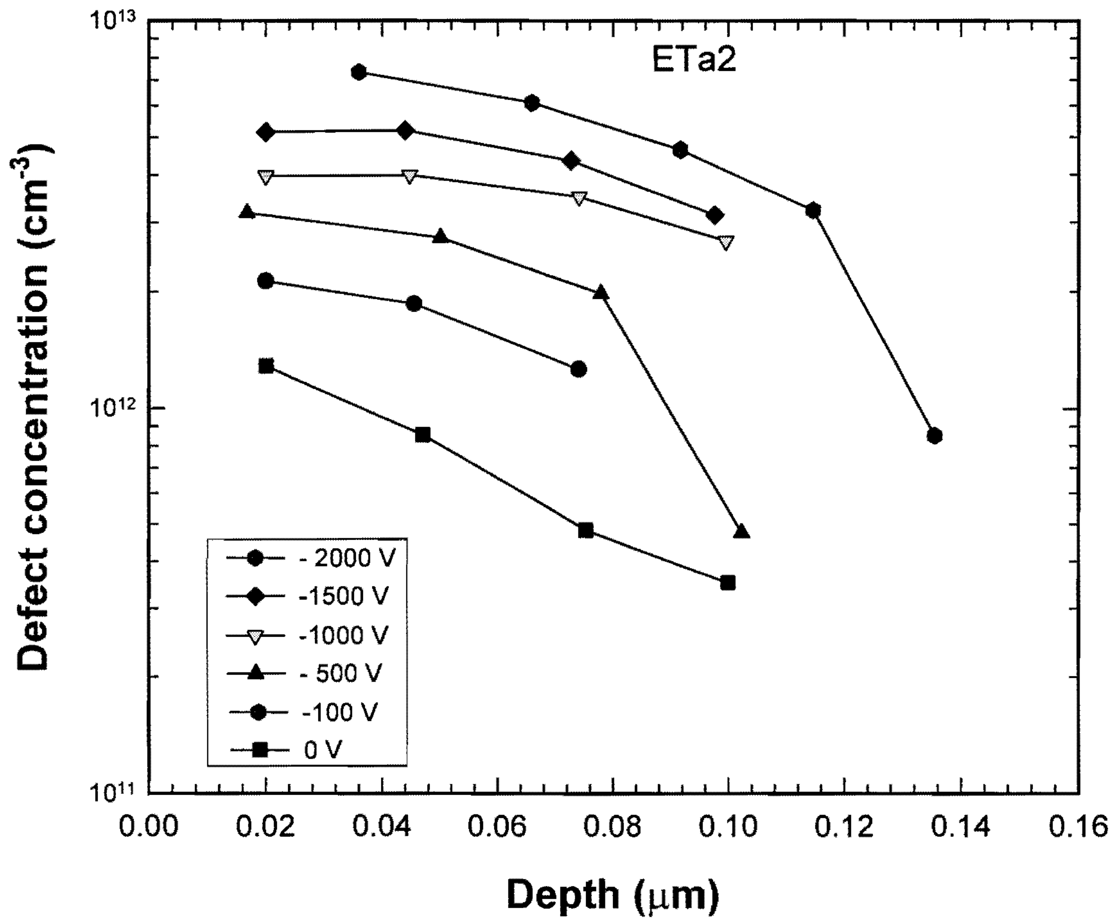

Fig 8.9 *Depth profiles (constructed from DLTS measurements) of the ETa2 defect introduced in n-GaAs during Ta Schottky contacts formed during the applied negative voltage.*

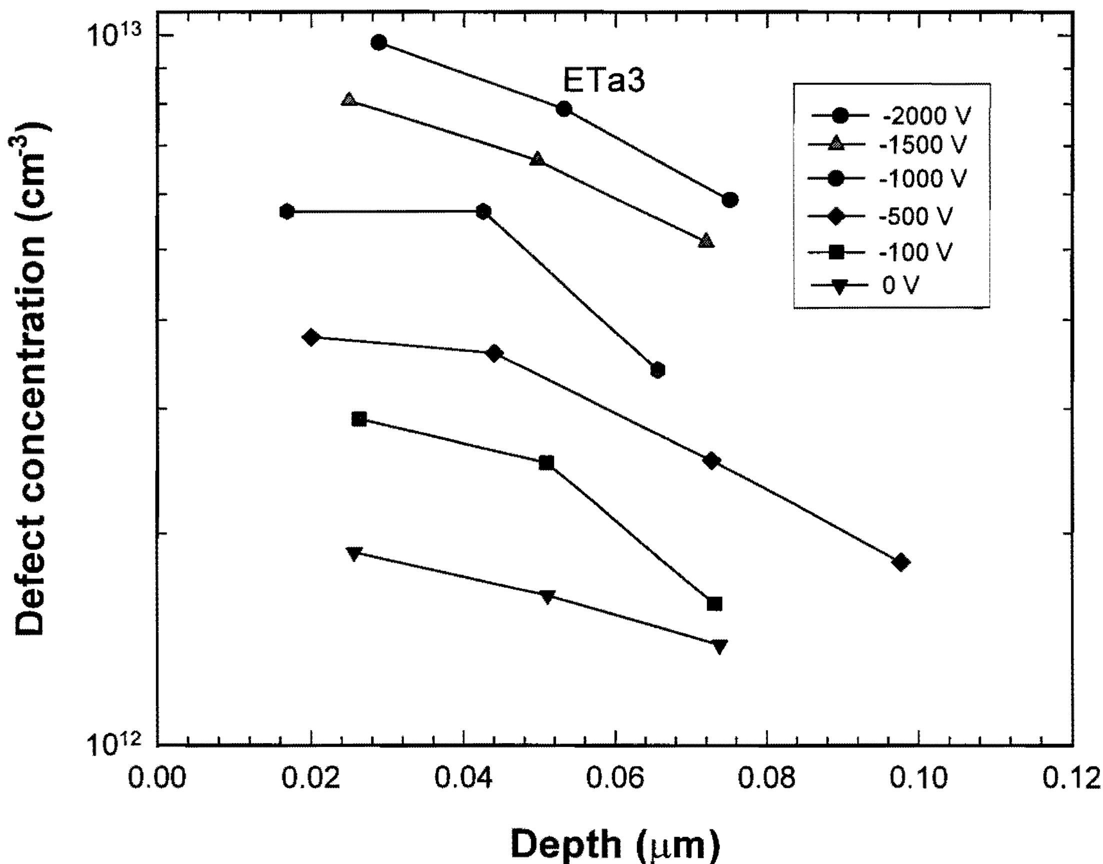

Fig 8.10 *Depth profiles (constructed from DLTS measurements) of the ETa3 defect introduced in n-GaAs during Ta Schottky contacts formed during the applied negative voltage.*

Comparing the defects introduced during EB deposition of Ta metal for the applied positive voltage (Fig 8.3) to those introduced during the applied negative voltage (Fig 8.7) to the substrate (GaAs), we find that there were three defects introduced. It was shown that the relative concentrations of those defects formed during EB deposition depend on the applied voltages. In order to explain the origin of EB deposition induced defects observed here we consider what happens to the GaAs during metallisation.

The heavy energetic Ta particles (ions or atoms) impinge on the sample and as the different voltage polarities were applied, different ions can be expected to reach the GaAs samples. The metal ions do not penetrate deep into the semiconductor but can transfer enough energy to cause displacement damage at and within several

atomic layers below the GaAs surface. Electrons can penetrate much deeper but cannot transfer enough energy via elastic collisions to cause displacement damage [7]. We also speculate that the defects observed after EB deposition may be caused by the x-rays produced when the electrons originating at the filament strikes the metal. X-ray induced damage has been reported [12] and it has been found to affect metal-oxide semiconductors (MOS) devices adversely. An increase in electron beam current would increase the x-ray intensity and hence increase the defect concentration. We therefore conclude that the EB deposition defects observed here result from the interaction of different particle types with the GaAs surface.

The relative heights of the DLTS peaks in Fig 8.3 and Fig8.7, which were used to calculate the defect concentrations, are not the same. Fig 8.3 shows that after EB deposition of Ta, the peak height of ETa2 has been relatively reduced with respect to that of ETa3. On the other hand, Fig 8.7 shows that the peak height of ETa2 has been relatively increased with respect to that of ETa3. The reasons for this apparent discrepancy may be the following, first the different in the applied voltages on the substrate. A second reason for this discrepancy in DLTS peak height may be related to the different particles reaching the substrate. It was noted that the defect concentration for all the EB induced defects increased with increasing the voltage to the sample, irrespective of positive or negative.

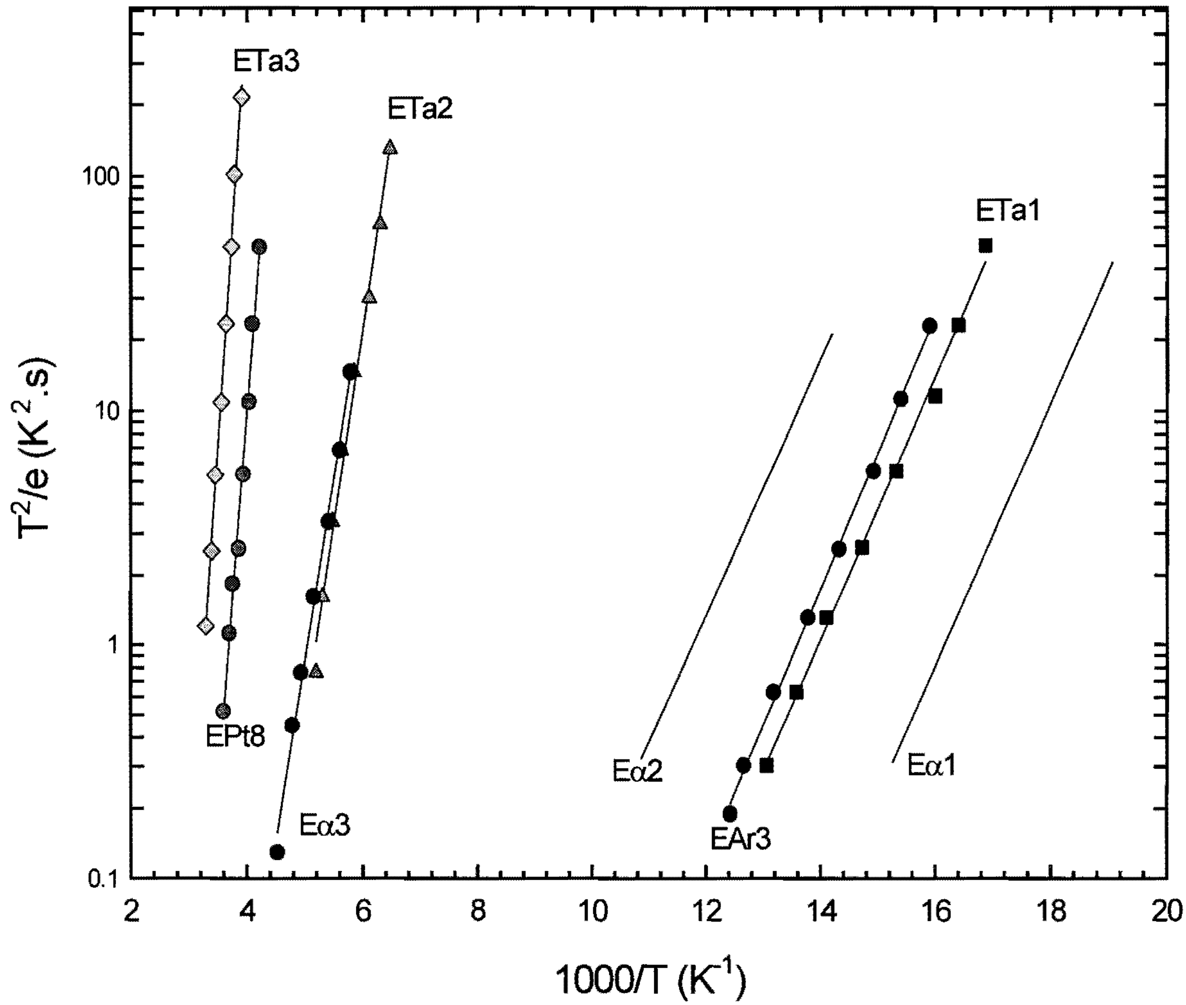

Fig 8.11 *Defect signatures of ETa1, ETa2, and ETa3 on an Arrhenius plot recorded at a quiescent bias of 0 V and a filling pulse of 0.2 V for ETa1, a quiescent bias of 0.5 V and a filling pulse of 0.7 V for both ETa2 and ETa3.*

The DLTS signatures of ETa1, ETa2 and ETa3 (activation energy E_t in the band gap and capture cross section σ_{na}) were calculated using the conventional assumption that (1) capture cross section (σ_{na}) is independent of temperature, and (2) the emission rate (e_n) of carriers by a trap varies with temperature according to the following equation:

$$e_n = \gamma_n T^2 \sigma_{na} e^{-E_t/kT}$$

where e_n is the electron emission rate from the defect site at a temperature T, k is Boltzmann's constant and the γ_n is a constant equal to 2.21×10^{20} cm^{-2} s^{-2} K^{-2} for an electron trap in GaAs [1]. In this study, the degeneracy factor (g) of 1 was used in all applicable calculations. Upon investigation of the DLTS spectra, there appeared only three defects (Fig 8.2 (b)). The pulse conditions chosen for the DLTS spectra in Fig 8.2(b) was not selected to maximize the peaks but to allow the best possible separation of the traps. The DLTS signatures of the three electron traps were determined from the Arrhenius graph (plot of T^2/e against 1000/T) represented in Fig 8.11 and the data are presented in table 8.1. From table 8.1, we see that these defects have electronic levels in the GaAs band gaps of 0.102 eV, 0.322 eV and 0.637 eV below the conduction band.

Table 8.1: *Electronic properties of defects introduced in epitaxial n-GaAs by EB deposition of Ta*

Defect label	E_T (eV)	σ_n (cm^2)	T_{peak}[a] (K)	Similar defects
ETa1	0.102 ± 0.004	1.9×10^{-15}	71	EA_r3 [8]
ETa2	0.322 ± 0.014	1.2×10^{-14}	183	Eα3[12]
ETa3	0.637 ± 0.029	9.2×10^{-13}	285	EPt8[6]

[a]Peak temperature at a lock-in amplifier frequency of 46 Hz. i.e. a decay time constant of 9.23 ms.

To clarify whether defects were new, their signatures were compared to defects detected from the same material by other authors. In comparing defect signatures, care was taken to ensure which degeneracy factor was used in the calculation of the defect characteristics. In table 8.1, reference is made to defects previously detected for GaAs with the same free carrier concentration. It was found that these defects have similar, if not identical signatures, as other defects were found after Ar-ion sputter etching (8), EB deposition of Pt (6), and alpha irradiation (12). ETa1 has a similar signature to EAr3 (from Ar sputter etching), ETa2 to Eα3 (from alpha irradiation) and ETa3 to EPt8 (from Pt EB deposition). This comparison indicates that the EB deposition induced defects observed here have similar "signatures" as those of defects previously observed in grown n-GaAs. Therefore, this shows that we have more or less the same defects. ETa1 was compared with the high-energy alpha particles induced defect on n-GaAs. The DLTS signature of the α-particles induced defects has therefore suggested that Eα1 and Eα2 have a point defect nature. ETa1 and Eα1 are supposed to be the same charge state of the same defect. However, it has been observed that their concentrations are strongly dependent upon the bias conditions chosen when acquiring the DLTS spectra. It appeared that their concentrations are strongly dependent upon the magnitude of the electrical field present during the measurement.

8.2 Summary

We presented the results of defects introduced during EB deposition of Ta contacts on n-GaAs. The introduction of three defects has been observed. DLTS spectra of control samples recorded using resistively deposited contacts, indicated that no defects with peaks between 20 and 350 K are present in significant concentrations. The DLTS peaks on the spectra Fig 8.3 and Fig 8.7 were obtained by applying the positive and the negative voltages to the sample. The signatures of the three defects were determined from Arrhenius plots. The electronic levels of these defects in the GaAs band gap were calculated as 0.102 eV, 0.322 eV and 0.637 eV below the conduction band for ETa1, ETa2 and ETa3 respectively.

The defects were found to have similar signatures to some of the defects detected in the same material after it has been exposed to other particles. The DLTS depth profiling showed that the concentration of these defects decreased with depth below the surface. It has been observed that ETa1 and Eα1 concentrations are strongly dependent upon the bias conditions chosen when acquiring the DLTS spectra.

References

1) S. A. Goodman, F. D. Auret, G. Myburg, and S. Schutte, Solid State Phenomena. **47** (1996) 391.

2) G. Myburg, and F. D. Auret, J. Appl. Phys. **71** (1992) 6172.

3) L. J. Bredell, F. D. Auret, G. Myburg, and W. O. Barnard, Appl. Surface. Sci. **50** (1991) 466.

4) F. D. Auret, S. A. Goodman, G. Myburg, and W. E. Meyer, J. Vac. Sci. Technol. B **10** (1992) 2366.

5) G. Myburg, F. D. Auret, W. E. Meyer, C. W. Louw, M. J. van Staden, Thin Solid Films. **325** (1998) 181.

6) G. Myburg, W. E. Meyer, F. D. Auret, H. Burger, W. O. Barnard, and S. A. Goodman, Mater. Sci. and Technol. **14** (1998) 1269.

7) F. D. Auret, G. Myburg, H. W. Kunert and W. O. Barnard, J. Vac. Sci. Technol. B **10** (1992) 591.

8) F. D. Auret, S. A. Goodman, G. Myburg and W. E. Meyer, Appl. Phys. A **56** (1993) 547.

9) S. X. Jin, H. P. Wang, M. H. Yuan, H. Z. Song, H. Wang, W. L. Mao, and G. G. Qin, Appl. Phys. Lett. **62** (1993) 2719.

10) W. O. Barnard, G. Myburg, F. D. Auret, S. A. Goodman and W. E. Meyer, J. Electron. Mater. **26** (1996) 1695.

11) Y. Zohta and M. O. Watanabe, J. Appl. Phys. **53** (1982) 1809.

12) D. V. Lang, J. Appl. Phys. **45** (1974) 3014.

13) S. A. Goodman, F. D. Auret and W. E. Meyer, Nucl. Instr. and Meth. in Phys. Res. B **90** (1994) 349.

CHAPETR 9:

CONCLUSION

Metallisation of semiconductors is a critical processing step during device fabrication. EB deposited layers exhibit a better adhesion as opposed to layers deposited by other methods. However, due to the energetic particles involved, EB deposition is damaging on an atomic scale and causes lattice disorder at and below the semiconductor surface. Investigations have shown that the barrier height of EB deposited Schottky contacts on n-type GaAs are lower than those of contacts deposited by a less damaging process, (like resistive evaporation). This barrier height alteration was ascribed to the introduction of defects in the semiconductor during EB deposition of Ta.

The main purpose of this study was to investigate the effect of GaAs substrate bias on Ta SBDs deposited by EB deposition on the electrical properties of the contact and GaAs material properties. In this study we addressed several aspects related to EB deposition of Ta Schottky contacts onto GaAs. The quality of these contacts on n-GaAs and the defects introduced there in were investigated as a function of applied positive and negative voltages to the sample. Characterization of the EB deposition of Ta resulted in the following main conclusions.

From the I-V results of Ta SBDs deposited with and without shielding the substrate from stray electrons during EB metallisation showed that the use of a shield is essential if higher quality devices are to be fabricated. From this, it is clear that the exposure of the semiconductor to stray electrons during metallisation causes non-ideal SBDs properties and should, therefore be avoided or minimized. We have established that EB deposition introduces defects in the band gap of the semiconductor when the substrate is biased. The barrier height decreased from 0.78 to 0.72 eV, accompanied by an increase in the ideality factor from 1.05 to 1.17 when positively biased and 1.05 to 1.19 when negatively biased. We have shown that the applied voltages cause reductions in the barrier heights and increases in the ideality factor.

From DLTS results, it appears that the increase in the reverse leakage current is due to the presence of defects with levels in the band gap (ETa1, ETa2 and ETa3).

Using DLTS, we have shown that resistive evaporation of Ni on n-GaAs does not introduce any defects. On the other hand, EB deposition introduced defects in the n-GaAs. This explains why the resistive evaporated contacts have significantly higher barrier heights than EB deposited contacts. For EB deposition, the defect concentration increased with increasing the applied voltage to the substrate. These results suggest that for the fabrication of high quality rectifying contacts to n-GaAs, resistive evaporation should be used. DLTS measurement confirmed the presence of defects with energy levels in the GaAs at and close to the GaAs surface. The concentration of these defects was found to increase with increasing the stray particle energy reaching the sample during deposition by increasing the voltage to the sample.

By applying a negative voltage on the substrate during metallisation, DLTS studies showed the presence of three prominent EB deposition induced defects, ETa1, ETa2, and ETa3. These defects act as electron traps in the n-type GaAs that was investigated and their energies in the band-gap are 0.102 eV, 0.322 eV and 0.617 eV below the conduction band. The concentration of the defects increased when the applied voltage was increased along the positive direction and when the applied voltage was increased along the negative direction. The Ta SBDs formed by EB deposition with the positive applied voltage, were found it to be of superior quality than the Ta SBDs formed at negative applied voltages under the same conditions. It appears that the defects ETa1, ETa2, and ETa3 are similar to EAr3, Eα3 and EPt8 introduced in GaAs by particle irradiations, respectively. The defects ETa2 and ETa3 are introduced in higher concentrations than ETa1. Depth profiles of each individual defect indicated a high defect concentration near the surface, which then sharply decreased away from the junction into the material. It appeared that as the voltage on the sample increases, the defect profiles move deeper into the material. The cause of the EB induced defects is unintentional bombardment of the GaAs by ionized particles originating in the region of the EB filament, any environment in the chamber or molten metal. The concentration of these defects can be minimized by adjusting the evaporation geometry, applying the low voltage to the sample and inserting a shield between the filament and the sample.

The fact that EB current resulted in formation of defects implies that the amount of damage can be minimized by optimizing deposition conditions in such a way that the lowest possible electron beam current is used.